

---

# **Comprehensive Vibration Assessment Program for U.S. EPR Reactor Internals**

ANP-10306NP  
Revision 1

## **Technical Report**

January 2013

AREVA NP Inc.

---

(c) 2013 AREVA NP Inc.

**Copyright © 2013**

**AREVA NP Inc.  
All Rights Reserved**

### Nature of Changes

Item	Sections or Pages	Description and Justification
000	All	Original Issue
001	All	For consistency, changes were made to verb tense and other grammatical changes
	Figure 3-1	Revised by adding pointers to show additional clarity and consistency with the Vibration Analysis Program (performed prior to the pre-operational tests) of the Regulatory Guide 1.20
	Section 4.0	Revised to address RAIs 407, 422, 458, 508, 522
	Table 4-19	Added Note 3 to provide additional clarity and definition of the FIV results that are presented in this table.
	Tables 4-26 to 4-37	Added to address RAIs 422, 508, 548, and 522
	Figures 4-41 to 4-72	Added to address RAIs 422, 508, 548, and 522
	Sections 5.5 and 5.6	Revised to address RAI 422
	Sections 6.1 and 6.2	Revised to address RAI 422
	Table 6-6	Added to address RAI 422
	Section 7.0	Revised to address RAI 522
	Section 8.0	Deleted Reference 13 and added References 17 to 28
	A.2.1	On page A-1, the second paragraph of this section was revised to provide a definition of "shear wave resonance" as used throughout Appendix A.
	A.2.1	On page A-2, the last paragraph of this page was revised to provide a better description of the acoustic mode in the standpipe and the main pipe for reasons of clarity.
	Sections A.2.1, A.2.3.3, and A.2.4	Revised to address RAIs 331, 422, and 522
	Sections B.3.1, B.3.2.2, and B.5	Revised to address RAI 422
B.3.3.1	The value of the crossing frequency was changed to be consistent with the value in Table B-3.	
Table B-3 & Figure B-9	Added to address RAI 422	
Appendix C	Added to address RAI 522	

---

## Contents

1.0	INTRODUCTION.....	1-1
2.0	DESCRIPTION AND CLASSIFICATION OF THE U.S. EPR REACTOR INTERNALS .....	2-1
2.1	General Arrangement.....	2-1
	2.1.1 Lower Internals .....	2-1
	2.1.2 Upper Internals .....	2-3
	2.1.3 Interface Cold Gaps.....	2-4
2.2	Flow Paths through the RV .....	2-5
2.3	Evolution of the U.S. EPR Reactor Vessel Internals .....	2-6
2.4	Classification of Reactor Internals in Accordance with Regulatory Guide 1.20.....	2-7
3.0	COMPREHENSIVE VIBRATION ASSESSMENT PROGRAM .....	3-1
4.0	VIBRATION AND STRESS ANALYSIS PROGRAM.....	4-1
4.1	General.....	4-1
4.2	RV Lower Internal Assembly .....	4-2
	4.2.1 HYDRAVIB Scale Model Tests.....	4-2
	4.2.2 Development of the 1/8 Scale Numerical Model .....	4-7
	4.2.3 Numerical Simulation of HYDRAVIB Mock-up Flow Condition... ..	4-34
	4.2.4 Conclusions of the FIV Numerical and Experimental Simulations .....	4-44
	4.2.5 Numerical Simulation of Full Scale Model (Pre-Operational) .....	4-45
	4.2.6 FIV Acceptance Criteria for the RV Lower Internals.....	4-85
	4.2.7 Response of the RV Lower Internals (Full Scale).....	4-88
	4.2.8 Conclusions .....	4-99
4.3	Flow Distribution Device (FDD) .....	4-100
	4.3.1 Testing Performed for the FDD .....	4-100
	4.3.2 Theoretical Analysis of the Flow Distribution Device .....	4-100
	4.3.3 FIV Acceptance Criteria for FDD .....	4-112
	4.3.4 Response of the FDD .....	4-112
	4.3.5 Conclusions .....	4-122

4.4	Irradiation Specimen Basket .....	4-123
4.5	RV Upper Internals .....	4-124
4.5.1	Theoretical Analysis of the RV Upper Internals (Full Scale).....	4-124
4.5.2	FIV Acceptance Criteria for the Column Supports.....	4-138
4.5.3	Response of the Column Supports.....	4-140
4.5.4	Conclusions .....	4-145
4.6	CRGAs and RCCAs .....	4-145
4.6.1	MAGALY Tests.....	4-146
4.6.2	CRGA Modal Characterization and Fatigue Tests .....	4-151
4.6.3	Theoretical Evaluation for the CRGA .....	4-153
4.6.4	FIV Acceptance Criteria for the CRGA Components.....	4-157
4.6.5	Response of the CRGA Components.....	4-158
4.6.6	Conclusions .....	4-162
4.7	Heavy Reflector Tie Rods .....	4-162
4.7.1	Description of Tests for the Tie Rod .....	4-162
4.7.2	Results of the Flow Test for the Tie Rods .....	4-163
4.7.3	Cyclic Loading of Tie Rods Created by Response of Heavy Reflector to Random Turbulence .....	4-164
4.7.4	Conclusions .....	4-165
5.0	VIBRATION AND STRESS MEASUREMENT PROGRAM .....	5-1
5.1	Objectives.....	5-1
5.2	Instrumentation.....	5-1
5.2.1	Permanent Instrumentation .....	5-1
5.2.2	Temporary Instrumentation .....	5-2
5.3	Test Conditions .....	5-21
5.3.1	Pre-Operational Tests .....	5-21
5.3.2	Initial Startup Tests and Full Power Tests .....	5-22
5.4	Acquisition of Test Data .....	5-24
5.4.1	Precautions to Ensure Quality of Data .....	5-24
5.4.2	Data Acquisition System.....	5-24
5.4.3	Process for Determining Frequency, Modal Content and the Maximum Values of Response.....	5-25
5.4.4	Bias Errors and Random Uncertainties .....	5-25

5.5	Acceptance Criteria for the Tests .....	5-25
5.6	Evaluation Plan for the Test Data.....	5-26
6.0	INSPECTION PROGRAM.....	6-1
6.1	Principles of the Inspection Program.....	6-1
6.2	Inspection Plan.....	6-1
7.0	CONCLUSION .....	7-1
8.0	REFERENCES.....	8-1
APPENDIX A: VIBRATION ASSESSMENT FOR THE RCS PIPING AND THE PIPING ATTACHED TO THE RSG.....		
	A.1 Scope .....	A-1
	A.2 Flow-Excited Acoustic Resonance .....	A-1
	A.3 Vibration Measurement Instrumentation .....	A-10
	A.4 Acceptance Criteria .....	A-10
APPENDIX B: VIBRATION ASSESSMENT OF THE RSG UPPER INTERNALS.....		
	B.1 Scope .....	B-1
	B.2 Operating Experience with RSG Upper Internal Design Similar to the U.S. EPR.....	B-1
	B.3 FIV Evaluation of the Primary Steam Separators.....	B-7
	B.4 FIV Evaluation of the RSG Steam Dryers .....	B-22
	B.5 FIV Evaluation of the Other RSG Upper Internal Components.....	B-24
	B.6 Conclusions.....	B-25
APPENDIX C: VIBRATION ASSESSMENT OF THE RSG TUBE BUNDLE.....		
	C.1 Overview of FIV Analysis Methodology Performed for the RSG Tube Bundle .....	C-1
	C.2 Flow and Vibration Test Models .....	C-2
	C.3 Analysis for Fluid-elastic Instability.....	C-5
	C.4 Analysis for Random Turbulence due to Cross Flow Conditions .....	C-6
	C.5 Analysis for Random Turbulence Induced Vibration due to Parallel Flow Conditions.....	C-10

---

C.6 Analysis for Vortex-Shedding Induced Vibration due to Cross Flow Conditions .....	C-12
C.7 Analysis for RCP Acoustic Pressure Fluctuations .....	C-14

---

**List of Tables**

Table 4-1	Dry Modal Frequencies – Measured vs. Computed Values .....	4-18
Table 4-2	Wet Modal Frequencies – Measured vs. Computed Values .....	4-23
Table 4-3	Displacements and Statistical Frequencies from the Scale Model Analysis of the HYDRAVIB Mockup Conditions .....	4-38
Table 4-4	Displacements Measured during the HYDRAVIB Mockup Flow Test ...	4-38
Table 4-5	Description of the Main Modes – Unloaded Core.....	4-47
Table 4-6	Description of the Main Modes – Loaded Core .....	4-48
Table 4-7	Summary of Modal Damping Ratios used for FIV Estimation .....	4-84
Table 4-8	FIV Displacement Limit for RV Core Barrel and Heavy Reflector .....	4-87
Table 4-9	Displacement Response of the RV Internals (HFT #17) .....	4-89
Table 4-10	Displacement Response of the RV Internals (Full Power, Steady State Normal Operating Condition) .....	4-89
Table 4-11	Modal Frequencies of the 1/8 Scale FDD .....	4-105
Table 4-12	Modal Frequencies of the Full Scale FDD (In-Water) .....	4-105
Table 4-13	Displacement Response of FDD to Random Turbulence at Different Shell Locations .....	4-115
Table 4-14	Maximum Stress in the FDD Support Columns Due to the Response of the FDD to Random Turbulence .....	4-116
Table 4-15	Reaction Loads in the FDD Support Columns Due to the Response of the FDD to Random Turbulence .....	4-117
Table 4-16	FDD Stress in the Cylindrical Shell Due to the Response of the FDD to Random Turbulence (psi, rms) .....	4-118
Table 4-16A	Response of the FDD to the RCP Acoustic Pressure Fluctuations.....	4-119
Table 4-17	Modal Damping Ratio (%) for Column Supports (Viscous) (Used only for Vortex-Shedding Excitation) .....	4-137
Table 4-18	In-Water Theoretical Natural Frequencies of the Column Supports....	4-141
Table 4-19	Evaluation for Vortex-Shedding Lock-in for the Column Supports.....	4-142
Table 4-20	Summary of FIV Results for the RV Upper Internal Column Supports.....	4-143
Table 4-21	Thermal-Hydraulic Inputs for the CRGA and the RCCA .....	4-155
Table 4-22	Susceptibility of CRGA Tie Rod to Vortex-Shedding Lock-In.....	4-159
Table 4-23	Susceptibility of CRGA C-Tube to Vortex-Shedding Lock-In .....	4-159
Table 4-24	Susceptibility of RCCA to Vortex-Shedding Lock-In.....	4-160

Table 4-25	CRGA FIV Results for Random Turbulence Excitation .....	4-161
Table 4-26	Modal Frequencies of the HR Tie Rods .....	4-166
Table 4-27	Damping Coefficients for the HR Tie Rods .....	4-166
Table 4-28	List of Sensors Used with the HYDRAVIB Mockup Testing .....	4-168
Table 4-29	Characteristic of the Sensors used with HYDRAVIB Mockup Testing.....	4-169
Table 4-30	U.S. EPR RCP Shaft and Blade Passing Frequencies (Design).....	4-169
Table 4-31	Static Forces Acting on the Support Columns.....	4-170
Table 4-32	Comparison of Natural & Vortex-Shedding Frequencies for the Column Supports.....	4-170
Table 4-33	Dynamic Amplification Factors for the RCP Acoustic Pressure Fluctuations .....	4-171
Table 4-34	Reduced Damping for the CRGA Control Rod Absorber (Viscous) ....	4-172
Table 4-35	Stress Results for Resonant Excitation of the HR Tie Rods (In-Air) .....	4-173
Table 4-36	Stress Results for Resonant Excitation of the HR Tie Rods (In-Water) .....	4-174
Table 4-37	Vibration Amplitude of LSP for Various Combinations of Pump Operation (from HYDRAVIB Mockup).....	4-175
Table 5-1	Instrumentation of the RV for Pre-operational Tests.....	5-5
Table 5-2	Instrumentation of the Lower Internals for Pre-operational Tests .....	5-6
Table 5-3	Instrumentation of Upper Internals for Pre-operational Tests .....	5-7
Table 5-4	Pre-Operational Test Program .....	5-23
Table 6-1	Visual Inspection of the Upper Internals on their Stand .....	6-3
Table 6-2	Visual Inspection of the Inside of Lower Internals (In RV).....	6-4
Table 6-3	Visual Inspection of the Outside of Lower Internals (On Their Stand) ....	6-4
Table 6-4	Visual Inspection of the RV Inside.....	6-5
Table 6-5	Visual Inspection of the RV Head.....	6-5
Table 6-6	U.S. EPR RPV and Internals Visual Inspection Plan .....	6-5
Table B-1	Comparison of RSG Upper Internals between the U.S. EPR and Other Plants Currently Operating .....	B-3
Table B-2	Pipe-Separator Displacements (RMS Response).....	B-14
Table B-3	Pipe-Separator Stress (RMS Response) .....	B-15
Table C-1	Acceptance Criteria for FIV Analysis of the U.S. EPR SG Tube Bundle .....	C-16

---

Table C-2	Summary of Fluid-Elastic Instability Analysis Results .....	C-16
Table C-3	Summary of Displacements due to Random Turbulence-Induced Vibration for Cross Flow .....	C-17
Table C-4	Summary of Stress due to Random Turbulence-Induced Vibration for Cross Flow .....	C-19
Table C-5	In-Plane U-bend Displacements for Column 113 on a Nodal Basis .....	C-21
Table C-6	Maximum Stresses for Flawed Tubes Resulting from Cross-Flow Turbulence-Induced Vibration .....	C-22
Table C-7	Summary of Displacements Due to Random Turbulence Induced Vibration for Parallel Flow .....	C-22
Table C-8	Summary of Stresses Due to Random Turbulence-Induced Vibration for Parallel Flow .....	C-23
Table C-9	Displacements Due to Vortex Shedding Induced Vibration.....	C-23
Table C-10	Stress Due to Vortex Shedding Induced Vibration .....	C-23

---

**List of Figures**

Figure 2-1	General Arrangement of the U.S. EPR RV Internals.....	2-8
Figure 2-2	U.S. EPR RV Lower Internals .....	2-9
Figure 2-3	U.S. EPR RV Heavy Reflector .....	2-10
Figure 2-4	U.S. EPR RV Upper Internals .....	2-11
Figure 2-5	U.S. EPR RV Upper Internals .....	2-12
Figure 2-6	Flow Paths within the Reactor Vessel .....	2-13
Figure 3-1	Comprehensive Vibration Assessment Program, including VMS Calibration .....	3-2
Figure 4-1	HYDRAVIB Mock-up .....	4-4
Figure 4-2	HYDRAVIB Test Loop .....	4-5
Figure 4-3	HYDRAVIB Instrumentation for the Flow Tests.....	4-6
Figure 4-4	HYDRAVIB Instrumentation – Implementation of Dynamic Pressure Sensors .....	4-7
Figure 4-5	Flow Chart for Scale Model Analysis.....	4-8
Figure 4-6	FEM of Core Barrel .....	4-11
Figure 4-7	FEM of Lower Support Plate and Flow Distributing Device.....	4-12
Figure 4-8	FEM of Heavy Reflector .....	4-13
Figure 4-9	FEM of Lower Internals and Core .....	4-14
Figure 4-10	HYDRAVIB Dry Mode Shapes CB Beam-Type Modes (Along Reactor 0°-top and 90°-bottom) .....	4-19
Figure 4-11	HYDRAVIB Wet Mode Shapes CB Beam-Type Modes (Along Reactor 0°-top and 90°-bottom).....	4-24
Figure 4-12	Dimensionless PSD for the Turbulence in the RV Downcomer .....	4-29
Figure 4-13	Dimensionless PSD of Turbulence in Front of Inlet Jets .....	4-32
Figure 4-14	Dimensionless PSD of the Turbulence in the RV Lower Plenum.....	4-34
Figure 4-15	Normalized Modal Covariance Matrix for the LSP Location.....	4-40
Figure 4-16	Response PSD and Corresponding Energy Distribution along Reactor 0° Axis (mockup conditions).....	4-41
Figure 4-17	Response PSD and Corresponding Energy Distribution along Reactor 90° axis (mockup conditions).....	4-42
Figure 4-18	Horizontal Displacements Levels Mapping for Mockup Conditions FIV Simulation .....	4-43

Figure 4-19	Wet Mode Shapes for Full Scale Model (Un-Loaded Core) .....	4-49
Figure 4-20	Wet Mode Shapes for Full Scale Model (Loaded Core).....	4-67
Figure 4-22	RV Lower Internal Response Locations for Displacements .....	4-90
Figure 4-23	RPSD and Corresponding Energy Distribution along Reactor 0° Axis .....	4-91
Figure 4-24	RPSD and Corresponding Energy Distribution along Reactor 90° Axis .....	4-92
Figure 4-25	Horizontal Displacements Levels Mapping for Reactor Conditions FIV Simulation.....	4-93
Figure 4-26	Axial Stress Distribution .....	4-95
Figure 4-27	Frequencies and Mode Shape Plots for the FDD.....	4-106
Figure 4-28	Deleted .....	4-110
Figure 4-29	Pressure PSD Loading for FDD (Log vs. Linear Scale) .....	4-111
Figure 4-30	FDD Cylindrical Shell Response PSD .....	4-120
Figure 4-32	FDD Cylindrical Shell Elements for Evaluation of Stress .....	4-121
Figure 4-35	MAGALY Mock-up.....	4-148
Figure 4-36	MAGALY - Simulated Flow Rates .....	4-149
Figure 4-37	Instrumentation for the Third Phase of MAGALY Tests .....	4-150
Figure 4-38	CALVA Bench .....	4-152
Figure 4-39	Control Rod Guide Assembly (CRGA) .....	4-156
Figure 4-40	Heavy Reflector Tie Rods .....	4-167
Figure 4-41	HR Tie Rod Mode Shape in Still Water (Mode 1).....	4-176
Figure 4-42	HR Tie Rod Mode Shape in Still Water (Mode 2).....	4-177
Figure 4-43	HYDRAVIB Instrumentation for Static Testing of Core Barrel.....	4-178
Figure 4-44	HYDRAVIB Instrumentation for Static Testing of Flow Distribution Device .....	4-179
Figure 4-45	HYDRAVIB Instrumentation for Modal Testing of Core Barrel .....	4-180
Figure 4-46	HYDRAVIB Instrumentation for Modal Testing of Heavy Reflector .....	4-181
Figure 4-47	HYDRAVIB Instrumentation for Modal Testing of Flow Distribution Device .....	4-182
Figure 4-48	HYDRAVIB Instrumentation for Modal Testing of Core Barrel Assembly (Core Barrel Instrumentation) .....	4-183
Figure 4-49	HYDRAVIB Instrumentation for Modal Testing of Core Barrel Assembly (Heavy Reflector Instrumentation) .....	4-184

Figure 4-50	Random Lift Coefficient for U.S. EPR Upper Internals .....	4-185
Figure 4-51	Mode Shapes for the Normal Support Column (axial load = -4500 lbs).....	4-186
Figure 4-52	Mode Shapes for the LMP Support Column (axial load = -3600 lbs).....	4-187
Figure 4-53	Mode Shapes for the CRGA Support Column (axial load = -7500 lbs).....	4-188
Figure 4-54	Mode Shapes for the Instrumentation Guide Tube .....	4-189
Figure 4-55	Displacement Response PSD for Normal Support Column .....	4-190
Figure 4-56	Displacement Response PSD for LMP Support Column .....	4-191
Figure 4-57	Displacement Response PSD for CRGA Support Column .....	4-192
Figure 4-58	Displacement Response PSD for Instrumentation Guide Tube .....	4-193
Figure 4-59	Acoustic Wave Impinging Normally on a Cylinder.....	4-194
Figure 4-60	CRGA and CRGA Column Support.....	4-195
Figure 4-61	CRGA Tie Rod Frequencies and Mode Shapes .....	4-196
Figure 4-62	CRGA C-Tube Frequencies and Mode Shapes (in-plane).....	4-198
Figure 4-63	CRGA C-Tube Frequencies and Mode Shapes (out-of-plane) .....	4-200
Figure 4-64	CRGA RCCA Frequencies and Mode Shapes (in-plane) Sheet 1 of 3 .....	4-202
Figure 4-65	CRGA RCCA Frequencies and Mode Shapes (out-of-plane) .....	4-205
Figure 4-66	CRGA Tie Rod Displacement Response PSD .....	4-208
Figure 4-67	CRGA C-Tube Displacement Response PSD (in-plane) .....	4-209
Figure 4-68	CRGA C-Tube Displacement Response PSD (out-of-plane).....	4-210
Figure 4-69	CRGA RCCA Displacement Response PSD (in-plane) (Between Bottom Flange/Guide Plate and Bottom End of RCCA).....	4-211
Figure 4-70	CRGA RCCA Displacement Response PSD (in-plane) (Between 5th Intermediate Guide Plate and Bottom Flange/Guide Plate) .....	4-212
Figure 4-71	CRGA RCCA Displacement Response PSD (in-plane) (Between RCCA Spider and 5th Intermediate Guide Plate).....	4-213
Figure 4-72	U.S. EPR CFD Model.....	4-214
Figure 5-1	Pre-operational Test Instrumentation - Overview .....	5-8
Figure 5-2	VMS Permanent Instrumentation .....	5-9
Figure 5-3	RV Bottom Head Instrumentation.....	5-10
Figure 5-4	Lower Internals Instrumentation .....	5-11

Figure 5-5	Lower Support Plate Instrumentation .....	5-12
Figure 5-6	Core Barrel and Heavy Reflector - Instrumentation .....	5-13
Figure 5-7	FDD Instrumentation .....	5-14
Figure 5-8	Upper Internals - Instrumentation.....	5-15
Figure 5-9	Upper Core Plate Instrumentation.....	5-16
Figure 5-10	Instrumented Locations of CRGA, CRGA Column and LMP Column ...	5-17
Figure 5-11	CRGA Guide Plate Instrumentation .....	5-18
Figure 5-12	CRGA Column Instrumentation.....	5-19
Figure 5-13	LMP Column Instrumentation.....	5-20
Figure A-1	Shear Wave Acoustic Resonance.....	A-12
Figure A-2	Positions of VMS Transducers in the MSL and the MFWL .....	A-13
Figure A-3	Positions of VMS Transducers in the Reactor Coolant System .....	A-14
Figure B-1	U.S. EPR RSG Upper Internals.....	B-4
Figure B-2	U.S. EPR RSG Two Stage Primary Steam Separators (Type S 335-2) .....	B-5
Figure B-3	U.S. EPR RSG Steam Dryers .....	B-6
Figure B-4	Pipe-Separator Frequencies and Mode Shapes (In-Plane X-Y Plots).....	B-9
Figure B-5	Pipe-Separator Frequencies and Mode Shapes (Out-of-Plane Z-Y Plots).....	B-10
Figure B-6	Single Sided Non-Dimensional PSD for Confined Annular Flow.....	B-11
Figure B-7	Pipe-Separator In-Plane Displacement Response PSD .....	B-16
Figure B-8	Pipe-Separator Out-of-Plane Displacement Response PSD .....	B-17
Figure B-9	Pressure PSD for Pipe-Separator Assembly.....	B-18
Figure C-1	Random Lift Coefficient for Random Turbulence due to Cross Flow (Per Reference 24).....	C-24
Figure C-2	Empirical Equations for the Random Pressure PSD (Recommended by various authors per Figure 9.5 of Reference 4) .....	C-25
Figure C-3	Random Lift Coefficient for the Analysis of Vortex-Shedding.....	C-26

**Nomenclature**

<b>Acronym</b>	<b>Definition</b>
CB	Core Barrel
CFD	Computational Fluid Dynamic
CRDM	Control Rod Drive Mechanism
CRDT	Control Rod Drive Tubes
CRGA	Control Rod Guide Assembly
FA	Fuel Assembly
FDD	Flow Distribution Device
FEM	Finite Element Model
FFT	Fast Fourier Transform
FIV	Flow-Induced Vibration
FSM	Fluid-elastic Stability Margin
FSRF	Fatigue Strength Reduction Factor
HFT	Hot Functional Testing
HR	Heavy Reflector
LMP	Level Measurement Probe
LSP	Lower Support Plate
NRC	U.S. Nuclear Regulatory Commission
PSD	Power Spectral Density
Prez	Pressurizer
PWR	Pressurized Water Reactor
RCCA	Rod Control Cluster Assembly
RCP	Reactor Coolant Pump
RCS	Reactor Coolant System
Re	Reynolds Number
RMS/rms	Root Mean Square
RPSD	Response Power Spectral Density
RSG	Re-circulating Steam Generator
RSS	Root Sum of the Squares
RTE	Random Turbulence Excitation
RV	Reactor Vessel
$S_t$	Strouhal Number
UCP	Upper Core Plate
USP	Upper Support Plate

---

<b>Acronym</b>	<b>Definition</b>
VSE	Vortex-Shedding Excitation
VMG	Vibration Monitoring Group
VMS	Vibration Monitoring System
XFreq	Crossing Frequency

## 1.0 INTRODUCTION

This report describes the comprehensive vibration assessment program for the U.S. EPR™ (U.S. EPR) reactor internals that verifies the structural integrity of the reactor internals for flow-induced vibration. The comprehensive vibration assessment program conforms to the guidance of Regulatory Guide (RG) 1.20, Revision 3 (Reference 1).

The design of the U.S. EPR reactor vessel (RV) internals is derived from French N4 and German Konvoi designs. However, the U.S. EPR RV internals include new features that could introduce some changes in the vibratory behavior compared to the reference units. The U.S. EPR reactor internals represent a first-of-a-kind design in size, arrangement, and operating conditions. Therefore, AREVA NP has classified the RV internals as "prototype" consistent with Reference 1.

Based on its "prototype" classification, a comprehensive vibration assessment program in conformance with Reference 1, which consists of three sub-programs, vibration and stress analysis program, vibration and stress measurement program, and inspection program, is established for the U.S. EPR and is discussed in this document.

The vibration assessments of the re-circulating steam generator (RSG) upper internals and the piping systems attached to the RSG, as well as the other reactor coolant system (RCS) piping systems, are provided in Appendix A and Appendix B. The vibration assessment of the RSG tube bundle is provided in Appendix C. The flow-induced vibration analysis of the RSG tube bundle is performed using the guidance of the 2004 ASME Boiler and Pressure Vessel (B&PV) Code, Section III, Appendix N-1300 [Reference 9(a)].

## **2.0 DESCRIPTION AND CLASSIFICATION OF THE U.S. EPR REACTOR INTERNALS**

### **2.1 General Arrangement**

The general arrangement of the U.S. EPR reactor vessel is shown in Figure 2-1. The RV internal structures contain two main assemblies, which are the lower internals and upper internals.

#### **2.1.1 Lower Internals**

The lower internals consist of the:

- Core barrel (CB) flange.
- CB cylinder.
- Irradiation specimen baskets.
- Lower support plate (LSP).
- Radial key inserts.
- Flow distribution device.
- Heavy reflector.

Further information on each of these components is provided in the following sections.

##### Core Barrel Flange

The core barrel outer diameter is machined to customize the fit up between the mating RV flanges. The core barrel transmits core and lower internal loads to the RV. The core barrel outer diameter is customized to the corresponding RV dimension in order to control the radial gap between the flanges. The radial gap controls lateral displacements in normal and faulted conditions.

##### Core Barrel Cylinder

The core barrel cylinder is composed of two cylindrical shells welded together. The upper section of the barrel comprises four integrated outlet nozzles located opposite the RV outlet nozzles. The core barrel cylinder provides the passageway for the reactor coolant from the core to the RV outlet nozzles. The external radius of the barrel nozzle is customized to the RV corresponding radius in order to control the radial gap, which restricts the bypass flow between the RV inlet and outlet nozzles.

##### Irradiation Specimen Baskets

Irradiation specimen baskets are attached to the outside of the core barrel lower shell at locations where the irradiation neutron flux is higher. The irradiation specimen baskets support, hold, protect, and guide the irradiation capsules to ensure adequate cooling of the capsules.

## LSP

The LSP is welded to the core barrel lower shell. The top face of the LSP supports and restrains the fuel assemblies (FAs) and the heavy reflector. The top face is equipped with fuel alignment pins (lower fuel alignment pins) at each FA location, which position, align, and restrain the FAs. The top face also contains heavy reflector positioning blocks that verify the proper gap between the heavy reflector and the core barrel. The bottom face of the LSP supports the flow distribution device and contains inlet holes under each FA location. A diaphragm at the base of each of the inlet holes homogenizes the flow rates at the FA inlets.

## Radial Key Inserts

The lower internals are positioned horizontally, with respect to the RV, by radial support keys and grooves machined in the LSP. The radial support keys are welded to and integral with the RV. Some of the radial support keys and corresponding LSP grooves provide circumferential centering. These keys and LSP grooves have radial key inserts to maintain tight lateral clearances. The radial key inserts are pinned and bolted in the LSP grooves.

The radial keys also provide a secondary support function by limiting the consequences of a postulated failure of the lower internals. The energy absorbed by the radial keys during a postulated failure is limited by the controlled vertical gaps.

## Flow Distribution Device

The flow distribution device is located below and attached to the LSP and is composed of a distribution plate and support columns. The flow distribution device provides a homogeneous flow distribution between the LSP holes.

## Heavy Reflector

The heavy reflector is located inside the CB between the core and the CB shells. The heavy reflector increases neutron efficiency due to its neutron reflective properties, protects the RV from radiation-induced embrittlement, improves the long-term mechanical behavior of the lower internals, and provides lateral support to maintain the geometry of the core. To avoid any welded or bolted connections close to the core, the heavy reflector consists of stacked slabs positioned one above the other. The heavy reflector rests on the LSP, but does not contact the upper core plate (UCP). The internal contour of the slabs conforms to the core and the external contour is cylindrical. The top slab is fitted with alignment pins that extend through the UCP to ensure proper alignment.

Because the heavy reflector is located between the core and the core barrel, the reflector limits the core bypass flow at the core periphery. The heavy reflector also provides lateral support to the core and contributes to the decrease of neutron fluence on the RV core shell.

## 2.1.2 Upper Internals

The upper internals consist of the:

- Upper support assembly (including the flange, shell, and the upper support plate (USP)).
- UCP.
- Control rod guide assemblies (CRGA).
- Columns.

### Upper Support Assembly

The upper support assembly is comprised of a circular skirt with an integrated flange and the USP. The skirt flange is welded to the USP. The upper support assembly flange is part of the internals hold-down stack in the RV and rests on the hold-down spring, which rests on the core barrel flange, which in turn is supported on the ledge machined in the RV flange. The upper internals flange is held in place and preloaded by the RV closure head flange. The outer diameter of the flange is customized to the corresponding vessel dimension in order to control the radial gap between the flanges. The radial gap controls lateral displacements in normal and faulted conditions.

### UCP

The UCP, which contains holes located opposite the FAs for core coolant outlet flow, encloses the top of the core cavity and is attached to the USP via columns. The UCP is designed to equilibrate the outlet flow from the core. The UCP contains fuel alignment pins at each FA location that position, align, and restrain the FAs.

### CRGA

The control rod guide tube assemblies provide a straight, low-friction channel to insert, withdraw, and drop the control rod drive mechanism (CRDM) drive shafts and the attached rod control cluster assembly (RCCA). The guide tube assemblies consist of a series of support plates held in place with tie rods and are located inside the housings of the support columns. The housings are attached to the top of the USP and the columns are attached to the bottom of the USP. The columns are also attached to the UCP. The housings and columns also protect the RCCAs from static and dynamic-type hydraulic loads and other mechanical loads.

### Columns

The columns attach the USP to the UCP and transmit the vertical forces to the RV closure head. The following is a description of the types of columns bolted to the bottom of the USP.

- The [ ] CRGA columns, which are located above the FAs that are equipped with RCCAs, serve as housings for the CRGAs. These columns also support the instrument guide tubes for the in-core instrumentation lances when the lances penetrate the upper plenum.

- The [ ] level monitoring probe (LMP) columns are located around the edge of the USP and protect the LMPs in the upper plenum.
- The [ ] normal edge columns provide support at the USP edge, including when the upper internals are removed to the refueling cavity storage stand.

### 2.1.3 Interface Cold Gaps

The design of the RV internals requires interface cold gaps between the internals and the RV and between the main parts of the internals. These cold gaps are:

- Functional cold gaps that are relative to the alignments of the equipment and to the limitation of core bypass flows under normal and upset operating conditions.
- Controlled cold gaps which are implemented to improve the vibratory behavior under normal, faulted, and beyond design conditions.

The cold gaps perform the following functions:

- Allow free withdrawal of the internals from the vessel in cold conditions.
- Avoid interference between components during temperature elevation transients (thermal inertia is higher for the vessel than for the internals).
- Limit RV internals to RV relative displacement during normal and faulted conditions.
- Allow for required bypass flows.

Further information on the cold gaps is provided in the following sections.

#### Functional Cold Gaps

The alignment components for the RV internal parts contain functional cold gaps. To reduce the outlet nozzle gap as much as possible, the diameter on the core barrel outlet nozzle is machined to customize its fit up with RV outlet nozzle. Reducing the outlet nozzle gap reduces the bypass flow at full power conditions. The gap between the heavy reflector and the CB (i.e., annulus thickness) allows a flow velocity in accordance with the needed cooling of the heavy reflector.

#### Controlled Cold Gaps

The controlled cold gaps for the RV internals are:

- To reduce the relative displacements between the top of the internals and the RV, the diameters of the CB flange and the upper support assembly flange are customized to the RV flange ledge.
- A lip on the heavy reflector bottom fits in a ledge machined in the LSP. The reduced radial gap between the ledge and the lip prevents sliding of the heavy reflector.
- The diameter of the UCP is customized to the corresponding inner diameter of the CB shell, with the gap between the UCP and the shell controlled to reduce possible lateral displacement.

- The radial keys include keys with and without lateral adjustments. The radial gap at the key ends and the vertical gap between the keys and the LSP are limited. The radial gaps limit the relative displacement between the LSP and the RV.

## 2.2 Flow Paths through the RV

The internals of the U.S. EPR reactor vessel channel the main coolant flow within the RV from the inlet nozzles to the outlet nozzles, via the core cavity (See Figure 2-6). Reactor coolant from the cold legs enters the RV through the inlet nozzles and flows into the downcomer, which is the annulus formed by the space between the CB and the RV inner wall. The flow then enters the lower plenum at the bottom of the RV below the flow distribution device (FDD), which is attached to the LSP. The flow then enters the FDD and is directed through the LSP and into the core region. After leaving the core, the heated reactor coolant passes through the UCP and enters the upper plenum, which is enclosed by the UCP, the core barrel, and the USP. The flow then goes through and around the columns attaching the UCP and USP to reach the RV outlet nozzles.

A part of the main flow through the RV does not participate in fuel rod cooling and is called core bypass flow. The total core bypass flow is divided as described below:

### Bypass Flow for RV Upper Dome

A portion of the bypass flow cools the RV upper dome, which is the area above the USP. The flow passes through the RV dome spray nozzles installed on the circumference of the CB and the USP flanges. The spray nozzles direct flow from the downcomer annulus to the upper dome. The flow is then directed from the upper dome to the upper plenum via the Control Rod Guide Tubes (CRGTs) and other orifices of the USP (aeroball tubes, instrument lances, etc.).

### Bypass flow for Heavy Reflector

Another portion of the bypass flow cools the heavy reflector slabs. This bypass flow is directed through cooling channels located in the slabs, the gap between the core and the slabs, and the gap between the CB and the slabs.

### Bypass Flow through Core Guide Thimbles

Bypass flow through the core guide thimbles cools the instrumentation and absorber rods guide tubes.

### Bypass From the RCS Inlet to Outlet Loop Nozzles

A small portion of the bypass flows goes from the downcomer annulus through the gap between the CB outlet nozzles and the RV outlet nozzles. This flow serves no function and is minimized by controlling the radial gap between the external radius of the CB outlet nozzle and the corresponding inner radius of the RV outlet nozzle.

### 2.3 Evolution of the U.S. EPR Reactor Vessel Internals

The features of the U.S. EPR RV internals are derived from international experience with the AREVA N4 units operating in France and the Siemens Konvoi designs operating in Germany. The U.S. EPR RV internals have the same design as the AREVA N4 units except for the scale, the CB, the CB flange, the design of the hold down spring, the upper internals support assembly, and the RV.

The U.S. EPR RV lower internals reflect the following evolutions from the N4 design:

- The flow cross section in the downcomer between the RV and the CB is increased.
- The number and shape of the lower radial supports at the bottom of the downcomer are modified.
- The incore instrumentation mounted in the RV lower head are replaced by a flow distribution device fastened under the LSP.
- The baffle assembly is replaced by the heavy reflector.

The CRGAs are derived from the Konvoi design, adapted to a [ ] fuel bundle configuration. The skeleton type CRGAs fit into support columns for protection from the flow conditions in the upper plenum. The design of the support columns of the upper internals of the U.S. EPR are similar to those in the Siemens Konvoi plants and have reliable operating experience. The top-mounted in-core instrumentation is also derived from the German Konvoi units. Nevertheless, this operating experience is not completely applicable to the U.S. EPR design because of the adaptation to the [ ] fuel bundle configuration and the distribution of the support columns in the upper plenum.

The international experience of these operating pressurized water reactor (PWR) designs shows that the RV internals vibrations can be induced by:

- The flow turbulences.
- Fluid-structure interactions (e.g., vortex shedding).
- Acoustic sources such as the main coolant pumps (rotation frequency, blade passing frequency) could also theoretically induce vibrations of the RV internals.

However, no problems due to other acoustic sources have been reported for these PWR units. The vibration of the lower internals is mainly due to flow turbulences in the downcomer that induce random low-frequency excitation (typically from 0 to 30 Hz) because the spectral density of the pressure fluctuations decreases rapidly when frequency increases. No fundamental changes in the sources of excitation or the structural response are expected for the U.S. EPR. However, the design changes that have been introduced through the evolution of the U.S. EPR can have a unique influence on the response of the lower internals. The changes to the design of the U.S. EPR that will have the most significant influence on the flow-induced vibration (FIV) response of the lower internals include:

- The larger cross section in the downcomer.

- The weight of the heavy reflector, which can influence the natural frequencies and the damping, and therefore the response of the lower internals.
- The lower radial CB supports, which can influence the excitation characteristics.
- The FDD.

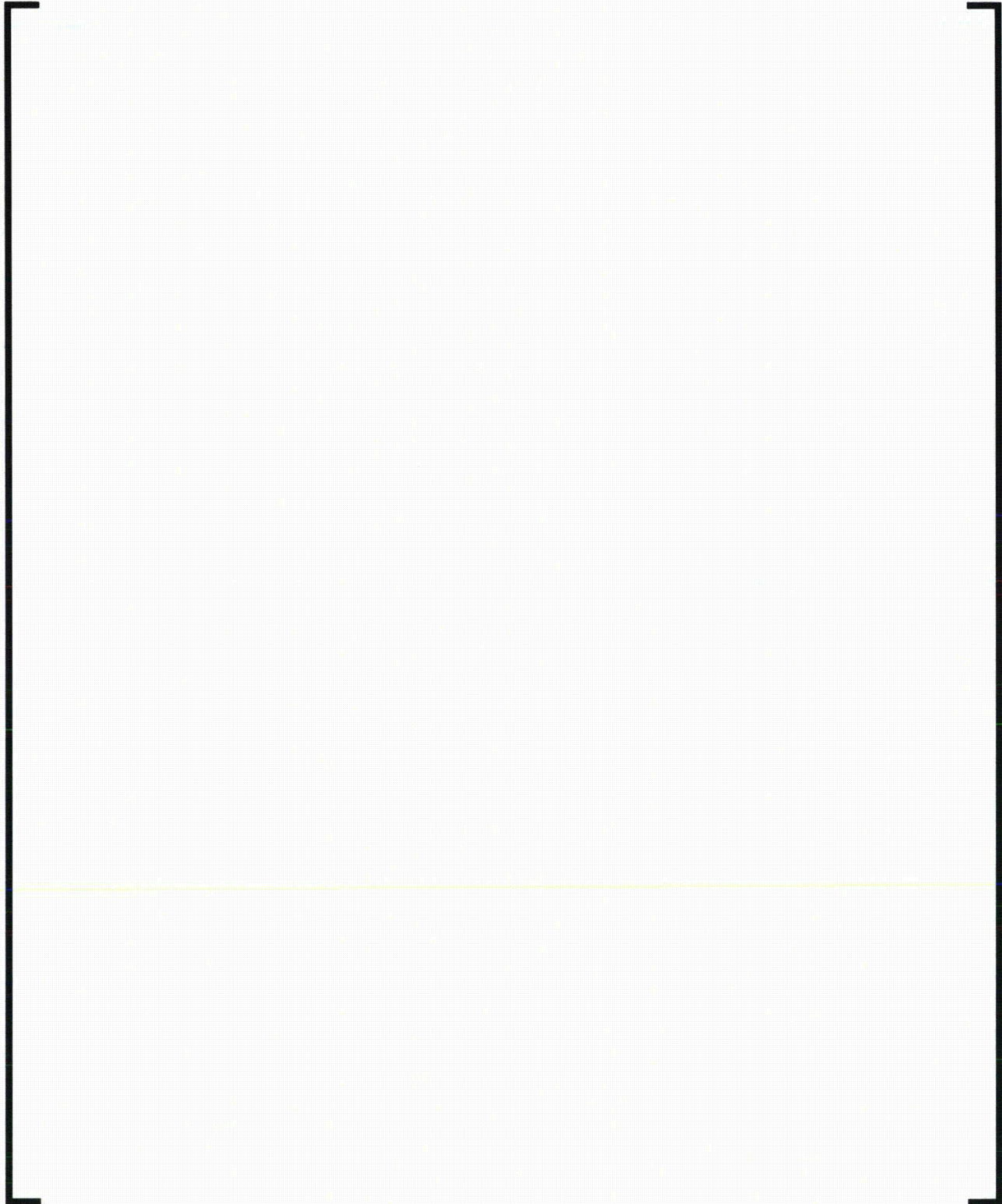
Regarding the upper internals, and more particularly the columns network in the upper plenum, phenomena like vortex shedding or fluid elastic instability are potential sources of strong vibrations.

## **2.4 Classification of Reactor Internals in Accordance with Regulatory Guide 1.20**

RG 1.20 (Reference 1) provides regulatory guidance for a comprehensive vibration assessment program to verify the structural integrity of reactor internals for FIVs prior to commercial operation. The extent of the verification measures recommended by Reference 1 for the comprehensive vibration assessment program depends upon the classification of the RV internals (prototype, non-prototype, etc.).

The design of the U.S. EPR RV internals is derived from French N4 and German Konvoi designs. However, the U.S. EPR RV internals include new features that could introduce some changes in the vibratory behavior compared to the reference units. The U.S. EPR reactor internals represent a first-of-a-kind design in size, arrangement, and operating conditions. Therefore, AREVA NP has classified the RV internals as "prototype" consistent with Reference 1.

**Figure 2-1—General Arrangement of the U.S. EPR RV Internals**



---

**Figure 2-2—U.S. EPR RV Lower Internals**

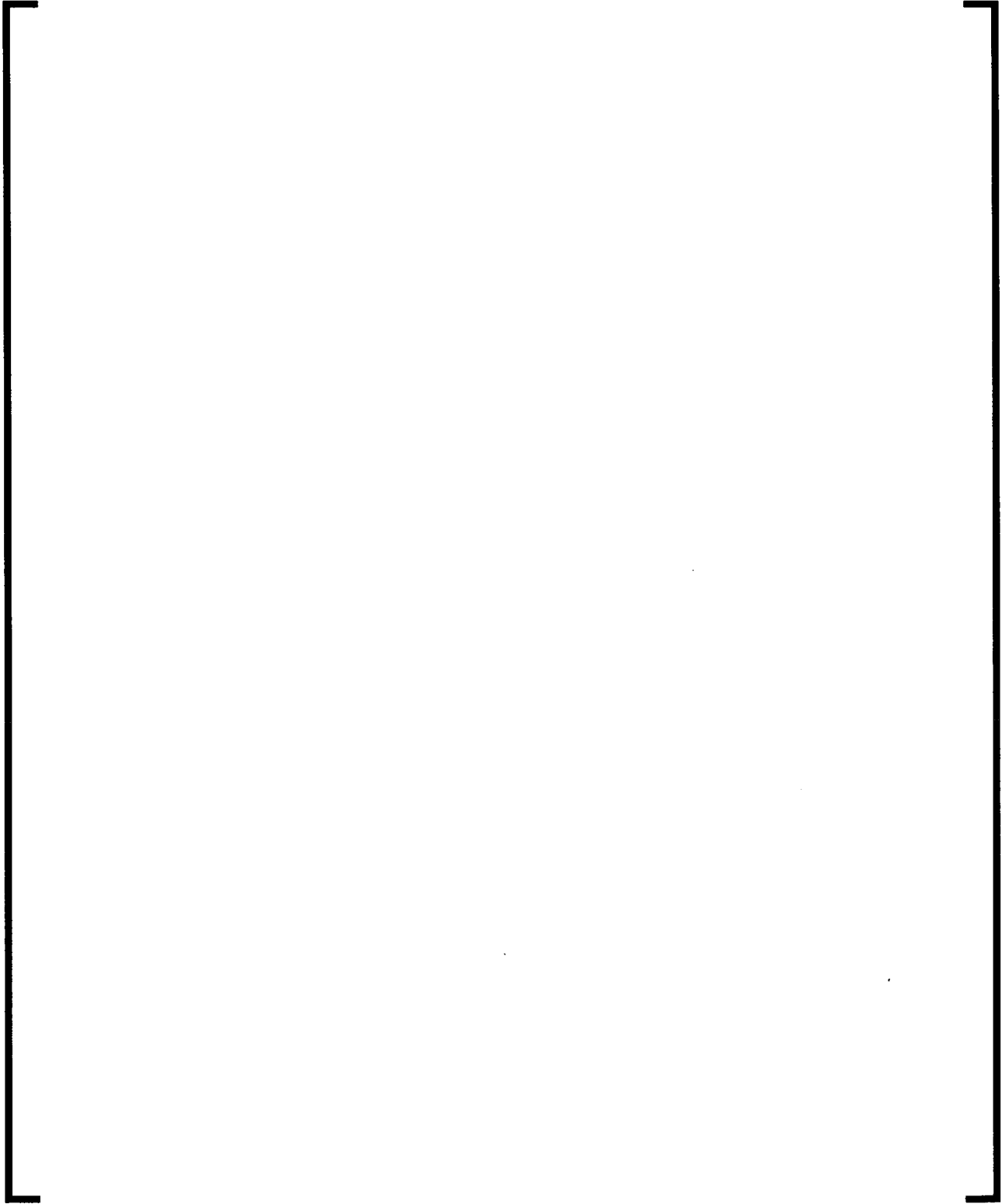


**Figure 2-3—U.S. EPR RV Heavy Reflector**

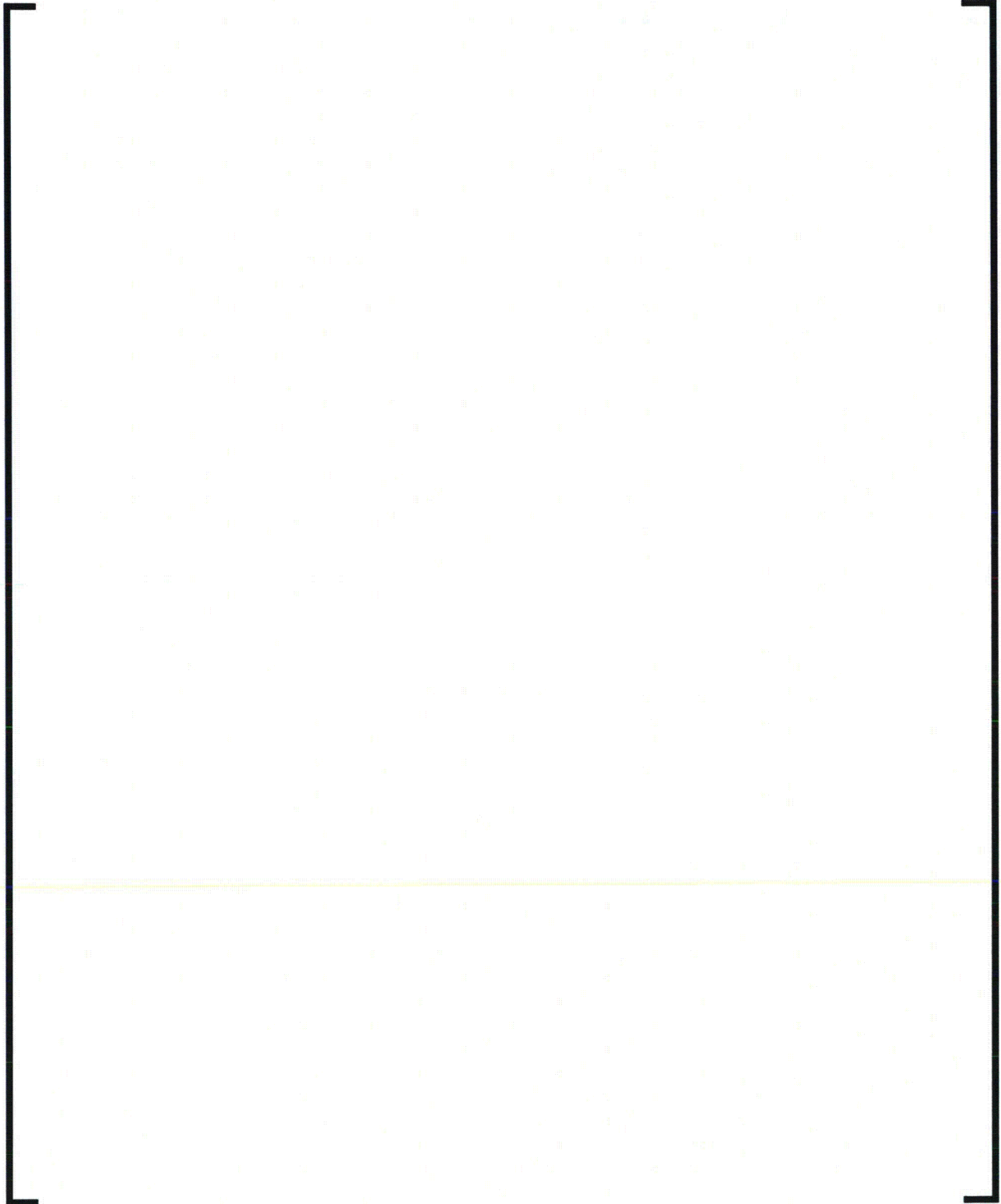
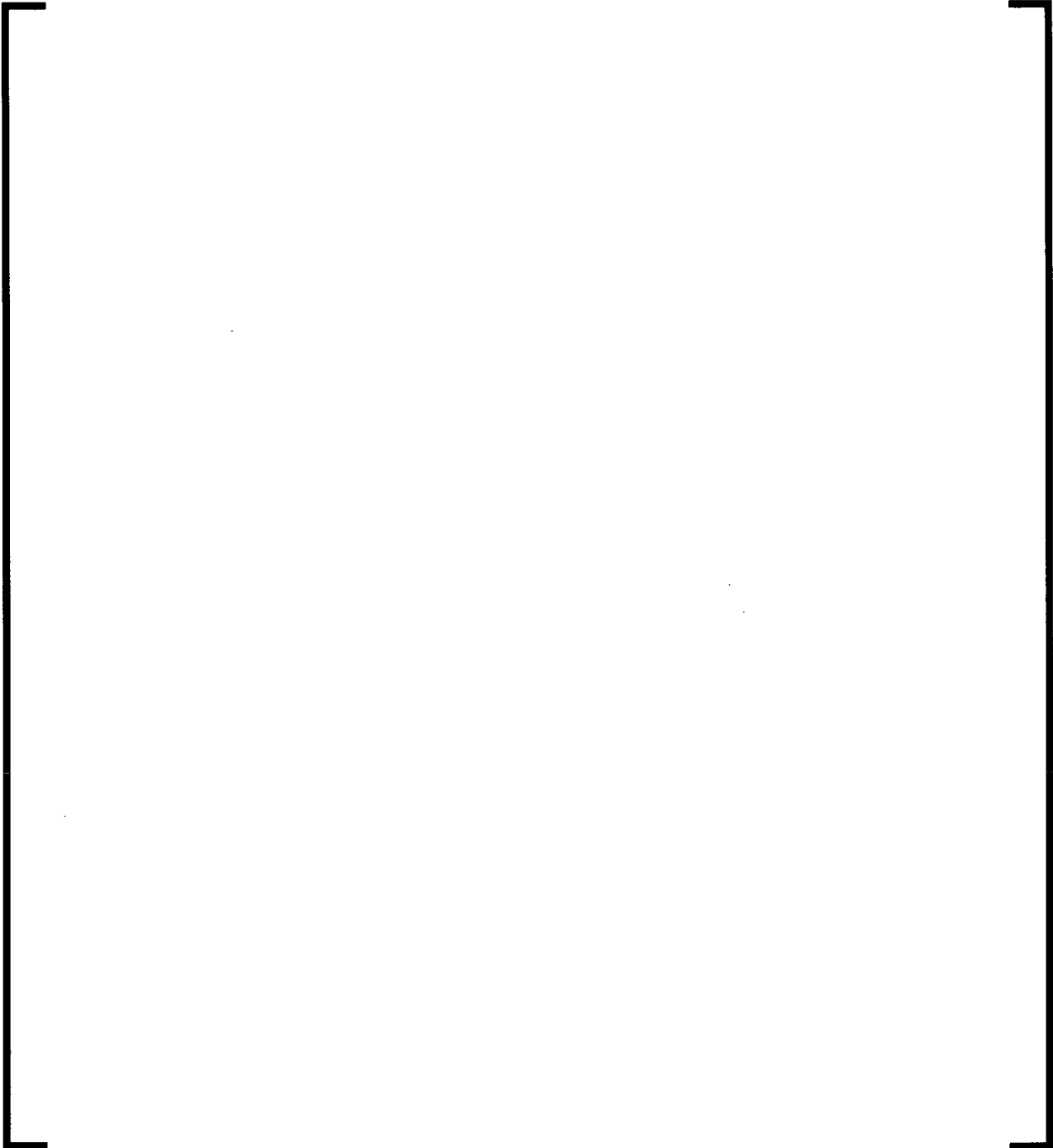


**Figure 2-4—U.S. EPR RV Upper Internals**

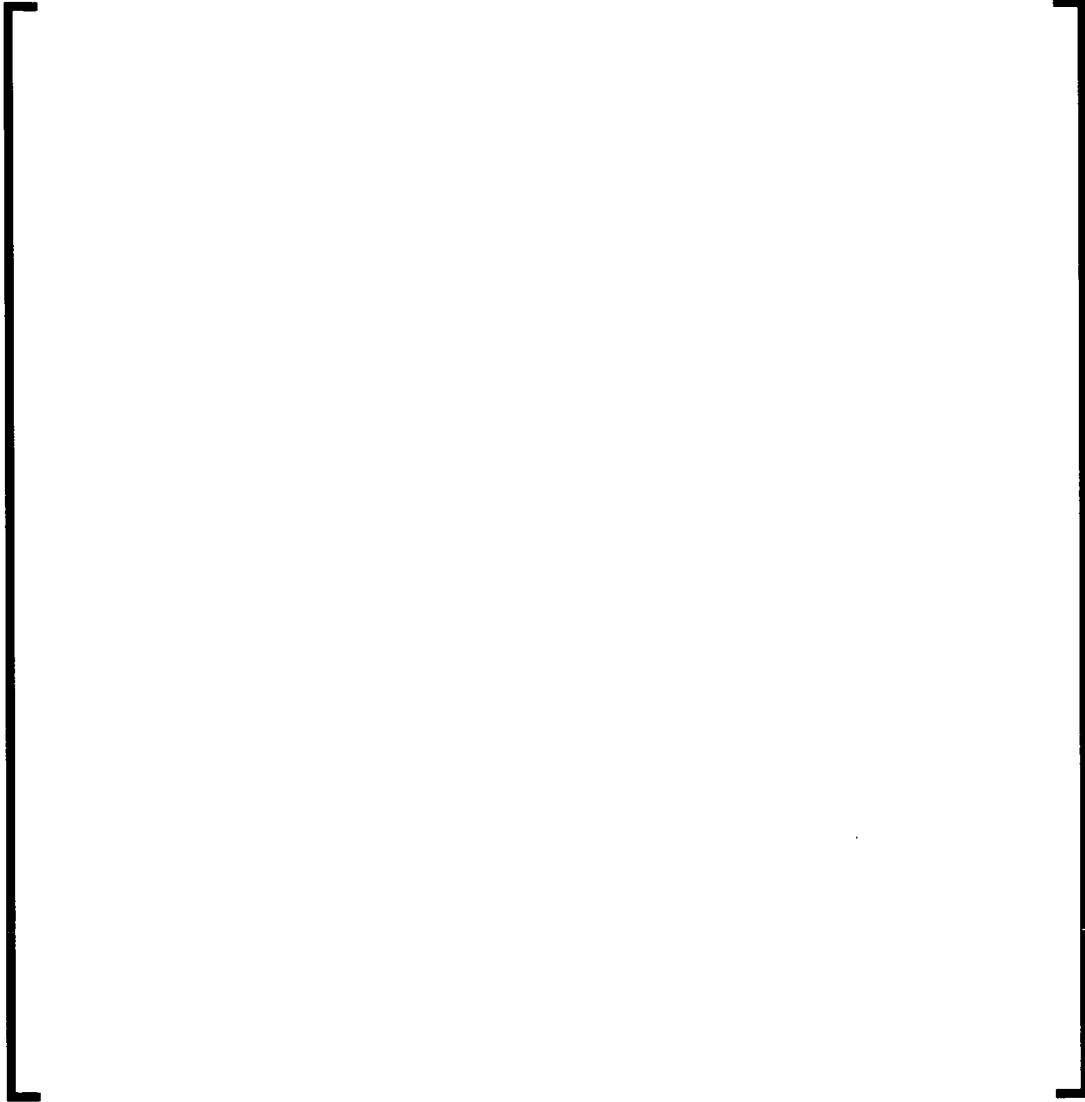


---

**Figure 2-5—U.S. EPR RV Upper Internals**



**Figure 2-6—Flow Paths within the Reactor Vessel**



### **3.0 COMPREHENSIVE VIBRATION ASSESSMENT PROGRAM**

As recommended by Reference 1, the U.S. EPR Comprehensive Vibration Assessment Program comprises three sub-programs. Consistent with the guidance of Reference 1 for the prototype classification of the U.S. EPR RV internals, the program includes:

- Vibration and stress analysis program.
- Vibration and stress measurement program.
- Inspection program.

Figure 3-1 presents the sub-programs and their sequences.

The vibration and stress analysis program is based on theoretical and experimental analysis and aims to predict the natural frequencies, the mode shapes, and the structural response of the reactor internals.

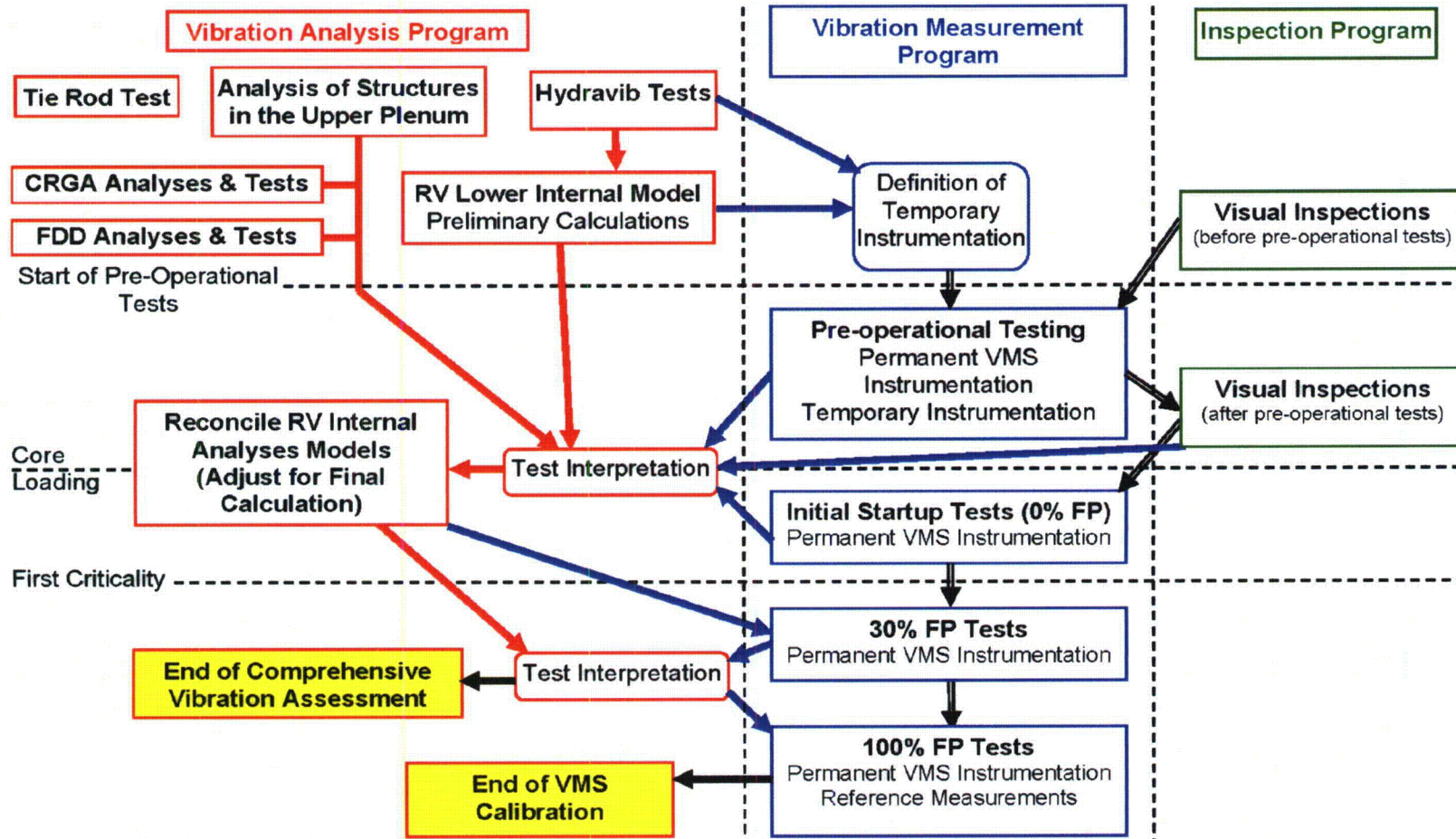
The vibration and stress measurement program consists of field measurements with temporary instrumentation during the pre-operational and/or initial startup testing. The vibration and stress measurement program verifies the structural integrity of the reactor internals, determines the margin of safety for steady state and anticipated transient conditions, and confirms the vibration analysis. If discrepancies are identified during the pre-operational testing between the vibration analyses and the measurement programs, a reconciliation of the analysis program will be made and the final comprehensive vibration assessment report for the U.S. EPR RV internals will demonstrate agreement between the analysis and the measurements.

The inspection program consists of the inspections of the RV and the RV internals before and after the pre-operational testing. The RV internals will be removed from the RV for these visual inspections, which will confirm that the vibratory behavior of the RV internals is acceptable.

The U.S. EPR RCS is equipped with permanent instrumentation, the vibration monitoring system (VMS), which includes displacement sensors installed on the RV head and excore instrumentation that provide continuous monitoring of the vibrations during full power operation. The VMS is calibrated during pre-operational testing using the temporary instrumentation of the RV internals and also during the initial startup testing after fuel is loaded in the fuel bundle.

The vibration analysis program, the vibration measurement program, and the inspection program are detailed in the following sections.

Figure 3-1—Comprehensive Vibration Assessment Program, including VMS Calibration



## **4.0 VIBRATION AND STRESS ANALYSIS PROGRAM**

### **4.1 General**

The objective of the vibration and stress analysis program for the U.S. EPR is to make a preliminary assessment of the vibrations of the RV internals through tests and theoretical analyses of scaled (reduced-scale) configurations. The methods and design inputs obtained for the reduced-scale configuration are then extrapolated to the full scale reactor configuration to demonstrate the integrity of the RV lower internals for flow-induced vibrations. Taking into account the difficulties in performing tests in dynamic similitude, the structures in the upper plenum are studied through full scale testing and theoretical evaluations. As shown in Figure 3-1, the main part of the vibration analysis program occurs before the pre-operational testing.

A combination of experimental testing and theoretical analyses (both scaled and full) are performed for the following U.S. EPR RV internal components:

- RV lower internal assembly (CB, HR, LSP, FDD, etc) – Section 4.2.
- FDD – Section 4.3.
- Irradiation specimen basket – Section 4.4.
- RV upper internals (CRGA columns, normal columns, LMP columns, and the instrumentation guide tubes) – Section 4.5.
- CRGAs and RCCAs – Section 4.6.
- Heavy reflector tie rods – Section 4.7.

## **4.2 RV Lower Internal Assembly**

### **4.2.1 HYDRAVIB Scale Model Tests**

The HYDRAVIB tests have two main objectives. The first objective is to make a preliminary and direct assessment of the lower internals (CB + LSP + FDD + HR) vibrations induced by the flow turbulences in the downcomer and in the RV bottom head, and to identify other potential sources of flow-induced vibration phenomena like vortex shedding (discrete frequency).

The second objective is to provide detailed input data for the construction and the validation of the overall finite element model (FEM) of the RV internals, which includes a characterization of the forcing function in the downcomer.

The HYDRAVIB mock-up represents at scale (1 / 8.168 or 1/8 scale) the lower internal structures consisting of the CB, LSP, FDD, HR, hold-down spring, irradiation capsule baskets, the RV inside, including the RV inlet nozzle, and the actual shape of the radial keys (See Figure 4-1). An equivalent device, representative in terms of stiffness and the first natural frequency, simulates the upper internals. The HYDRAVIB tests are performed in cold water and in hydro-elastic similitude.

The following locations of potential interference resulting in the non-linear interaction with the interfacing structures of the lower internal assembly are simulated with the HYDRAVIB mock-up:

- UCP/UCP guide pins.
- LSP/radial keys.
- CB outlet nozzles/correspondent RV surfaces.

Four pipes (See Figure 4-2), which represent the cold legs, including the elbow at the RV inlet at scale, feed the mock-up. Four additional pipes simulate the hot legs at scale. Four pumps (one per loop) generate the required flow rate, allowing a flow velocity at the RV inlet up to 116 percent of the nominal flow rate. Acoustic dampers are implemented to avoid parasitic excitations due to the pumps.

#### **4.2.1.1 Test program**

The test program is developed in four phases:

- Stiffness measurements.
- Modal characterizations in air.
- Modal characterizations in still water.
- Flow tests.

The first three phases of the test program are essential to the interpretation of the flow tests. The overall FEM is adjusted to accurately model the experimental test data.

The stiffness measurements (phase 1) are performed to characterize the boundary condition at the CB flange and the interaction of the structural components of the lower internals, considering the stiffness of the hold-down spring and the cantilever stiffness of the CB.

Modal characterizations (phases 2 and 3) are performed for the individual components (CB alone) and on assembled components (CB + HR). This allows a detailed analysis of the results, particularly for the fluid couplings between the CB and HR.

Flow tests (phase 4) are carried out with steady state flow velocities up to about 116 percent of the best estimate flow rate and several configurations of active loops (4/4, 3/4, 2/4 and 1/4).

#### 4.2.1.2 Instrumentation

For the first three phases, specific instrumentations, including force transducers, displacement sensors, and accelerometers, are used depending upon the objective of the tests. Figure 4-43 through Figure 4-49 provide the type and location of the instrumentation on each of the structural components of the HYDRAVIB mockup that are used for phase 1, 2, and 3 for testing. Figure 4-3 and Figure 4-4 provide the instrumentation that is used with the HYDRAVIB mockup for flow tests (phase 4). The types of instrumentations used for the testing include:

- Accelerometers sensitive in the radial direction in order to measure the vibration amplitudes (shell modes and beam modes).
- Accelerometers sensitive in the tangential direction in order to measure the vibration amplitudes (torsion modes and beam modes).
- Displacement sensors at the LSP level in order to measure the low frequency vibration amplitudes (beam modes) and quasi-static motions.
- Strain gauges on the FDD column in order to assess static and quasi-static motions acting on the FDD.
- Strain gauges on the CB just below the flange in order to measure the vibration amplitudes (beam modes) and quasi-static motions (low frequency motions).
- Dynamic pressure sensors distributed along the RV wall in the downcomer.

The type and specification for the sensors used with these tests are identified respectively in Table 4-28 and Table 4-29.

**Figure 4-1—HYDRAVIB Mock-up**

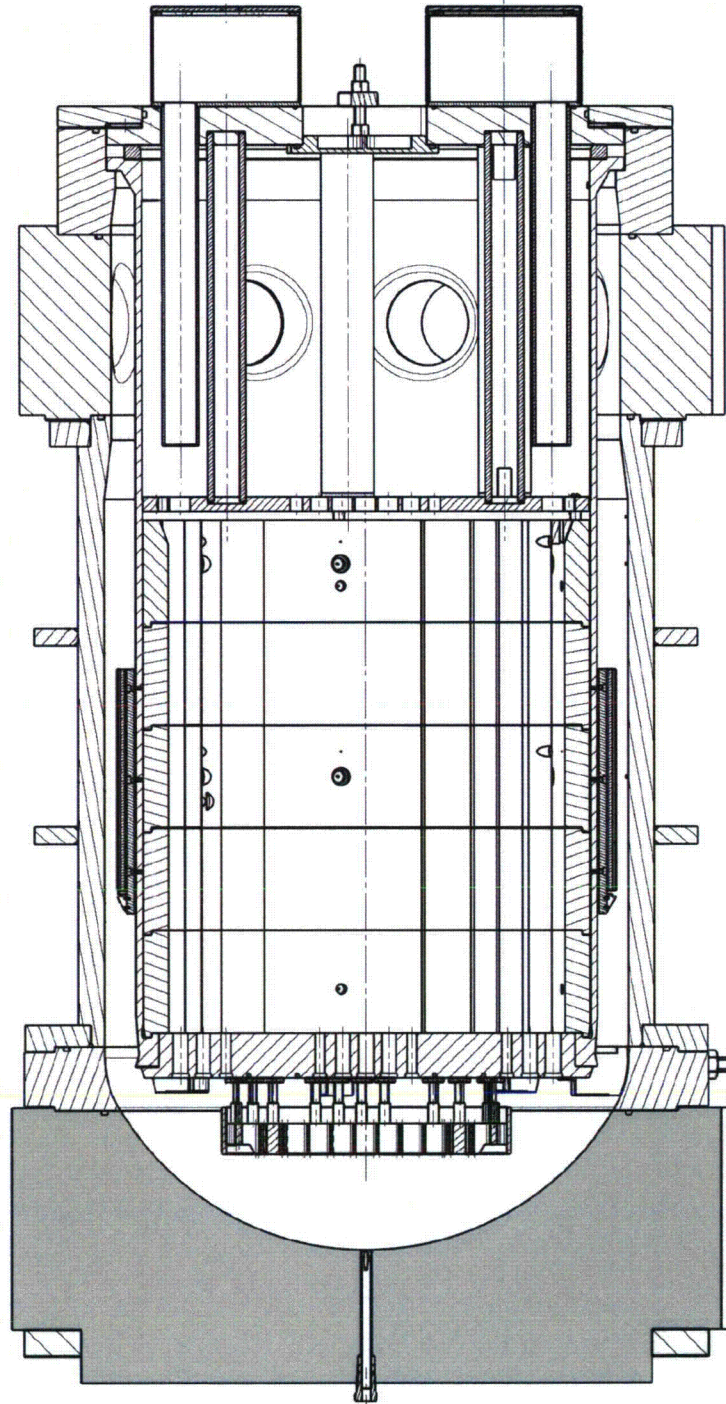
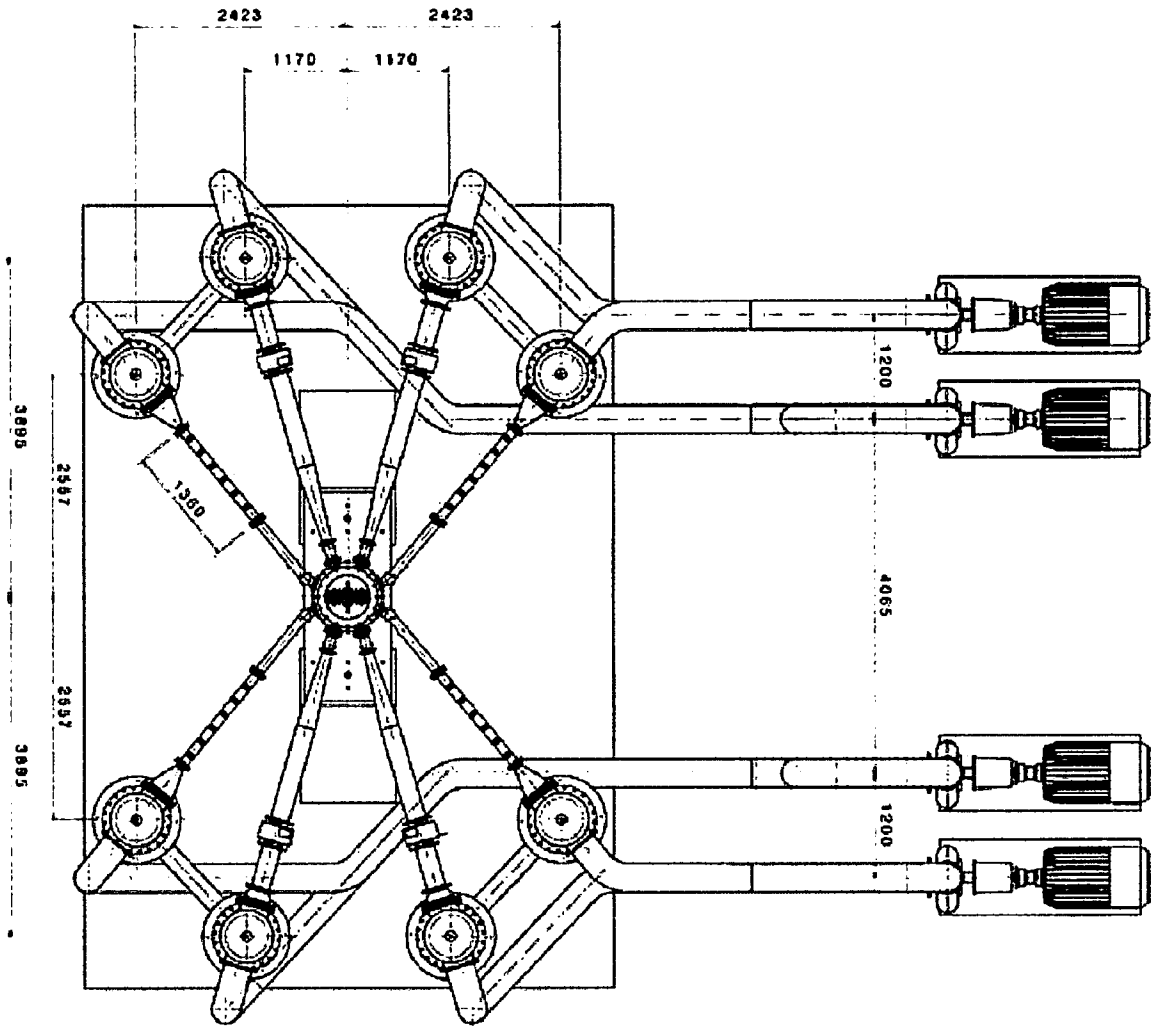
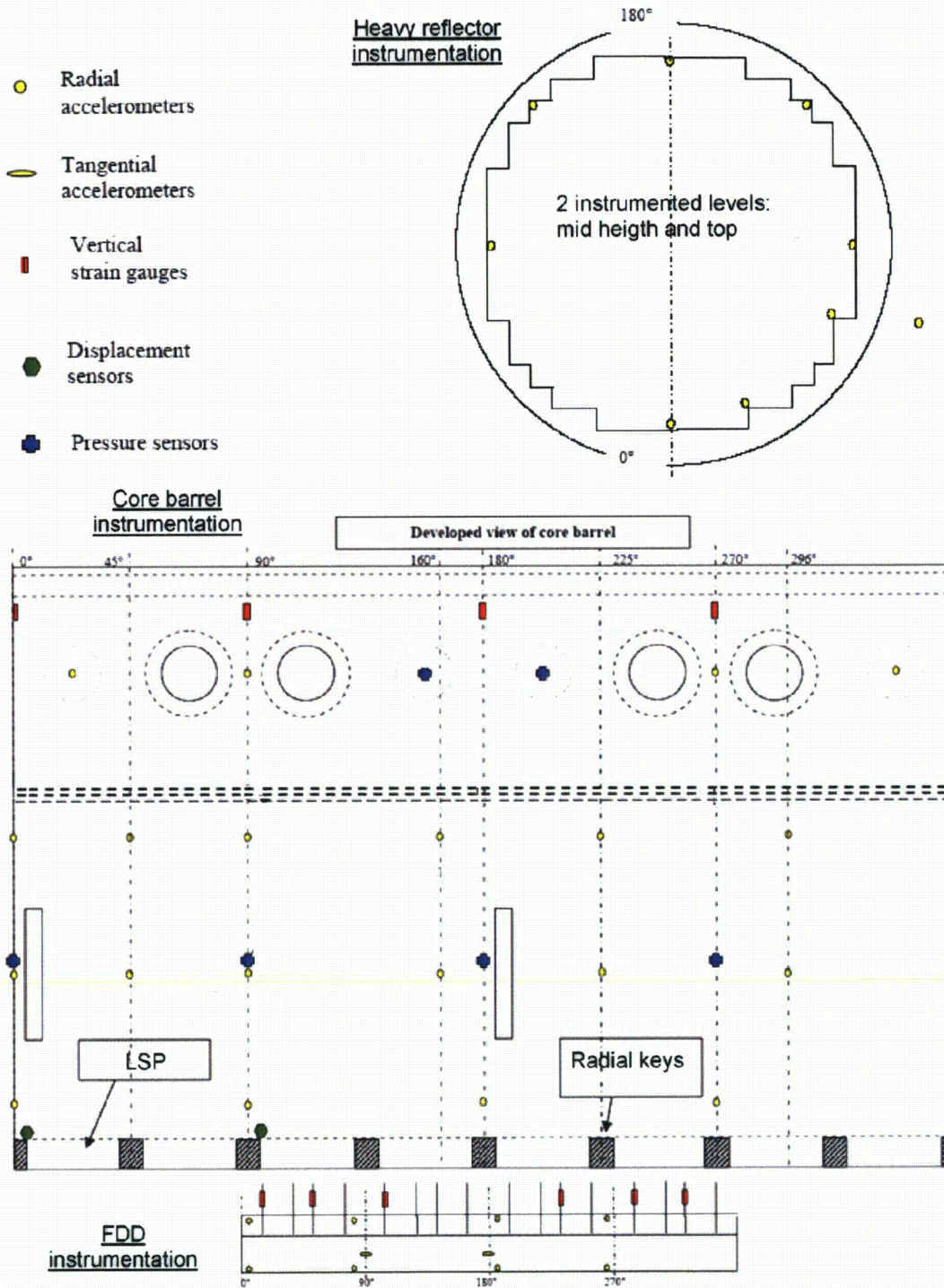


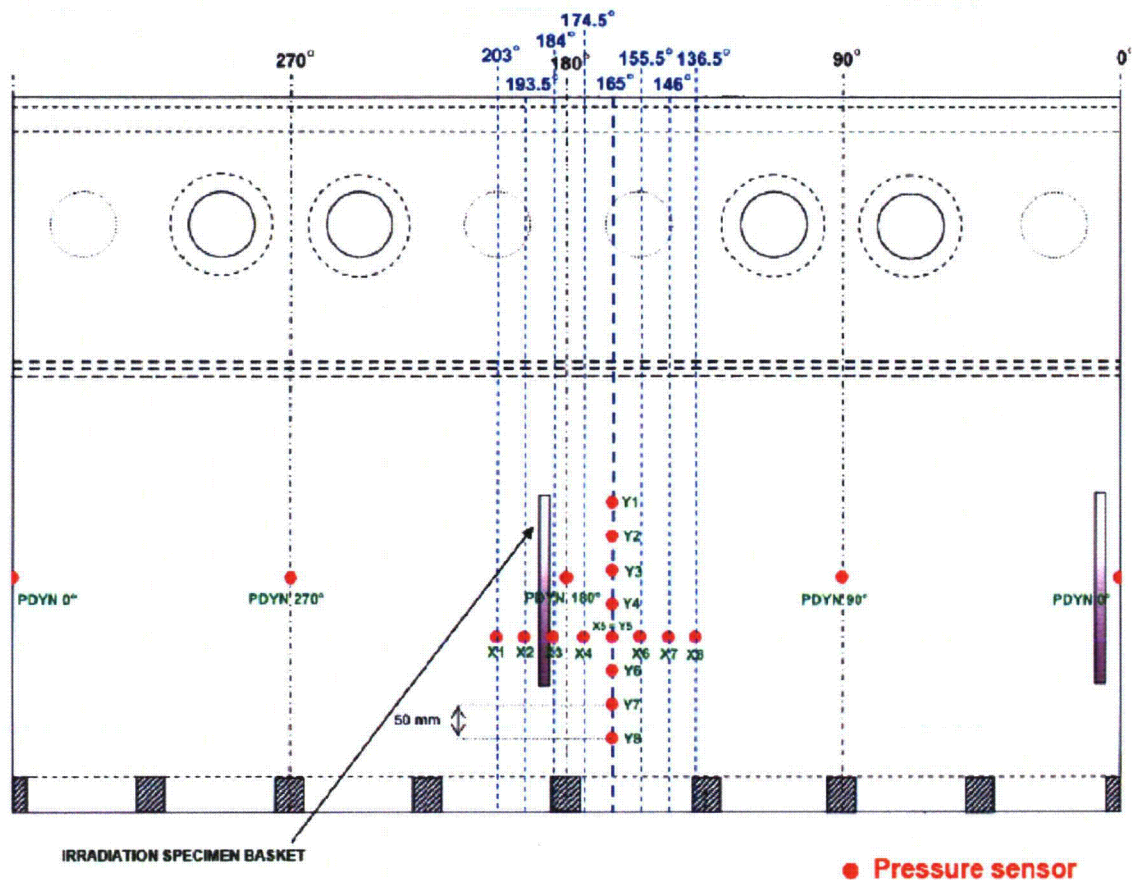
Figure 4-2—HYDRAVIB Test Loop



**Figure 4-3—HYDRAVIB Instrumentation for the Flow Tests**



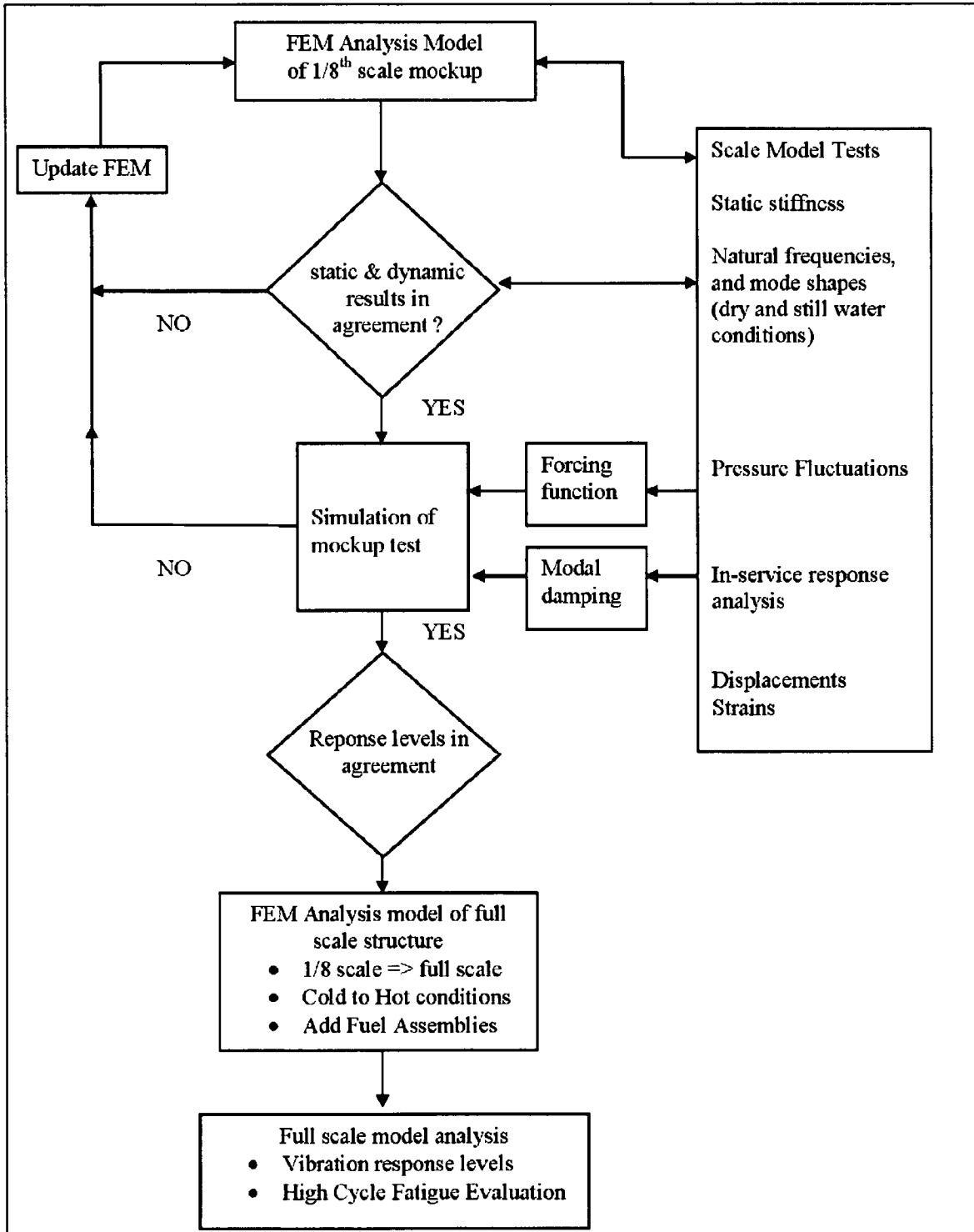
**Figure 4-4—HYDRAVIB Instrumentation – Implementation of Dynamic Pressure Sensors**



**4.2.2 Development of the 1/8 Scale Numerical Model**

The development of the scale model analysis of the HYDRAVIB mock-up is shown in Figure 4-5 which provides a flow chart outlining the method used to develop and validate the scale model. A three dimensional model of the RV and the RV internals is built using the finite elements code ANSYS. The validation of the methodologies applied to the scale model analysis is described in Section 4.2.3.2 and Section 4.2.4.

**Figure 4-5—Flow Chart for Scale Model Analysis**



#### 4.2.2.1 Structural Model

The structural model of the RV lower internals includes the CB, the LSP, the HR, the FDD, and the FAs. The CB shell is modeled with plate elements and the HR is modeled with solid elements. The FAs are included in the model as a unique, equivalent beam representing the FAs. The RV lower internal assembly is restrained at the elevation of the CB flange.

The LSP is significantly stiffer than the other components of the lower internals and is not modeled in detail. Rather, the LSP is modeled as a series of solid elements with the density of the elements corrected to account for the flow holes. The elastic modulus of the LSP is scaled to obtain the same bending mode frequency as that obtained on a more detailed, local model.

The FDD is comparatively lighter and more flexible than the LSP and is included as a non-structural lumped mass located on the CB axis at the elevation that corresponds to the center of gravity for the FDD. It is connected to the LSP with force/moment distributing equations.

#### 4.2.2.2 Fluid-Structure Coupling

The width of the RV downcomer is relatively small compared to its mean diameter. Consequently, the confinement effects of the fluid can be significant relative to the dynamics of the internals. This fluid domain is modeled in detail in the global FEM using a series of brick-shaped fluid elements along the height of the downcomer.

The water annulus between the HR and the CB is thin so that the confinement effects of the fluid will play a prominent role for the modes involving relative motion of the HR and CB. Similar to the RV downcomer annulus, the HR/CB annulus is introduced as a layer of brick-shaped fluid elements.

For the cases where the FAs are not included in the model, the effects of the hydrodynamic mass of the fluid contained by the boundaries of the HR simply acts as a non-structural, added mass. This hydrodynamic mass is added as a series of lumped masses on the vertical axis of the CB. Each mass is laterally connected to the HR (or CB shell, depending on the elevation) using force distributing equations, strictly adding no stiffness to the system.

Vertically, the added mass effect of the fluid entrained in the LSP is estimated by [

] which leads to the following formula:

$$[ \quad ]$$

Where:



**Figure 4-6—FEM of Core Barrel**

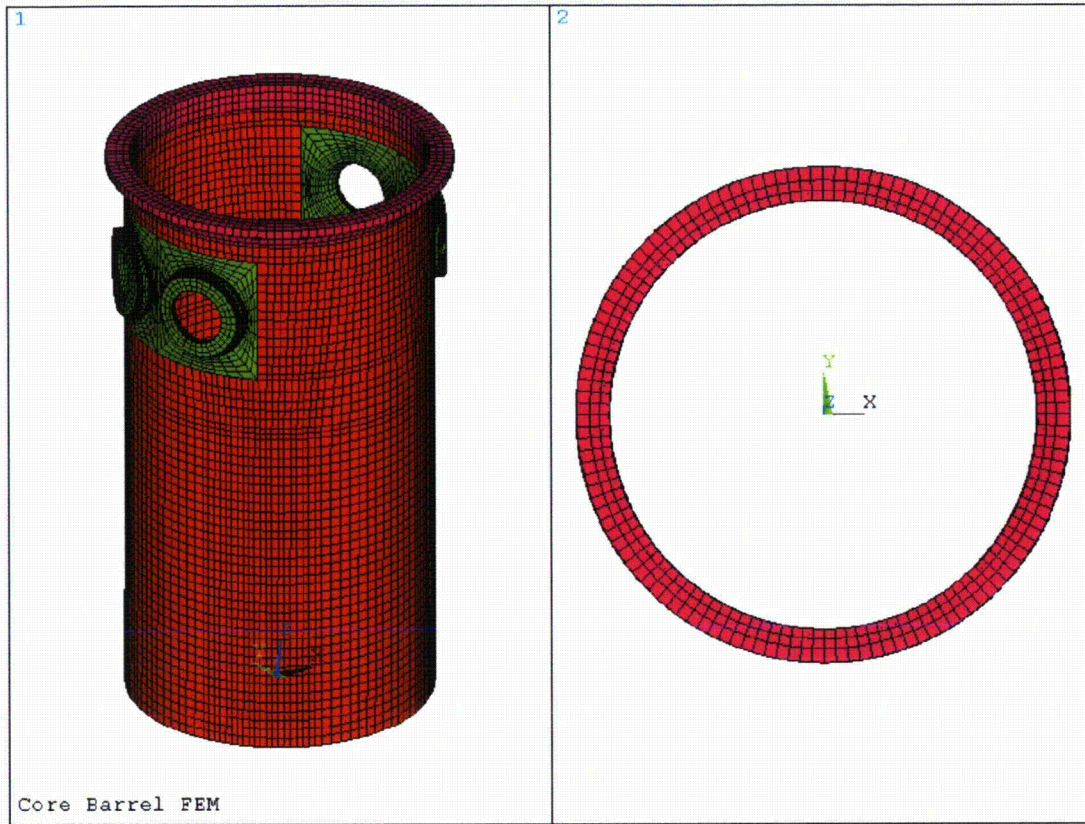


**Figure 4-7—FEM of Lower Support Plate and Flow Distributing Device**

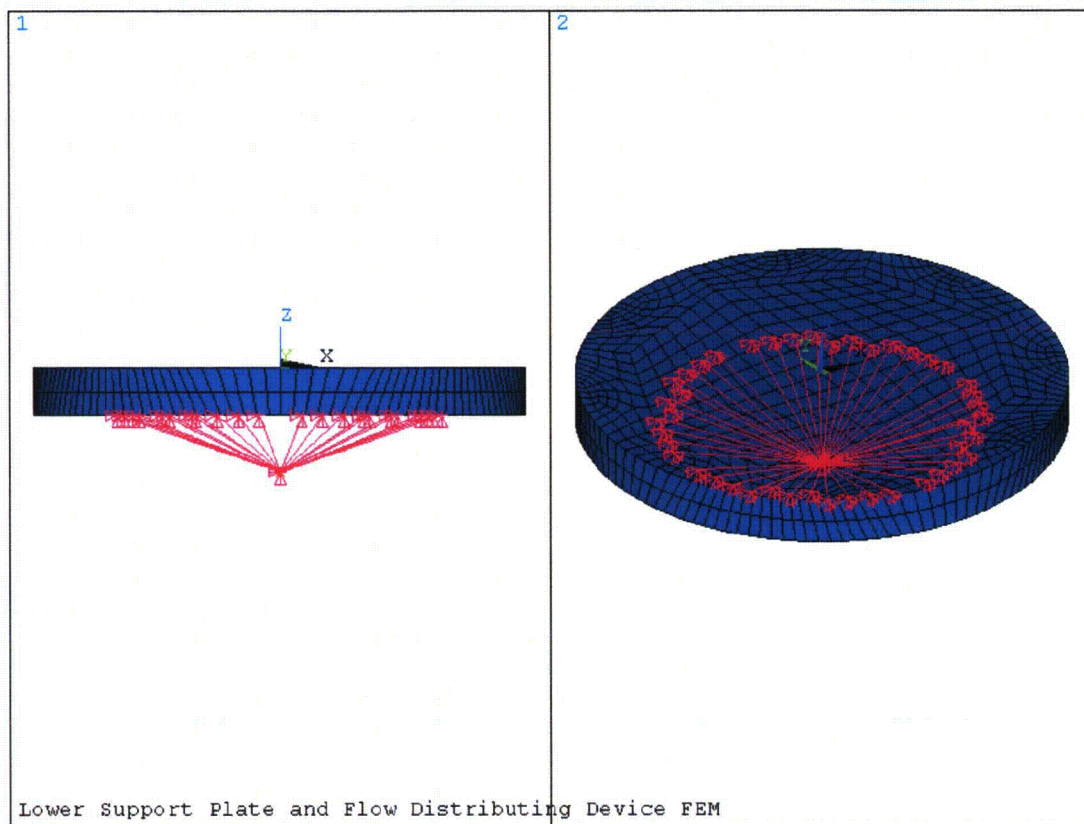
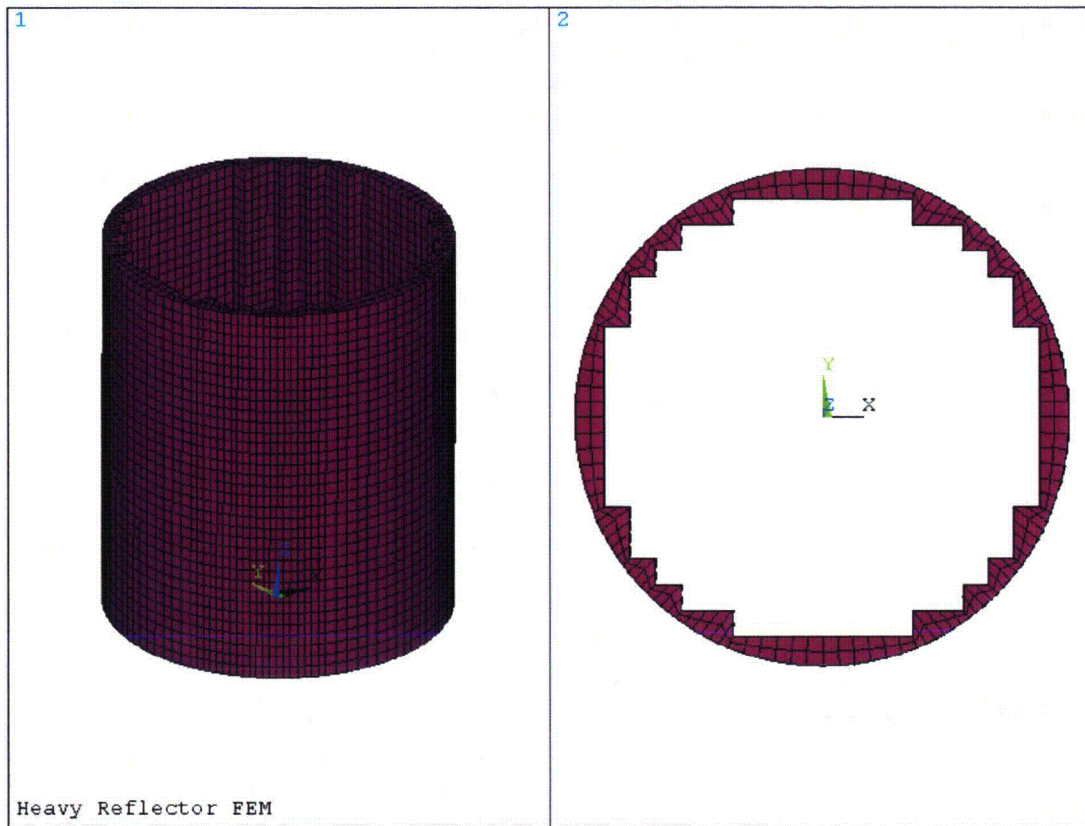


**Figure 4-8—FEM of Heavy Reflector**





### 4.2.2.3 Modal Characterization

Prior to the modal characterization test, static tests are performed on the HYDRAVIB mock-up to verify that the stiffness of the lower internal assembly and its restraint at the CB flange is modeled accurately. This is accomplished through characterization tests with the hold-down ring to determine the stiffness for the one dimensional translational spring elements that are used with the FEM at the CB flange juncture.

The bending stiffness of the mockup is assessed by recording the applied load and resulting displacement at the LSP elevation. The load and displacement measurements are performed for a range of LSP displacements between 0 and 0.002 inches in the two transverse directions to yield a linear relationship between the stiffness and the displacement and confirm the absence of any spurious gaps within the mockup. A mean stiffness value equal to [ ] or [ ] is obtained.

To confirm the accuracy of the stiffness of the spring elements used to represent the CB flange juncture of the numerical model, the bending stiffness of the lower internal assembly is assessed by imposing the loading scheme applied in the static test to obtain a linear relationship of the stiffness of the lower internal assembly versus lateral displacement at the LSP elevation. The stiffness values computed along each axis of the numerical model are as follows:

$$K_{NS} = [ ] \text{ (for the north-south direction).}$$

$$K_{EW} = [ ] \text{ (for the east-west direction),}$$

for a mean stiffness value of [ ].

The difference in stiffness between the two translational directions is due to the presence of the hot leg nozzles. The stiffness values obtained through FEM calculation correlates closely with the values obtained through the experimental observations

Applying an ideal "clamped boundary condition" at the CB flange location would represent an infinite stiffness of the translational spring elements, which would increase the modal frequencies of the CB lower assembly and result in a reduction in the response of the CB to turbulence. Spring elements for the boundary conditions are conservatively applied to both the scale and full scale analytical models.

After obtaining the numerically derived modal solution for the dry and wet modal frequencies (considering the hydrodynamic effects of the fluid), a comparison of the experimentally derived modal solution is performed as the bases for the validation of the numerical solution.

#### Dry Modal Frequency Comparison

The comparison of the dry modal frequencies is provided in Table 4-1. The corresponding mode shapes are graphically displayed in Figure 4-10. These results demonstrate that the CB

“pendulum” modal frequencies are similar using either the experimental or numerical approaches. Past experience has consistently shown that this mode is the most significant contributor to the motions of the internals.

It was observed during these tests that the modal frequencies of the HR are consistently overestimated by the numerical model, which suggests that the HR model is stiffer than the mockup and is interpreted as a consequence of the method by which the slabs and elements of the HR are modeled. Because the HR is a highly integrated part, the discontinuities of the HR structure tend to reduce its stiffness compared to a continuous one. No attempt is made to update the model to precisely match the experimentally obtained frequencies because these values are only representative of the HR mockup structure. This lack of agreement between the HR frequencies does not significantly impact the response of the HR or the lower internal assembly for the reasons identified below.

- The “rocking” mode ( $M=1$ ) of the HR slabs, either in air or in water, is a rigid body mode. Because all of the flexibility is from the shell of the CB, the lateral stiffness of the HR has an extremely low influence on its dynamic behavior. The majority of the kinetic energy comes from the mass and motion of the HR (in air) or from the HR/CB annulus (in water) and the potential strain energy is stored in the shell of the CB. Even a large deviation in the “beam” stiffness of the HR would not result in a significant drop in response of the HR. Although it would appear to be counter-intuitive, the accurate modeling of the stiffness of the CB shell is an essential parameter that is very influential in the prediction of the dynamic response of the HR.
- The coupled modes of the HR/CB are mainly shell type modes. The physical mockup of the HR and numerical modeling scheme are sufficiently accurate for the characterization of these shell type modes and the corresponding dynamic behavior of the lower internals.

#### Wet Modal Frequency Comparison

The purpose of the second series of validation tests on the scale model is to verify that the hydrodynamic effects are correctly captured by the numerical method. A significant decrease in modal frequency is anticipated and observed for the two CB “beam type” modes because they involve considerable hydrodynamic effects and the HR beam-type modes. An even higher drop in modal frequencies is expected and observed for the “shell type” modes of the CB and HR due to the coupling of the HR and the CB through the thin water annulus between these structures. Instead of obtaining uncoupled shell type modes of the HR or CB, coupled modes are expected and observed.

The comparison of the wet modal frequencies is provided in Table 4-2. The corresponding mode shapes are graphically displayed in Figure 4-11.

#### Differences between the Wet and Dry Testing

As reported in Table 4-2, the CB shell modes and the HR beam and shell-type modes are not identified in the experimental results because of the high damping effect induced by the thin fluid layer that separates the HR outer and the CB inner surfaces. This damping has been estimated

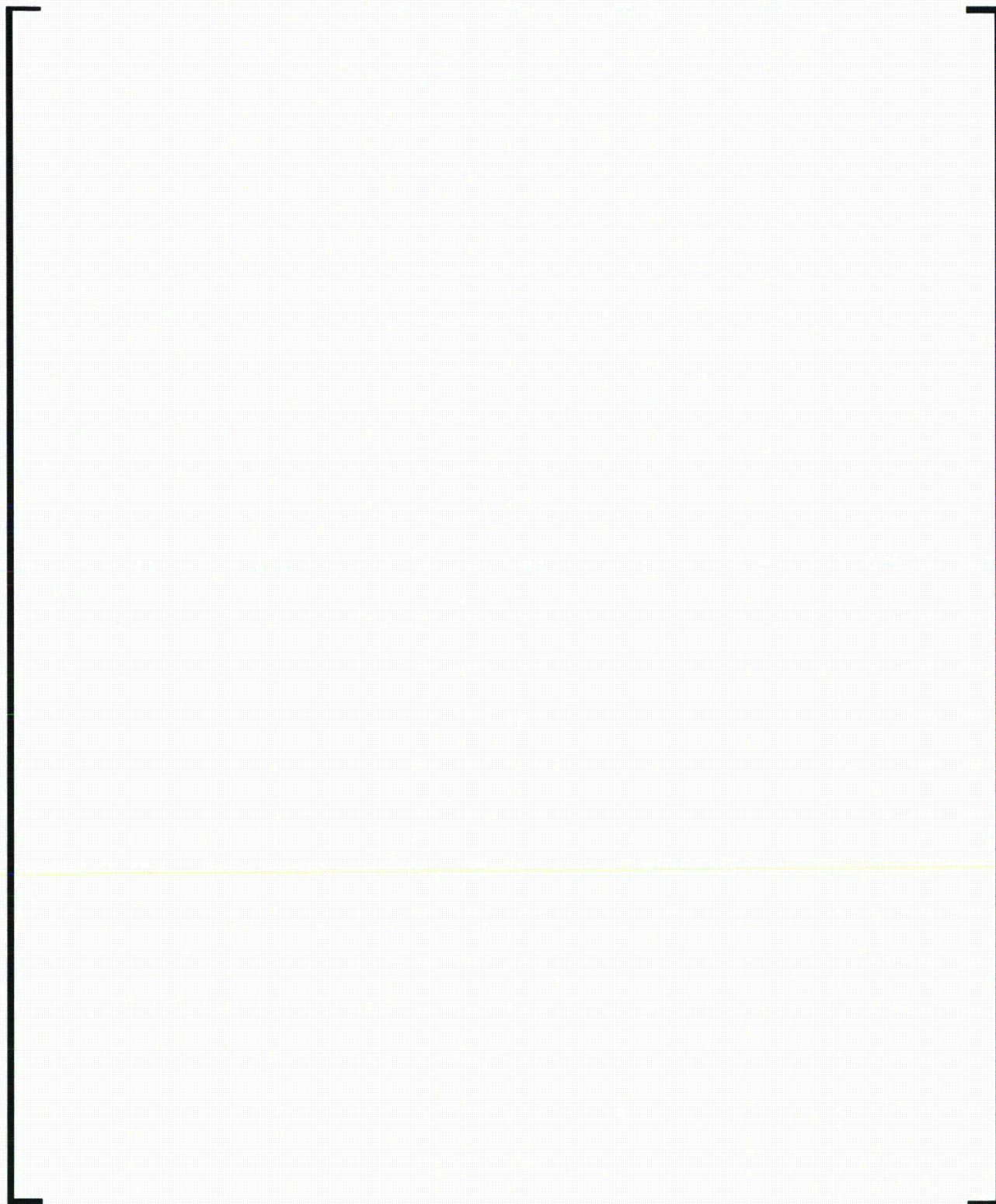
to be about [ ] percent of critical damping (at mockup scale, cold conditions and without flow). During the HYDRAVIB flow tests, there is a [ ] inch/second flow velocity in the annular gap between the CB and HR, which induces additional damping. The amplification of these modes is inhibited by these two additional sources of damping such that the resonance peaks of these modes cannot be extracted from the measurements. Supplementary testing performed with the HYDRAVIB mockup to validate this observation and conclusion was performed using various thicknesses of the HR/CB annulus and fluid temperatures.

As reported in Section 4.2.3.2, the response of the RPV lower internal assembly is dominated by the global beam mode motion of the CB. Therefore, the "shell type" modes obtained numerically in Table 4-2 are not influential to the dynamics of the LSP and they do not produce significant motion of the LSP or the fuel bundle. Sections 4.2.3.2 and 4.2.7.1 provide additional validation of the numerical models for the HYDRAVIB mockup and the full scale design respectively in regard to the dominance of the CB pendulum mode to the response of the lower internal assembly.

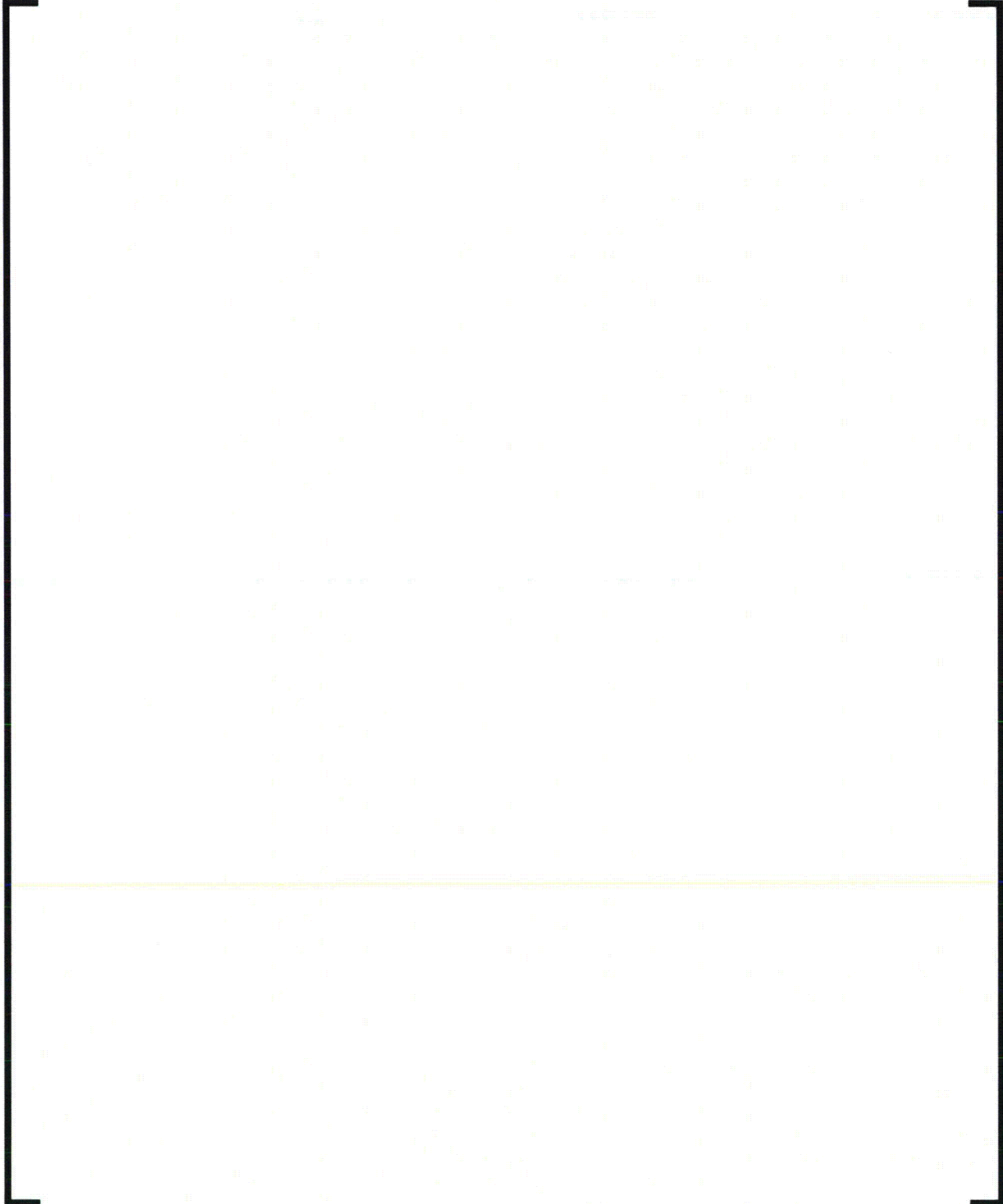
**Table 4-1—Dry Modal Frequencies – Measured vs. Computed Values**

A large, empty rectangular frame with brackets on the left and right sides, indicating a table that has been removed or is otherwise blank. The frame is composed of thick black lines.

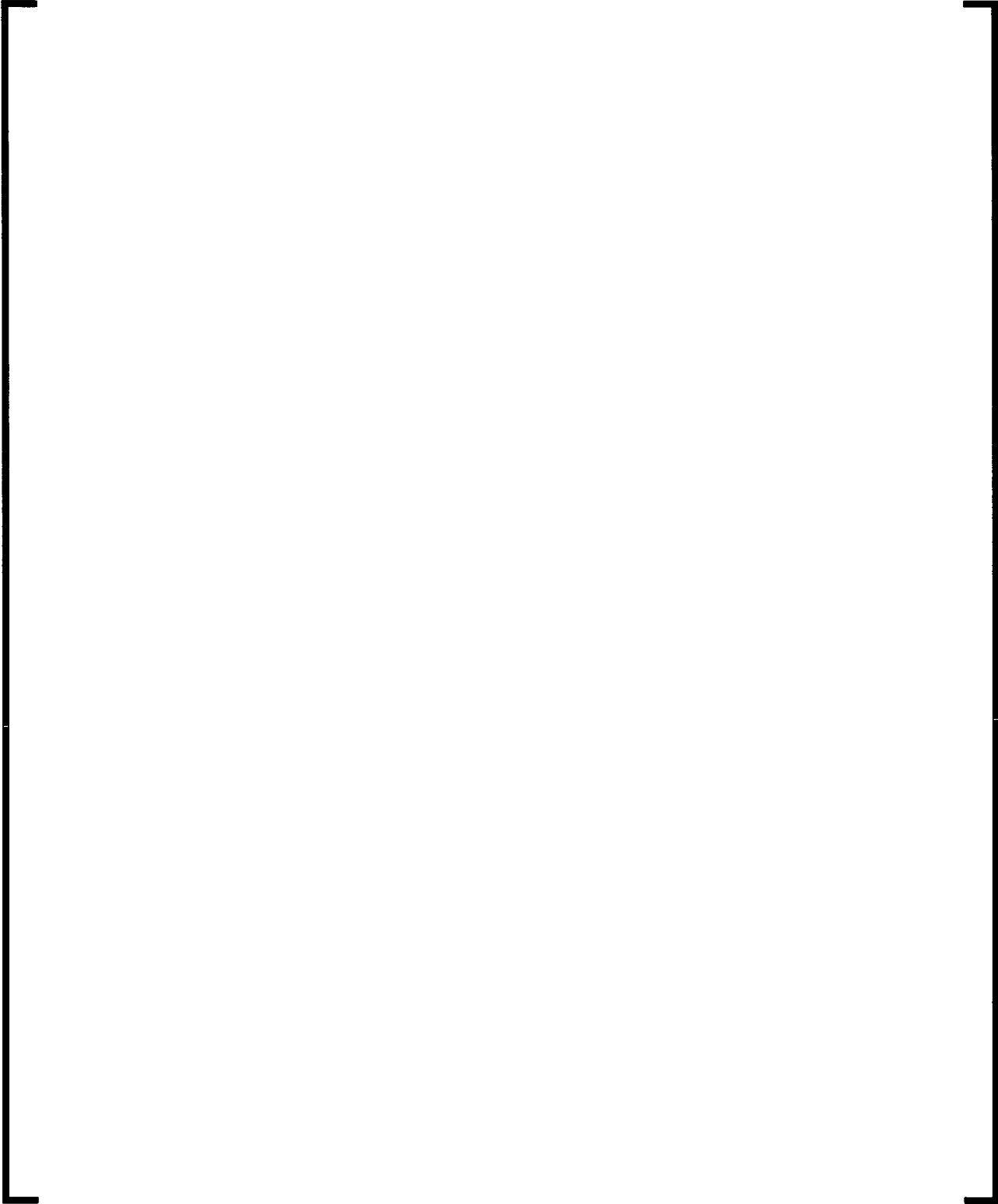
**Figure 4-10—HYDRAVIB Dry Mode Shapes  
CB Beam-Type Modes (Along Reactor 0°-top and 90°-bottom)**



**HR Shell Modes "N=2" (Along Reactor 45°-top and 90°-bottom)**



**HR Rocking Modes (Along Reactor 0°-top and 90°-bottom)**



---

**HR Shell Modes (N=3)**

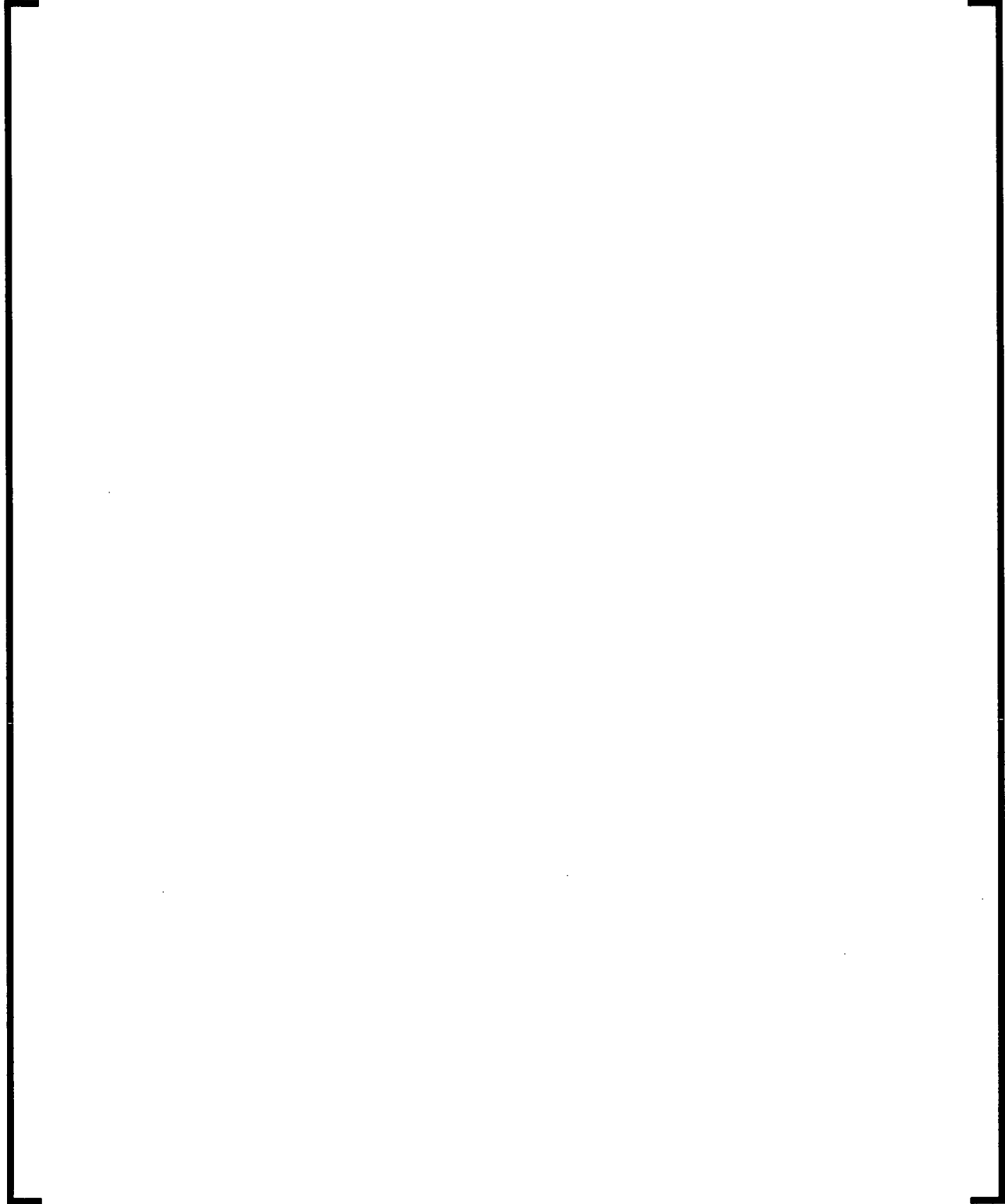


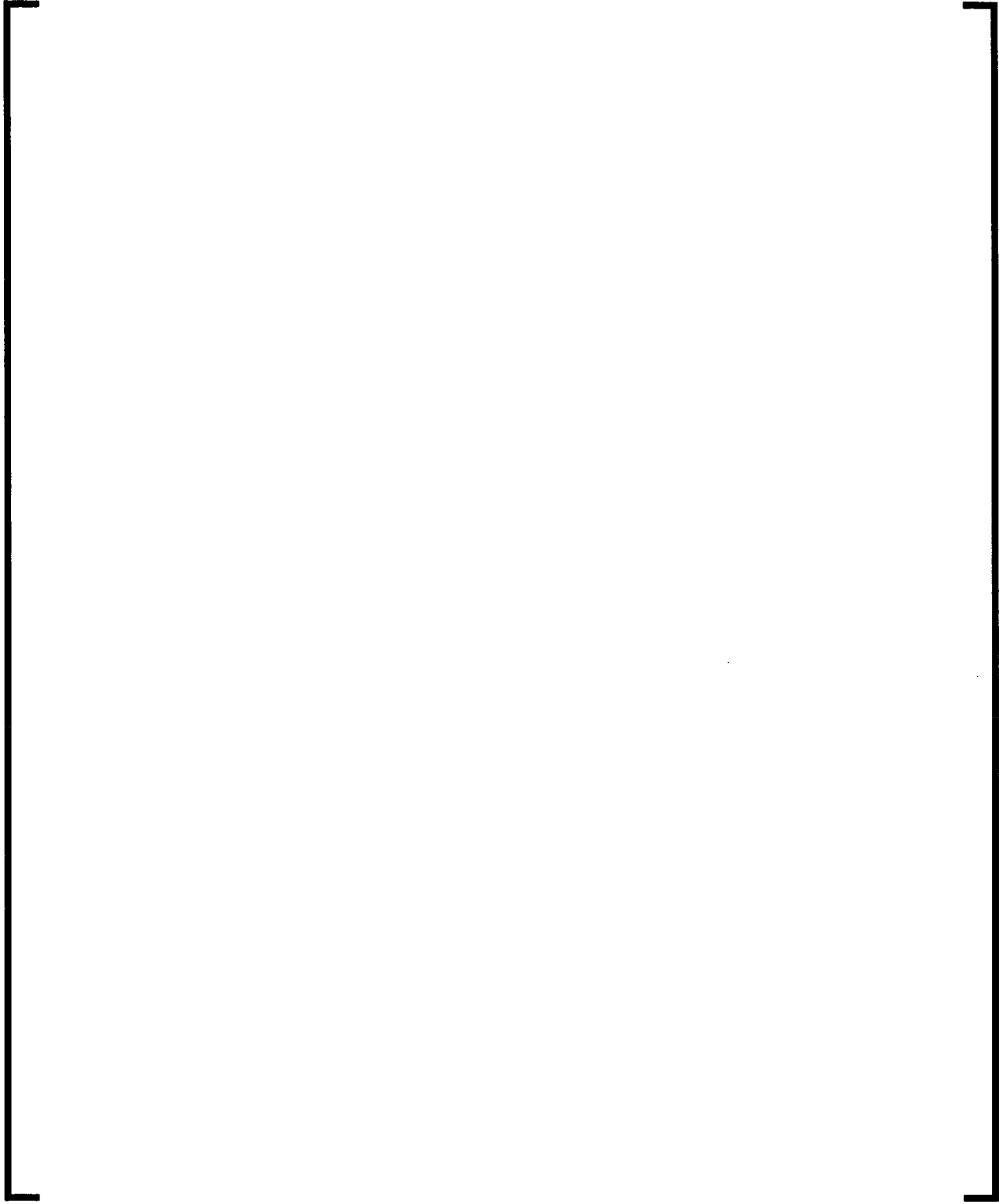
**Table 4-2—Wet Modal Frequencies – Measured vs. Computed Values**



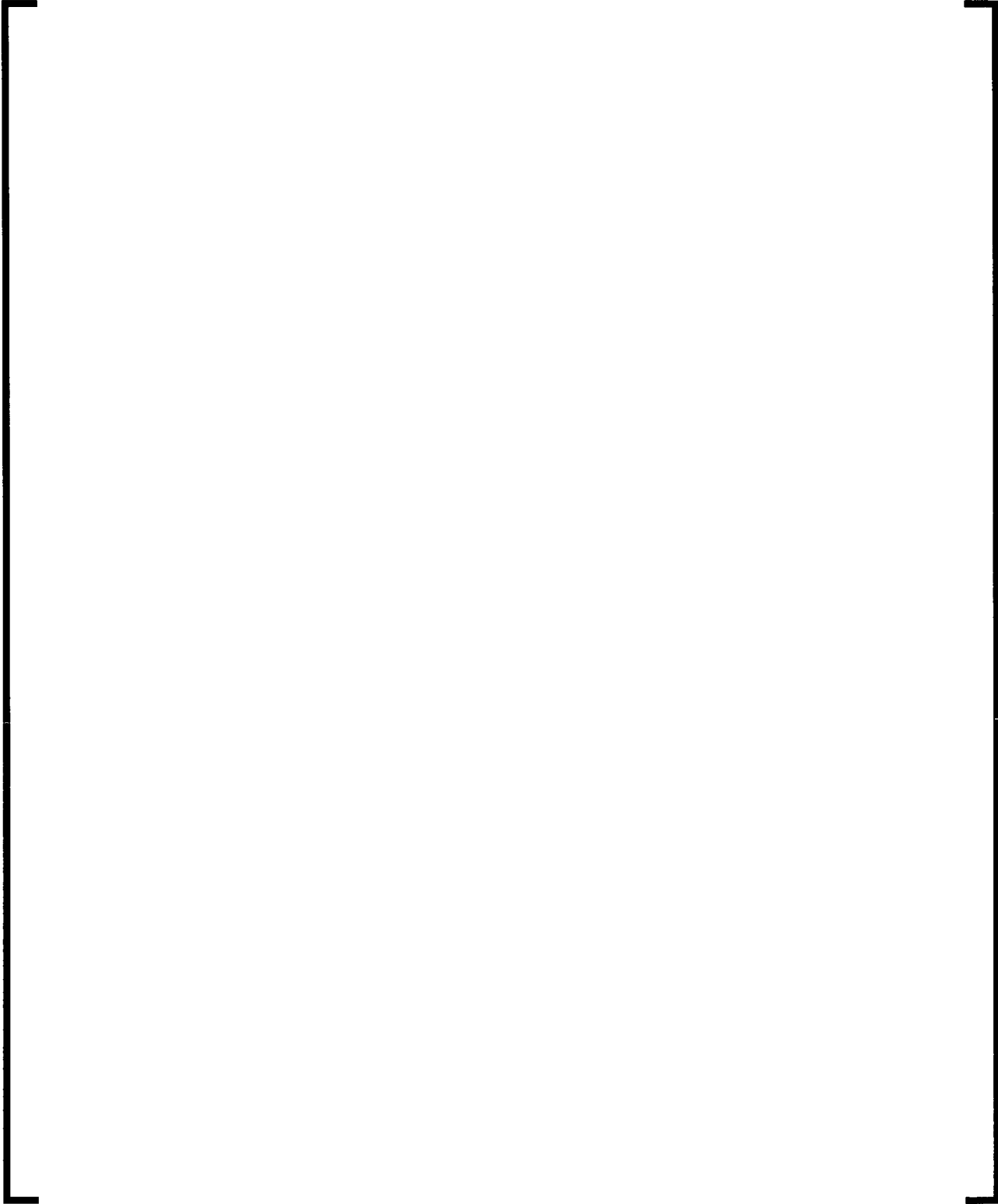
Notes for Table 4-2:

1. The corresponding mode shapes are graphically displayed in Figure 4-11.

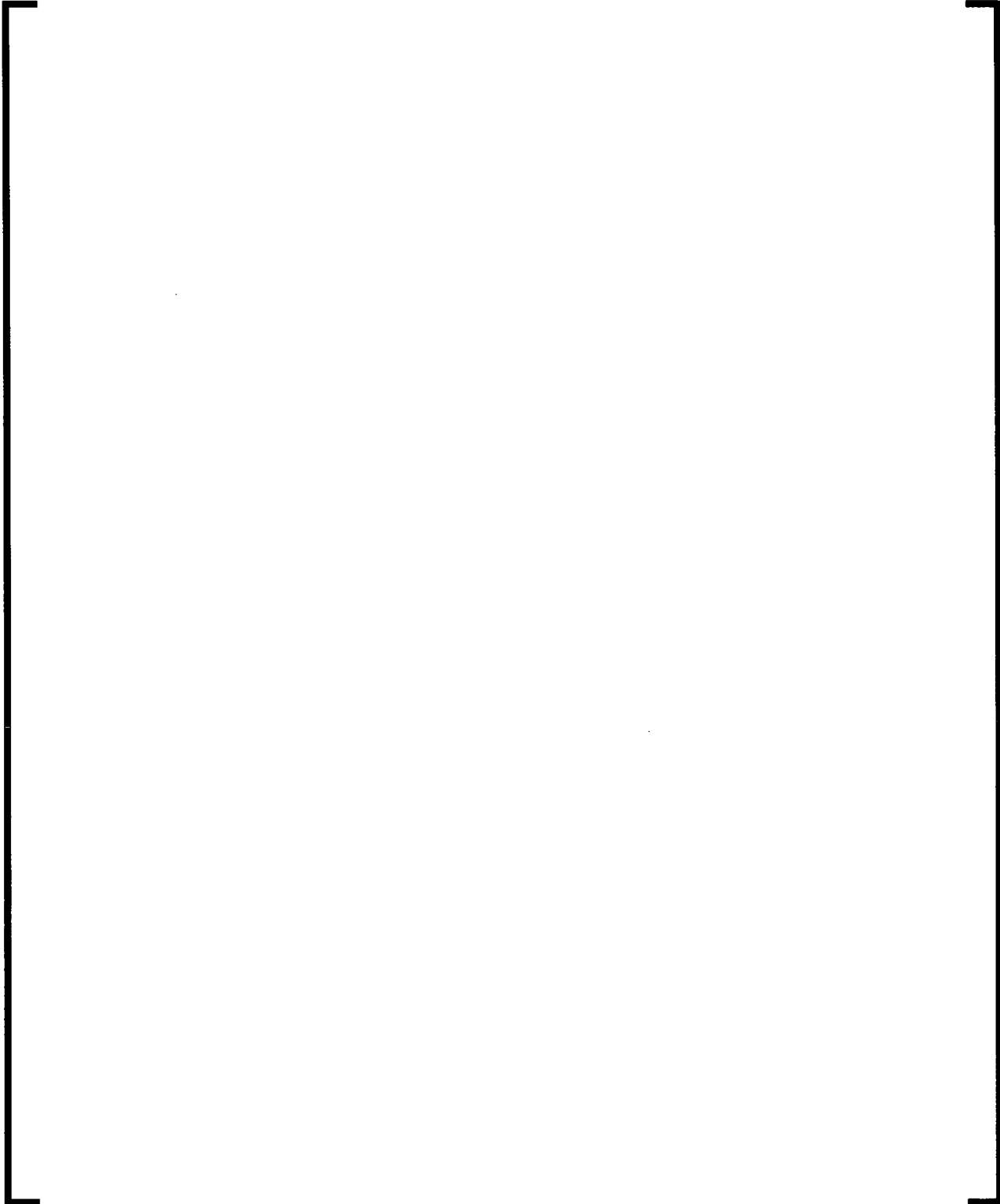
**Figure 4-11—HYDRAVIB Wet Mode ShapesCB Beam-Type Modes  
(Along Reactor 0°-top and 90°-bottom)**



**HR Shell Modes "N=2"**



**HR Rocking Modes (Along Reactor 0°-top and 90°-bottom)**



#### 4.2.2.4 Forcing Functions

The excitations of the RV lower internals due to pressure fluctuations in the turbulence are applied to the structure as power spectral densities (PSDs) with the relevant correlation lengths. These pressure excitations are developed from the dynamic pressure measurements performed in the HYDRAVIB mock-up during the flow tests. Three unique PSDs that represent the level of turbulence in the upper and lower CB and in the lower plenum are derived from the flow tests.

These unique PSDs include:

- PSD to define the turbulence in the downcomer annulus.
- PSD to define the turbulent excitation created by the impingement of the cold leg flow upon the CB.
- PSD to define the turbulence in the lower plenum for the LSP.

The pressure fluctuations were measured by piezoelectric sensors with integrated electronics type, PCB 112A21, 113A21 or WM105C02. The dynamic response of these sensors and the static calibration supplied by the manufacturer is verified. The resulting root mean square (RMS) level of the pressure fluctuations is accurate to within  $\pm 5$  percent. The signals from the sensors are conditioned in a Bruël & Kjaer type 2694 rack. The fluctuations are acquired via a dynamic NI – PXI 1045 system, then recorded using an internal software package developed under Labview. The data is processed using the MATLAB scripts in order to determine the RMS values, to calculate the PSD, and to determine the coherence functions and the cross-power.

During the tests, the signals are sampled at 2 kHz. The acquisition period is 60 seconds. The frequency resolution used in processing the data is 0.5 Hz with an overlap of 67 percent and a time domain Hanning weighting window. Each result is a mean of 90 spectra over an analysis range extending to 1 kHz.

Forcing functions are not derived to account for the turbulence in the by-pass flow between the CB and HR. The thin annulus between these two components reduces the maximum correlation length to the size of the annulus. The coherence of the forcing function is not sufficient to excite the model frequencies of the CB and HR.

##### 4.2.2.4.1 Excitation due to Turbulence in RV Downcomer

The downcomer turbulent pressure fluctuation is the primary forcing function on the reactor CB. A series of dedicated tests are conducted on the 1/8 scale mockup, aiming at accurately defining the turbulent pressure amplitude, frequency content, and correlation patterns. After reduction, the following empirical formulas are retained.

Power Spectral Density:

Dimensionless quantities are as follows;

$$[ \quad ]$$

Where:

$$S_i = f \frac{D_h}{V}$$

- The following numerical values are obtained through curve-fitting of the averaged PSD curves obtained along the length and circumferential directions in the downcomer.

$$[ \quad ]$$

The resulting dimensionless pressure PSD curve is displayed in Figure 4-12.

The dimensional pressure PSD(f) is defined as follows:

$$[ \quad ]$$

Where:

$$\Delta P = \frac{1}{2} \rho V^2 \quad (\text{Dynamic pressure})$$

$D_h$  = Downcomer hydraulic diameter.

$f$  = Forcing frequency.

$S_t$  = Strouhal number.

$V$  = Fluid mean velocity in the downcomer.

$\rho$  = Fluid density.

**Figure 4-12—Dimensionless PSD for the Turbulence in the RV Downcomer****Correlation Patterns:**

Representative correlation patterns are used along with the dynamic pressure PSD. Following the common practice, the correlation decay curves are fitted using an exponential shape. The coherence value is expected to decay exponentially with increasing distance between measurement points as defined by the relation;

$$\Gamma_{ij}(f, d) = \exp(-d / \lambda)$$

The coherence function between the pressure signals ( $p_i$  and  $p_j$ ), separated by a distance “d” is defined by the relation,

$$\Gamma_{ij}(f) = \frac{|P_{ij}(f)|}{\sqrt{P_{ii}(f)P_{jj}(f)}}$$

Where the following notations are used:

$P_{ii}$   $P_{jj}$  Auto-power spectral density of pressure at location i (resp. j).

$P_{ij}$  Cross-power spectral density of pressure signals at locations  $i$  and  $j$  (complex values).

Cross-correlation calculated on a series of axially and circumferentially positioned pressure sensors provide the following relationships for the downcomer (at a location remote from the inlet jets):

$$[ \quad ]$$

Where:

$f$  = Forcing frequency.

$t$  = Downcomer annulus width.

$V$  = Downcomer flow velocity.

Phase Relationships:

Measurements of the mean phase lag between upstream and downstream locations show that the ratio between convective ( $U$ ) and mean flow velocities is fairly constant and has a value between [ ] which is typical of axial flows. The following value for the ratio between the convective and mean flow velocities is applied:

$$[ \quad ]$$

Where:

$$[ \quad ]$$

**4.2.2.4.2 Excitation due to the Inlet Jets**

Another source of localized, yet highly energetic excitation is the jet impingement effects that exist in the vicinity of the four inlet nozzles to the RV downcomer. Measurements performed on the mockup confirm that the inlet jets behave as similar, un-correlated turbulent sources.

Power Spectral Density

Using a curve-fitting process similar to that previously explained, the following empirical formulas for the dimensionless turbulent PSDs are obtained from the HYDRAVIB flow test.



Where:

$$S_t = f \frac{D_h}{V}$$

The resulting dimensionless pressure PSD curve is displayed in Figure 4-13.

The dimensional pressure PSD(f) is defined as follows;



Where:

$$\Delta P = \frac{1}{2} \rho V^2 \text{ (Dynamic pressure)}$$

$D_h$  = Inlet nozzles diameter.

$f$  = Forcing frequency.

$S_t$  = Strouhal number.

$V$  = Fluid mean velocity at inlet (cold leg) nozzles.

$\rho$  = Fluid density.

Because of the limited number of sensors, correlation patterns are not determined during the HYDRAVIB flow test. The pressure field in front of each inlet jet is assumed [

] This simple and conservative assumption is integrated  
into the analysis.

**Figure 4-13—Dimensionless PSD of Turbulence in Front of Inlet Jets****4.2.2.4.3 Excitation of the Lower Support Plate**

The CB, being relatively slender, primarily responds as a beam, with the dominant motion in the horizontal plane. Nevertheless, the vertical excitation created by turbulence in the RV lower head plenum to the LSP is included in the 1/8 scale model analysis.

Power Spectral Density

The dynamic pressure sensor, located at the bottom of the RV, shows that the PSD curve in this region follows the classical Dryden shape obtained in fully developed turbulent flows.



Where:

$$S_t = f \frac{D_h}{V}$$

The resulting dimensionless pressure PSD curve is displayed in Figure 4-14.

The dimensional pressure PSD(f) is defined as follows;

$$\Delta P = \frac{1}{2} \rho V^2$$

Where:

$$\Delta P = \frac{1}{2} \rho V^2 \text{ (Dynamic pressure)}$$

$D_h$  = Downcomer hydraulic diameter.

$f$  = Forcing frequency.

$S_t$  = Strouhal number.

$V$  = Fluid mean velocity in the downcomer.

$\rho$  = Fluid density.

$$\Delta P = \frac{1}{2} \rho V^2$$

**Figure 4-14—Dimensionless PSD of the Turbulence in the RV Lower Plenum****4.2.3 Numerical Simulation of HYDRAVIB Mock-up Flow Condition**

The analytical model of the HYDRAVIB mockup flow conditions is created using the techniques implemented by ANSYS. The accuracy of the analytical model, the simulation of the fluid-structure interaction, and the forcing functions is verified against the HYDRAVIB flow test results.

A modal damping ratio for the CB beam-type modes of [ ] percent of critical was applied to the scale model analysis. This damping ratio was obtained by post-processing the test results obtained with the HYDRAVIB mockup and using the half-power bandwidth method to evaluate the horizontal components of motion at the LSP elevation. The modal damping ratio includes a minor correction to negate the effect created from the bias induced by fast fourier transform (FFT) windowing and noise reduction so that the final damping value is lower when compared to the measured value.

Linear velocity displacement transducers (LVDT) installed at the LSP elevation measure the relative displacement time histories between the LSP and CB. By installing the instrumentation at the LSP elevation, the measurement and detection of the pendulum mode of the CB, as well as the higher order mode shapes, is possible. Therefore, only the damping relevant to the CB beam type mode is obtained.

Calculations are performed to benchmark the [ ] percent damping value for all types of modes, including the shell type modes. The response of the shell modes is observed to be insignificant during mockup conditions; therefore, the application of this damping value to the shell type modes is acceptable from an analytical perspective.

In the mockup conditions, the damping values for shell type modes are much higher than that of the beam modes, and a more realistic value for this damping would be at least five times higher. Therefore, the use of the [ ] percent damping value in the numerical models for the shell type modes has no appreciable influence on the response of the shell modes. The impact of the damping values for the shell type modes on the response of the CB is negligible; therefore, no attempt is made to determine actual damping values.

This damping ratio is determined from damping tests performed in a water environment at ambient temperatures with excitation at the middle and bottom elevation of the CB, at the top of the HR, and at the LSP. In-air damping tests are also performed. The accelerometers are located around the circumference and along the length of both the CB and HR to verify that the beam and shell modes are detected for the computation of this damping ratio. (See Figure 4-45, Figure 4-46, Figure 4-48, and Figure 4-49.)

The methodology implemented with ANSYS to perform analysis of the flow excitation due to random turbulence is reviewed in the following section.

#### 4.2.3.1 FIV Methodology Implemented by ANSYS

The FIV methodology implemented by ANSYS is conducted using the standard random vibration response analysis method. This multi-step method includes the following steps:

1. Determine the structural frequencies and eigenvectors of the fluid-structure model.
2. Determine the response of the RV lower internal assembly to each individual PSD, which includes a single jet impingement PSD, the lower plenum PSD, and the downcomer PSD, through the following process:
  - a. Compute the participation factors.
  - b. Compute the modal response power spectral densities (RPSDs) and integrate with respect to frequency to obtain modal direct and co-variance terms.
  - c. Combine modal solution to obtain the displacement response.
3. Compute the global response of the RV lower assembly by quadratically combining the individual responses for the single jet impingement, the lower plenum, and the downcomer PSDs.
4. The nodal RPSDs are evaluated using the standard equation:

$$S_{di}(\omega) = \sum_{j=1}^n \sum_{k=1}^n \Phi_{ij} \Phi_{ik} \left( \sum_{l=1}^{r_1} \sum_{m=1}^{r_1} H_j^*(\omega) H_k(\omega) S_{lm}(\omega) \right)$$



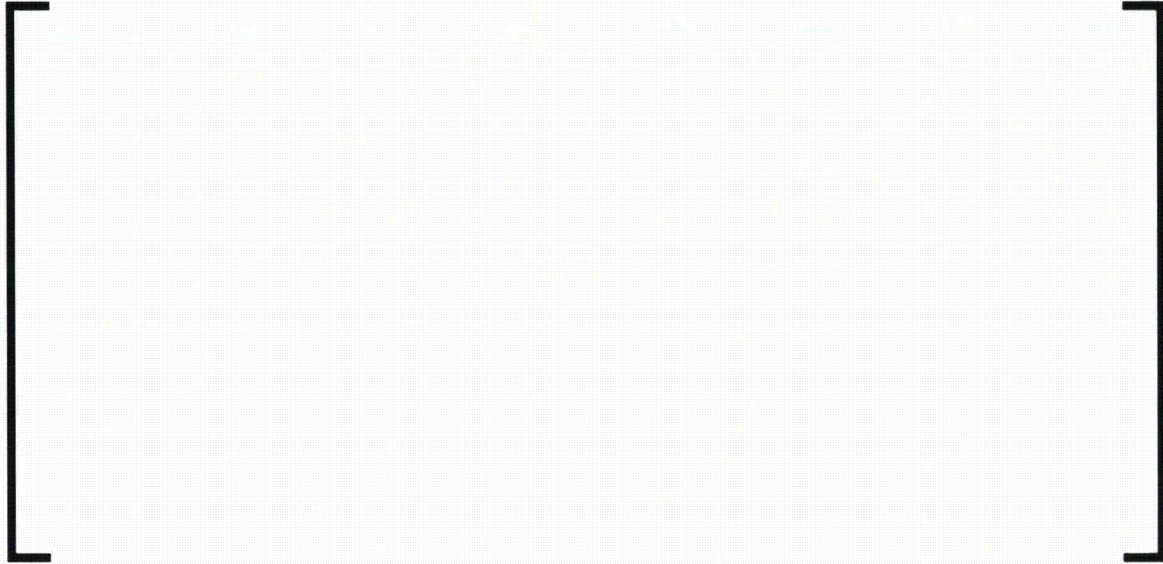
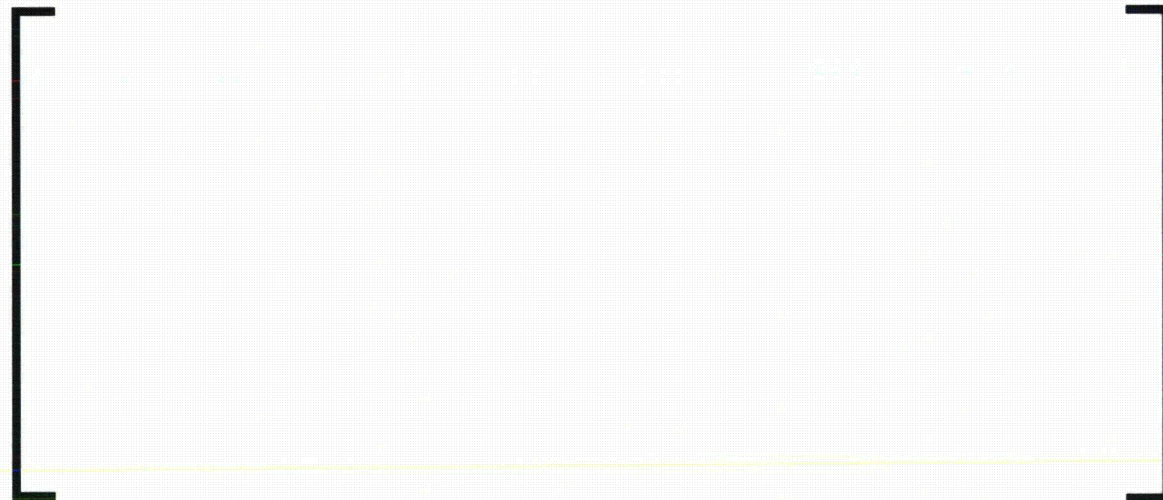
For each of these locations, the following quantities are computed:

- Response PSDs (unit: millimeters<sup>2</sup>/Hz).
- Broadband response (0 -100 Hz)(unit: mil, rms).
- Band-limited response i.e. beam mode contribution (45 – 75 Hz)(unit: mil, rms).
- Statistical frequency (unit: Hz).

These results are summarized in Figure 4-16 and Figure 4-17. From these figures, the FIV motion of the lower internals primarily consists of:

- [
- The statistical results for the response of the internals of the scale mode are provided in Table 4-3. The corresponding displacement fields are shown in Figure 4-18. These results confirm that [

]

**Table 4-3—Displacements and Statistical Frequencies from the Scale Model Analysis of the HYDRAVIB Mockup Conditions****Table 4-4—Displacements Measured during the HYDRAVIB Mockup Flow Test**

Notes for Table 4-3 and Table 4-4:

1. The results are applicable to four pumps running with 100 percent flow.
2. Location "LSP" represents a location on the LSP with an elevation of 0.0 inches above the LSP upper face.
3. Locations "CB\_A1", "CB\_A2" and "CB\_A3" respectively represent locations on the CB with elevations of 11.4, 20.9 and 31.5 inches above the LSP upper face.
4. Locations "HR\_A1" and "HR\_A2" respectively represent locations on the HR with elevations of 12.5 and 21.9 inches above the LSP upper face.

5. The measured and computed wet modal frequencies of approximately 67 Hz for the core barrel (CB) global "pendulum" mode that are reported in Table 4-2 are determined in still water. The first beam mode frequency of approximately 58 Hz identified in Table 4-4 is measured during tests with flow. The comparison of these two frequencies refers to the same pendulum mode of the CB. The inconsistency in frequency is due to differences in the boundary conditions that are created by the two different types of tests. During the flow tests, strain in the RPV head mock-up that is created by the internal pressure slightly alters the stiffness of the boundary condition at CB flange, thereby creating a difference in the measured frequency of the first mode.
6. The statistical frequencies obtained by both experimental and numerical means are estimated using the Rice formula, as defined by the following expression, which is also presented in the Section 4.3.4.1

$$f_{\text{stat}} = \sqrt{\frac{\int_0^{+\infty} f^2 G_d(f) df}{\int_0^{+\infty} G_d(f) df}}$$

Which makes use of the following notations:

$G_d(f)$  single-sided displacement Power Spectral Density (unit: length<sup>2</sup>/Hz)

$f$  frequency (unit: Hz)

The equation above for  $f_{\text{stat}}$  is used to determine the statistical frequency from the experimentally derived response PSDs. Equivalently, the statistical frequencies calculated with ANSYS are derived with the following relation

$$f_{\text{stat}} = \frac{1}{2\pi} \frac{\text{velocity}_{\text{rms}}}{\text{displacement}_{\text{rms}}} ;$$

The second equation for  $f_{\text{stat}}$  is strictly equivalent by virtue of conservation of energy.

whereby:

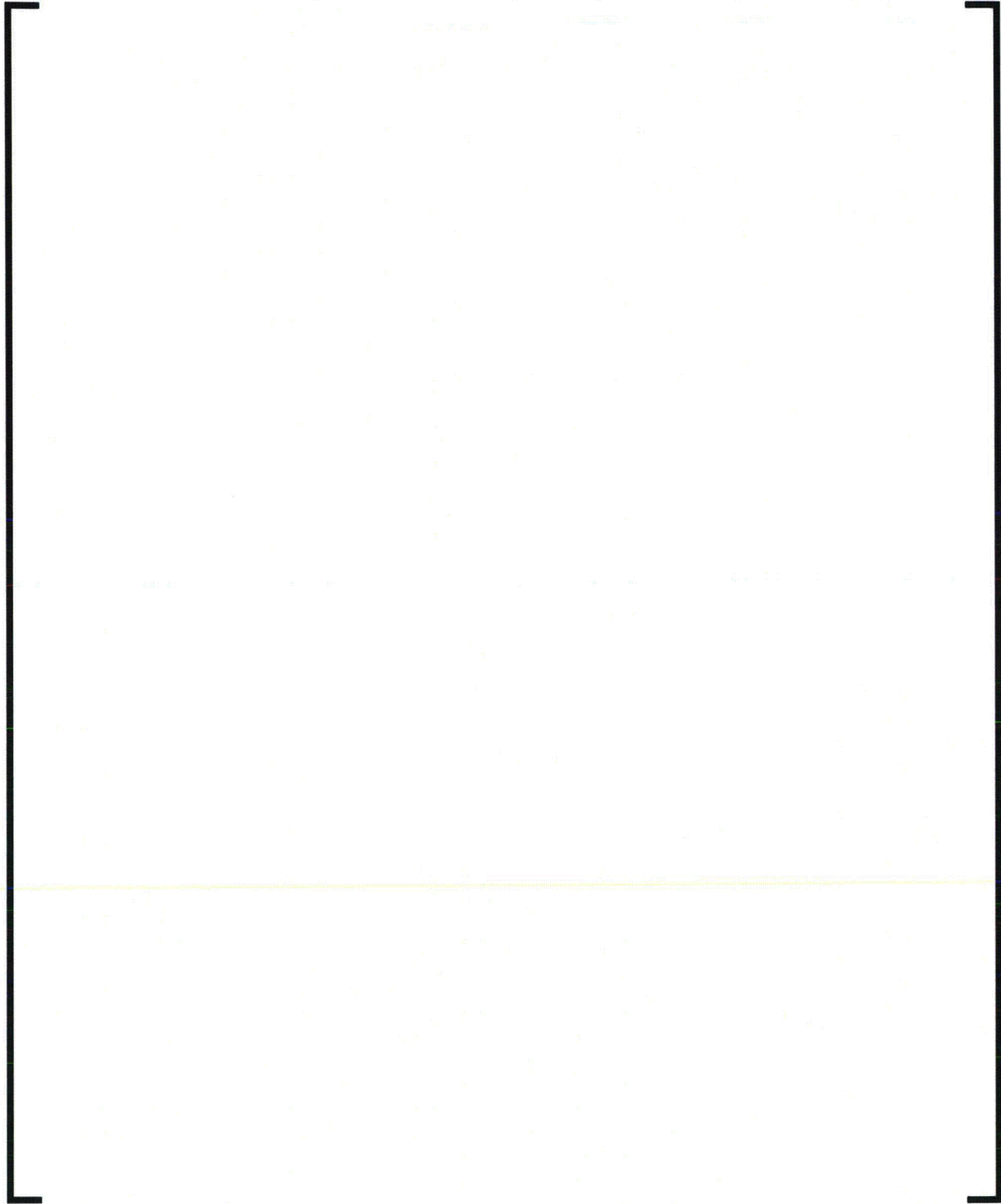
$$\text{displacement}_{\text{rms}} = \sqrt{\int_0^{+\infty} G_d(f) df}$$

$$\text{velocity}_{\text{rms}} = \sqrt{\int_0^{+\infty} (2\pi f)^2 G_d(f) df}$$

**Figure 4-15—Normalized Modal Covariance Matrix for the LSP Location**

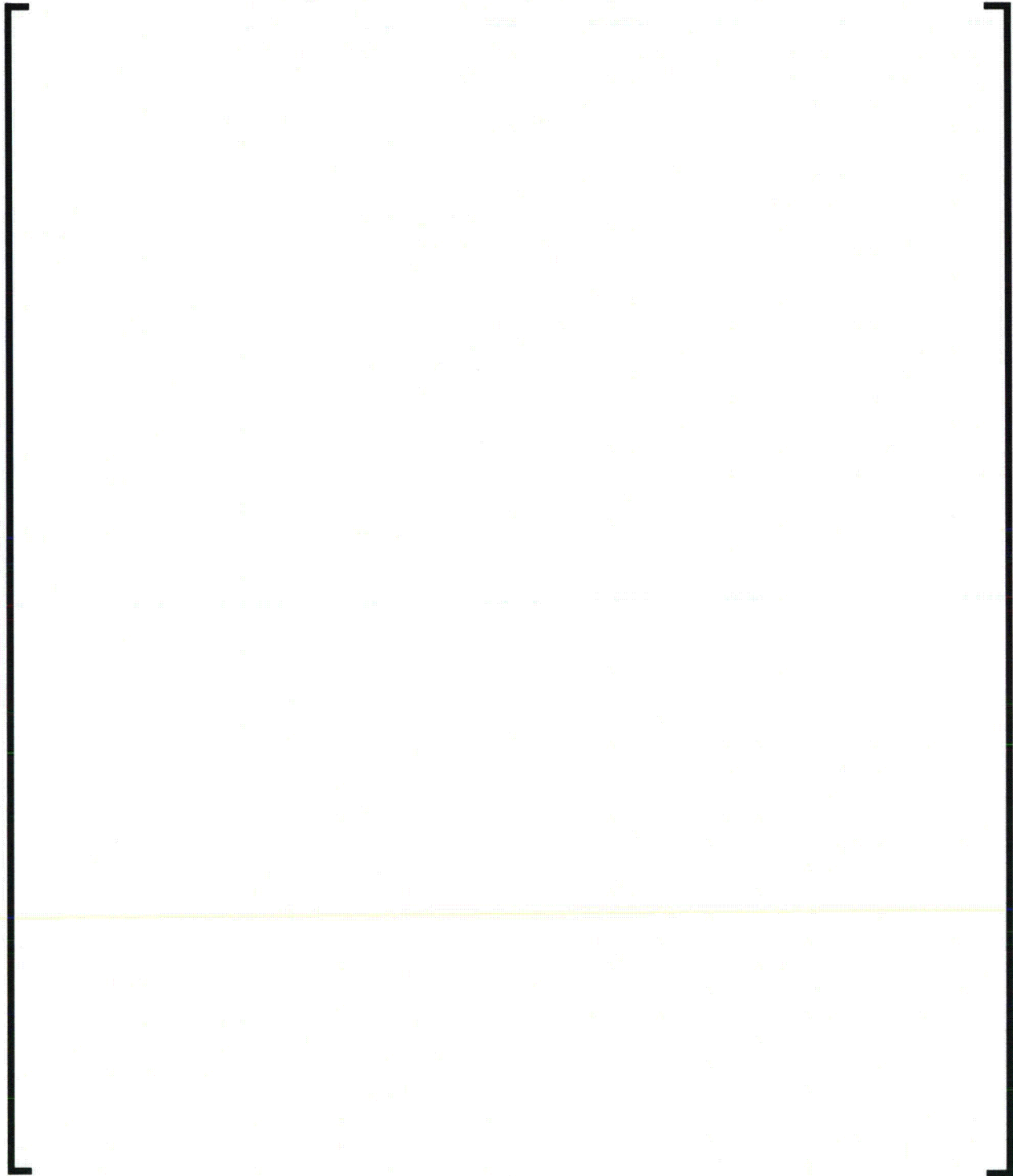


**Figure 4-16—Response PSD and Corresponding Energy Distribution  
along Reactor 0° Axis (mockup conditions)**



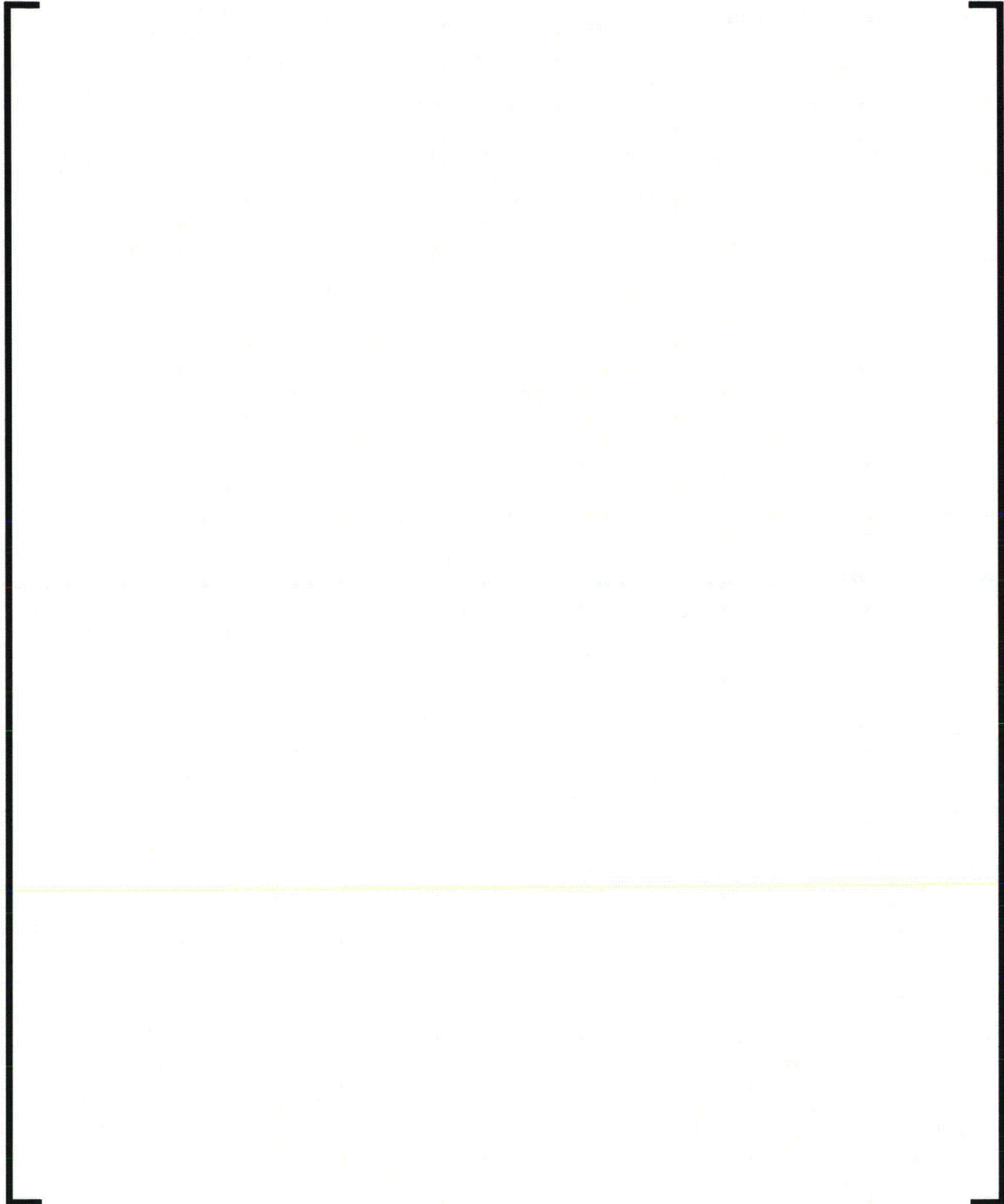
Units: (millimeter)<sup>2</sup> / Hz

**Figure 4-17—Response PSD and Corresponding Energy Distribution  
along Reactor 90° axis (mockup conditions)**



Units: (millimeter)<sup>2</sup> / Hz

**Figure 4-18—Horizontal Displacements Levels Mapping for Mockup  
Conditions FIV Simulation**



Units: micrometers,rms

#### 4.2.4 Conclusions of the FIV Numerical and Experimental Simulations

As stated in Section 4.2.1, the intent of the HYDRAVIB mockup is to assess the vibrations of the lower internals due to flow excitation resulting from random turbulence and vortex-shedding. Due to the patterns of flow in the lower internals, flow excitation of the lower internals as a result of vortex-shedding is not possible. This assertion is confirmed by the absence of fluid velocity related spectral peaks in all of the dynamic pressure measurements obtained during the flow tests.

Regarding flow excitation created by random turbulence, the results of the scale model FIV analysis compare acceptably well with those obtained from the HYDRAVIB mockup flow test as shown in Table 4-3 and Table 4-4. The broadband displacement values at the LSP level, which are dominated by the approximately [ ] mils, rms [ ] are consistent with the displacement values measured experimentally (about [ ] mils, rms). The statistical frequencies also have agreement (about [ ] Hz calculated vs. [ ] Hz measured). Therefore, the numerical model adequately captures the essential features and FIV response of the lower internals to allow its use for the extrapolation to reactor conditions without modification.

The mockup test confirms that the pressure fluctuations in the lower plenum [ ] Considering the worst-case scenario [ ] the numerically obtained displacement response at the center of the LSP is about [ ] mils, rms and slightly less than [ ] mils, rms at its perimeter. Over [ ] percent of the response energy corresponds to the quasi-static response of the CB. This result is expected because the CB axial mode frequency is equal to [ ] Hz, which is considerably higher than the cutoff frequency of the excitation of about [ ] Hz provided with the PSDs. [ ]

## 4.2.5 Numerical Simulation of Full Scale Model (Pre-Operational)

A three dimensional full scale model of the RV and its internals is built using the ANSYS finite element code. The methods and design inputs essential to obtaining agreement between the experimental and numerical simulation of the 1/8 scale model, which are developed during the HYDRAVIB testing (See Section 4.2.2 and Section 4.2.3), are implemented into the full scale model of the RV lower internals. The full scale model contains all of the relevant structural components that are influential to the dynamic behavior of the RV lower internals, which include:

- CB and LSP.
- HR.
- The mass of the flow distribution device.
- Upper internals.
- Hold-down spring.
- Interfaces with the RV.
- FAs (for calculation with core).

The numerical simulation for the full scale model is first performed for the hot functional testing (HFT) condition, or more specifically Test #17 with four reactor coolant pumps (RCPs) operating and fluid temperature at 578°F (See Table 5-4), which is also representative of the hot standby conditions (0 percent power). A uniform temperature equal to 578°F is applied to the structure and the fluid.

The response of the RV lower internals during full power, steady state normal operating conditions is adjusted from the FIV results of the hot functional test #17 through the use of a scaling factor. This scaling factor is based upon the ratio of the dynamic pressure term for the fluid conditions in the RV downcomer between the full power operation and the HFT. The implementation of this method is conditionally acceptable with the demonstration that the core has an insignificant influence on the FIV behavior of the lower internals.

### 4.2.5.1 Modal Analysis

The numerical analyses are performed to obtain a modal solution using reactor, hot shutdown conditions with a uniform temperature equal to 578°F. The possible interfacing contact locations (i.e., the radial and tangential keys, CB nozzles, UCP) are assumed to be open, which is confirmed by the results of the analysis. Closed gap conditions would stiffen the structure, resulting in higher natural frequencies, and a lower response to turbulence.

#### 4.2.5.1.1 Unloaded Core Analysis

The main modes are summarized in Table 4-5. As described in Section 4.2.3.2; [

]

#### 4.2.5.1.2 Loaded Core Analysis

For transverse motion, the core acts as a flexible beam with a first bending mode frequency in the vicinity of [ ] Hz, where the first beam-type modes of the internals has a natural frequency about [ ] Therefore, only the higher order bending modes of the FAs (or core) can couple with the CB. Because these modes involve relatively little mass, no significant impact to the transverse behavior of the CB is expected. Moreover, [

]

- Minimal amplification is expected for the CB/HR beam-type modes.
- A slight reduction in natural frequencies of the CB/HR beam-type modes is expected.
- Near-zero impact is expected for the CB/HR shell-type modes.
- For axial (vertical) motion, the core is firmly connected to the LSP so that its mass nearly follows the LSP out-of-plane motion. Consequently, a significant decrease is expected in the frequency of the global axial mode of the lower internals assembly.

The results of the modal analysis are summarized in Table 4-6.

#### 4.2.5.1.3 Rationale for the Configuration and Selection of Dynamic Parameters

The unloaded core condition is expected to yield the higher vibratory levels because the transverse motion of the lower internals is of primary interest. The structural frequencies of the lower internals are not significantly altered by the loaded core, but the loaded core does add a significant amount of damping such that amplitudes obtained with the fuel are bounded by the unloaded core. In addition, the unloaded core is more directly comparable to the hot functional tests.

The dynamic parameters and principles used for the mockup-scale computations are retained. However, in order to perform the random vibrations analysis of the RV internals, the following inputs obtained from the mockup-test are modified:

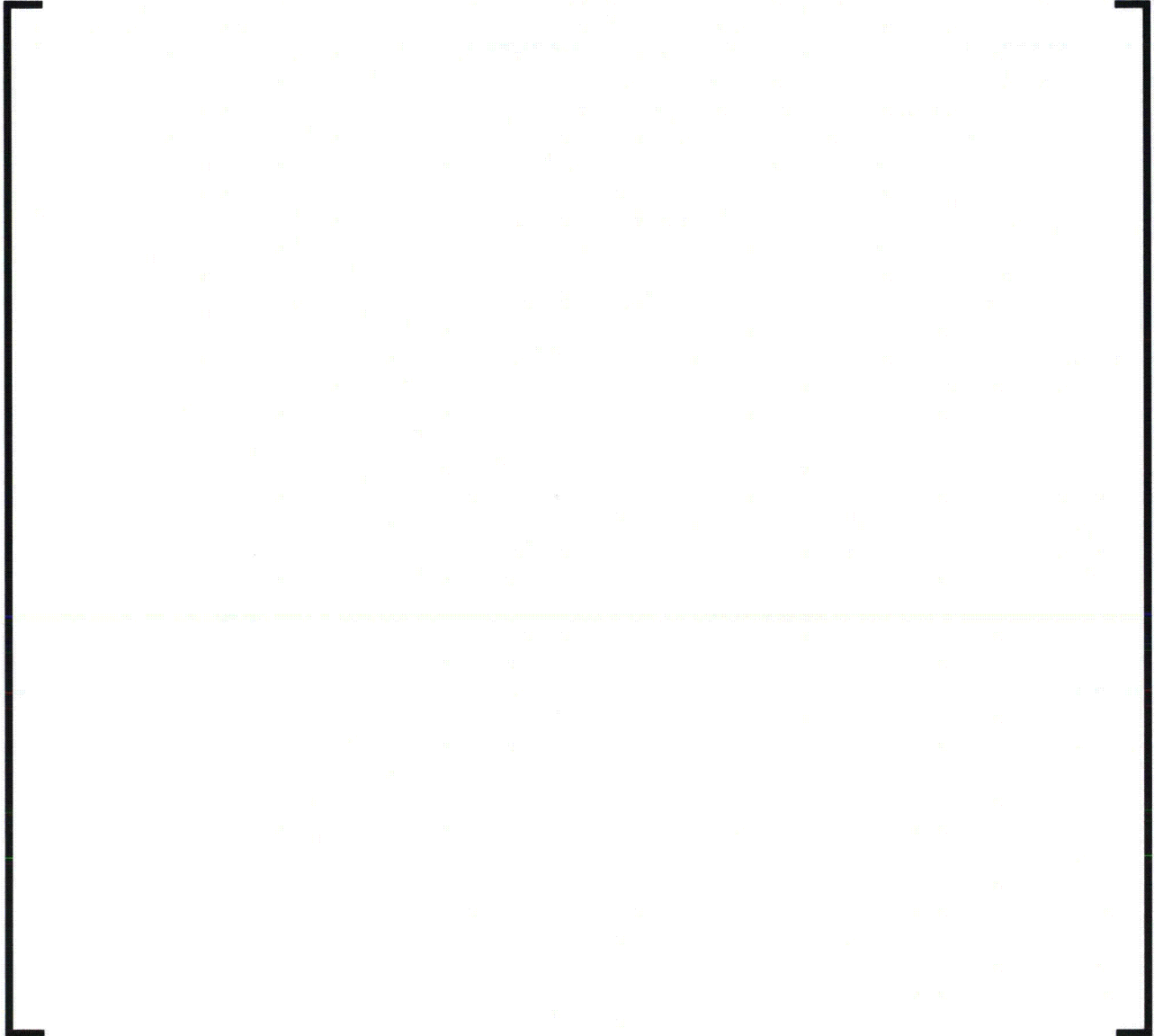
- Forcing functions (Section 4.2.5.2).
- Modal damping ratios (Section 4.2.5.3).

**Table 4-5—Description of the Main Modes – Unloaded Core**

Notes for Table 4-5:

1. Figure 4-19 provides the graphical representation of the mode shapes for the unloaded core.

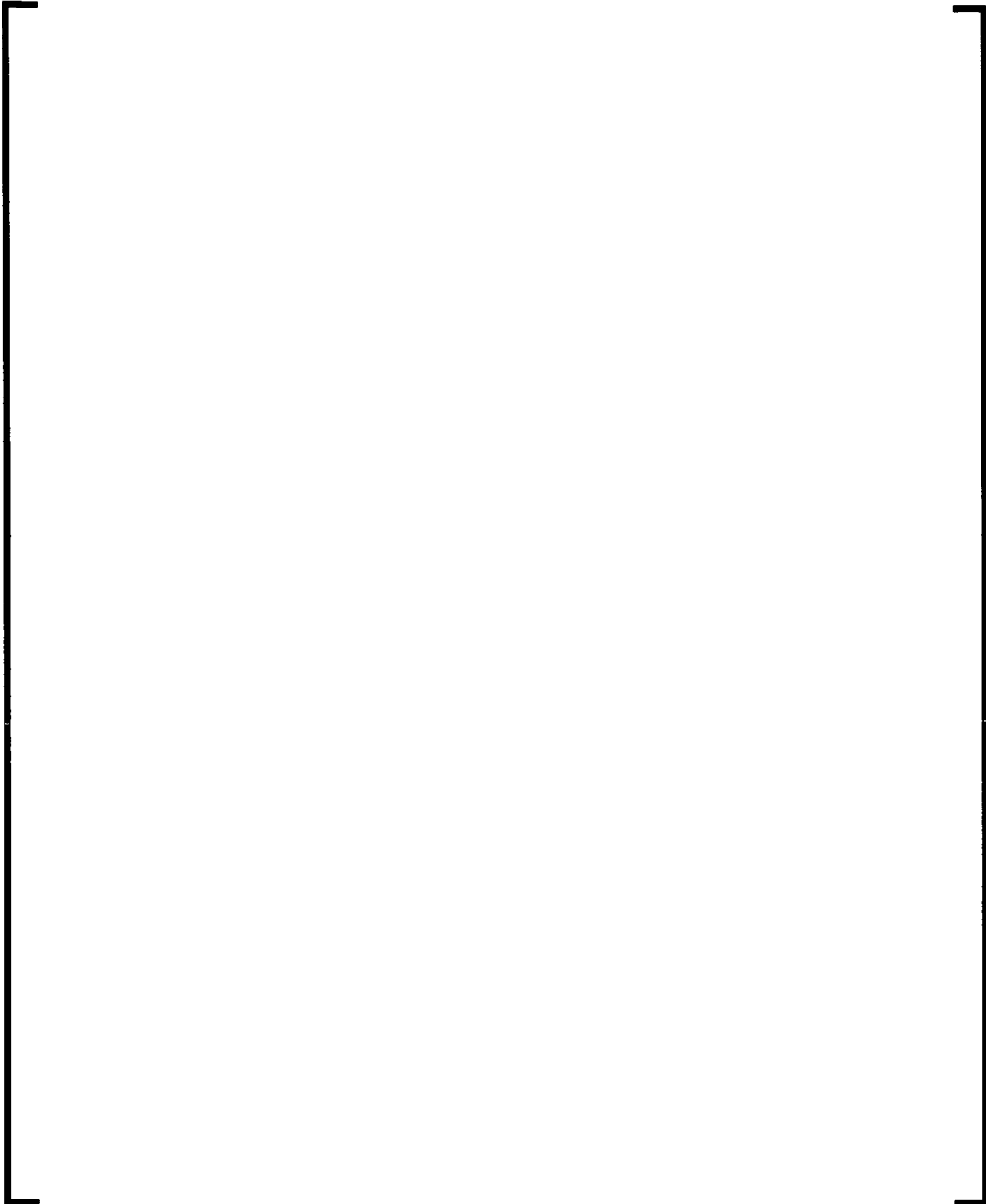
**Table 4-6—Description of the Main Modes – Loaded Core**

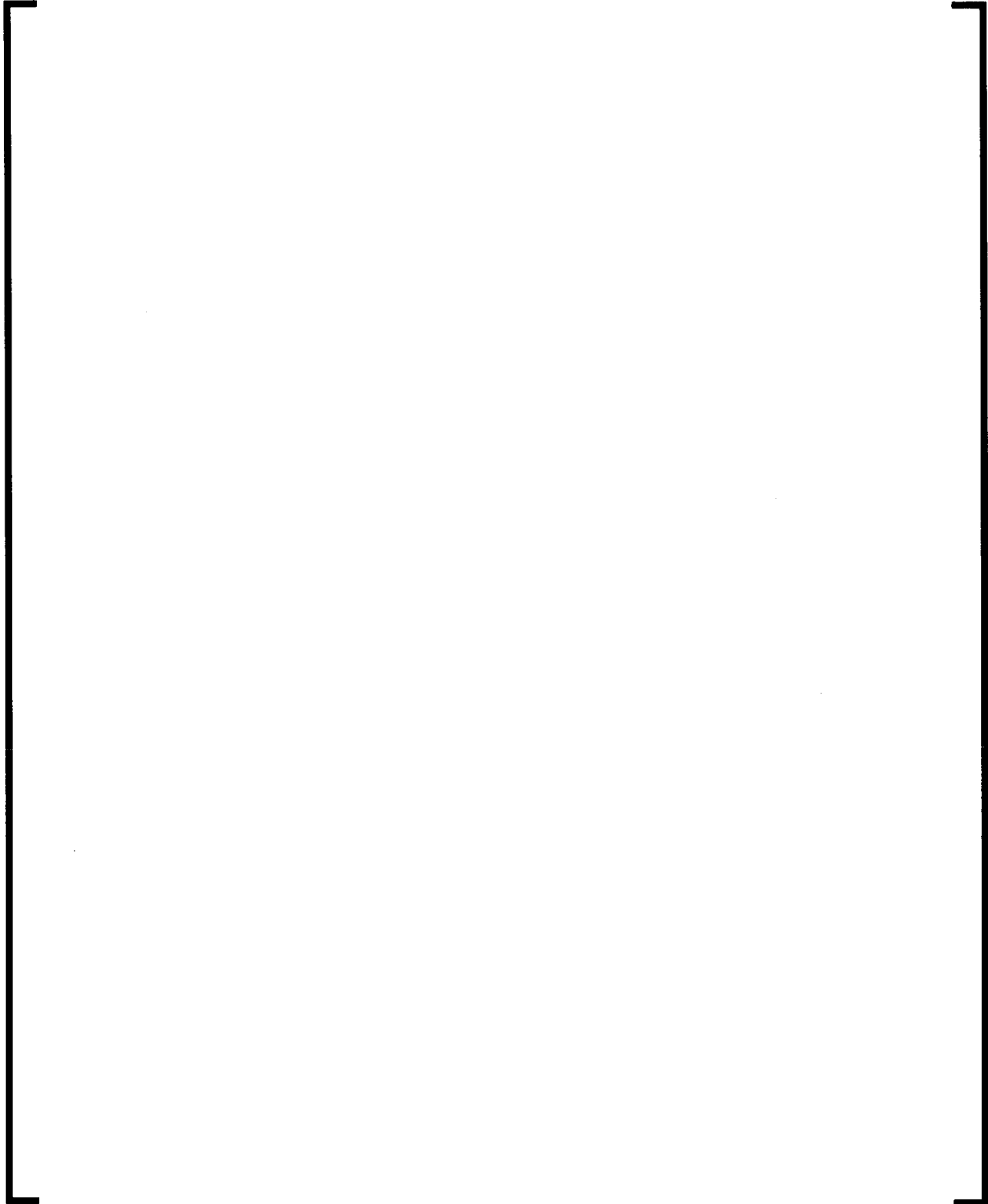


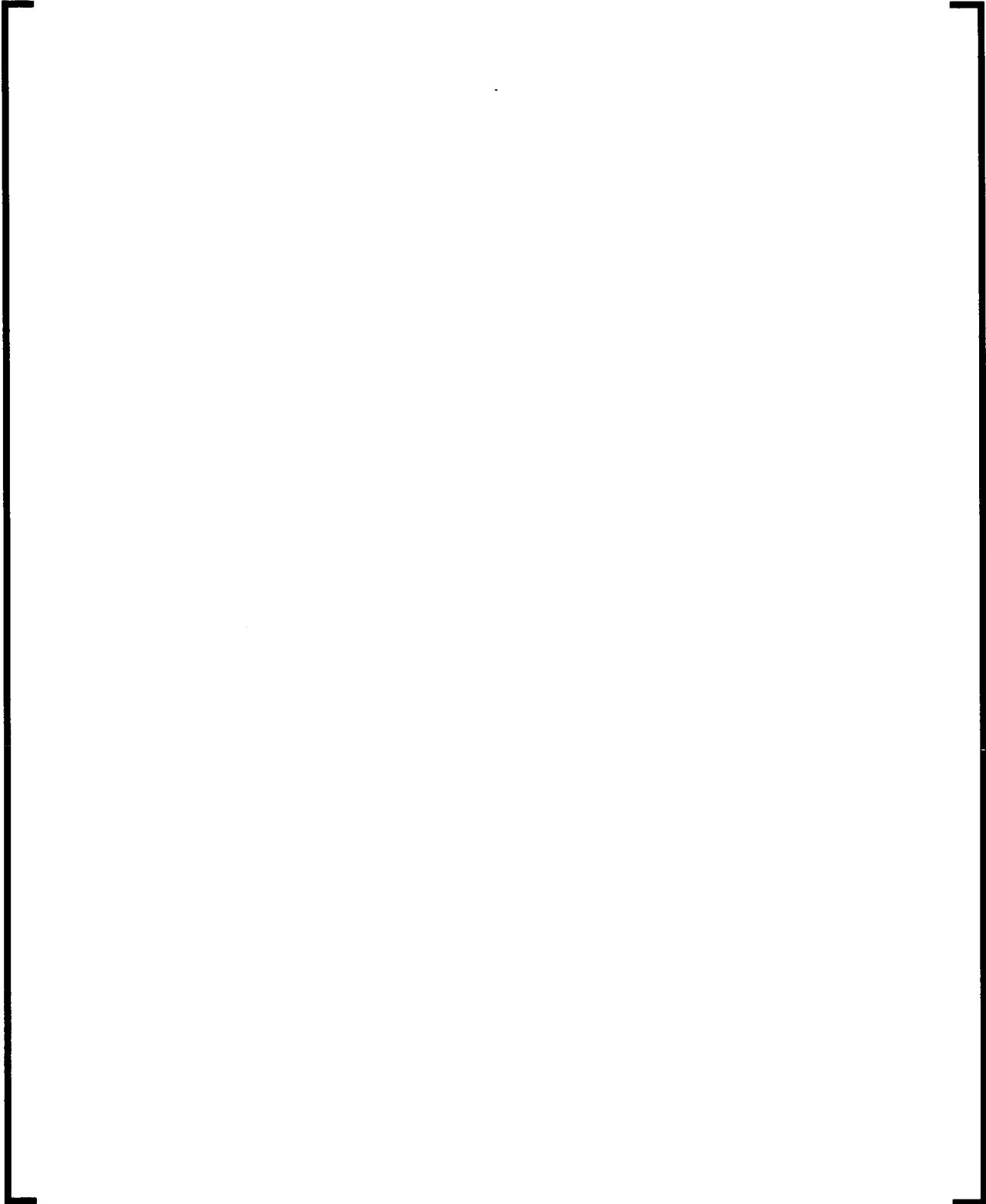
Notes for Table 4-6:

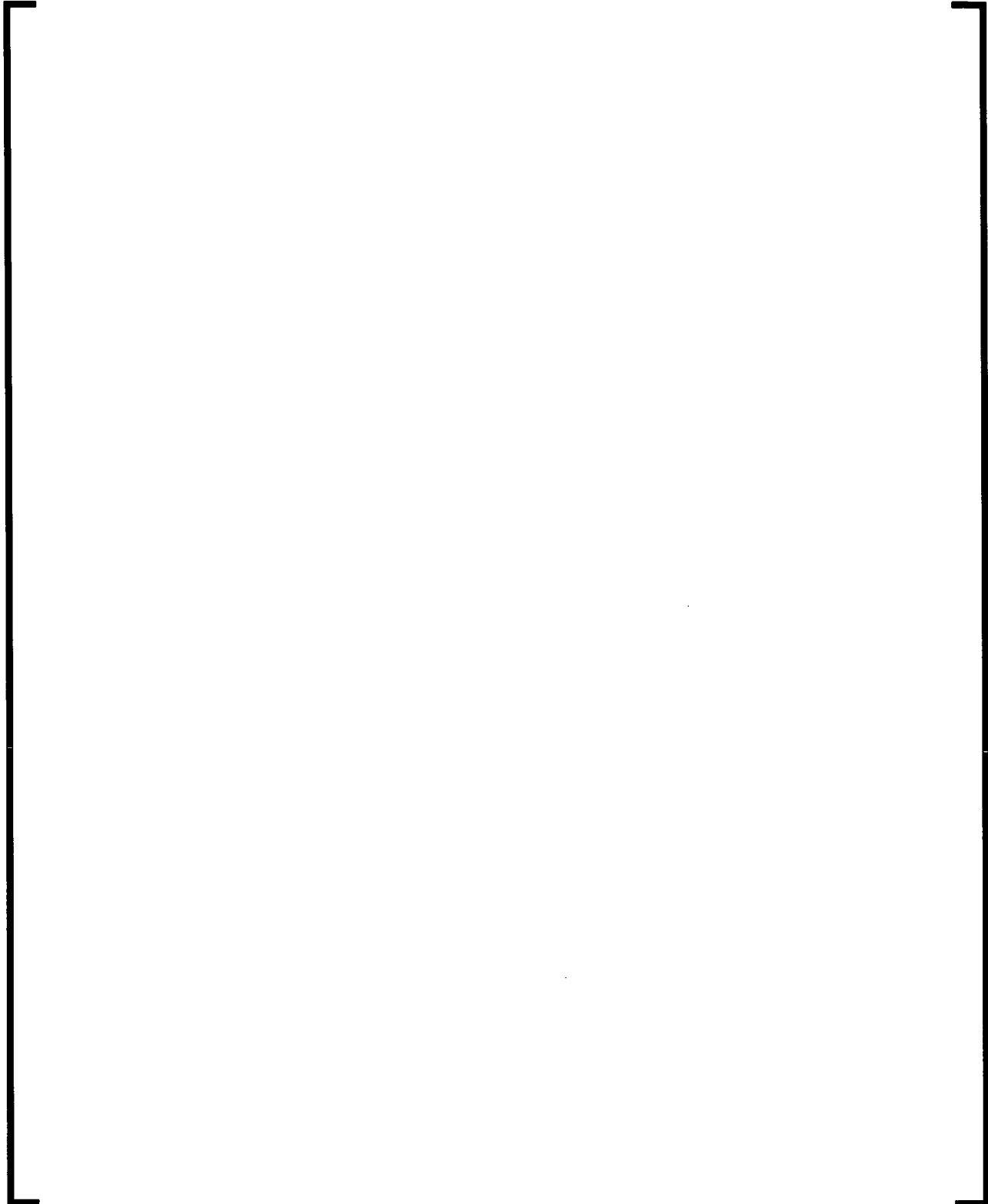
1. Figure 4-20 provides the graphical representation for the mode shapes for the loaded core.

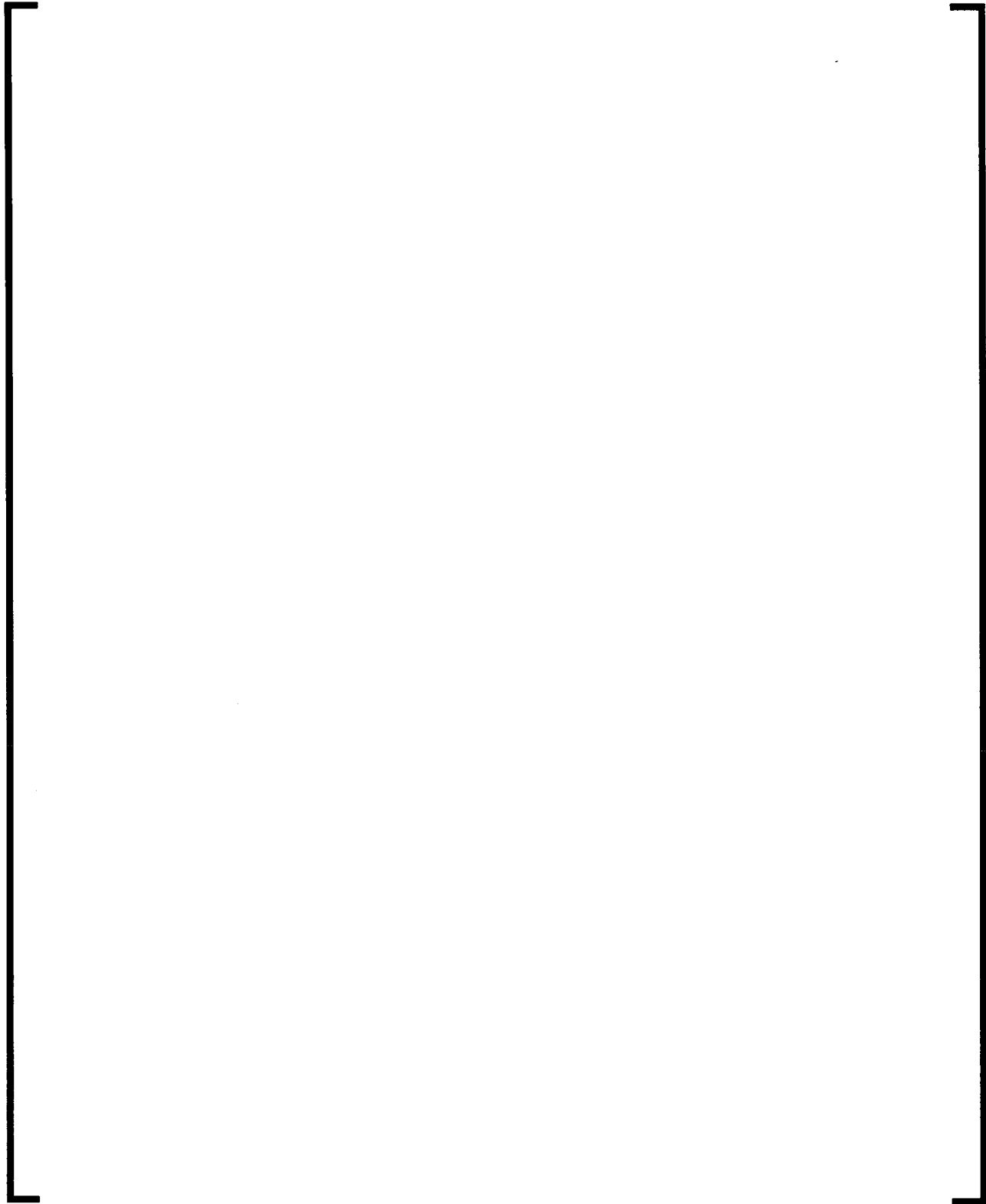
**Figure 4-19—Wet Mode Shapes for Full Scale Model (Un-Loaded Core)**

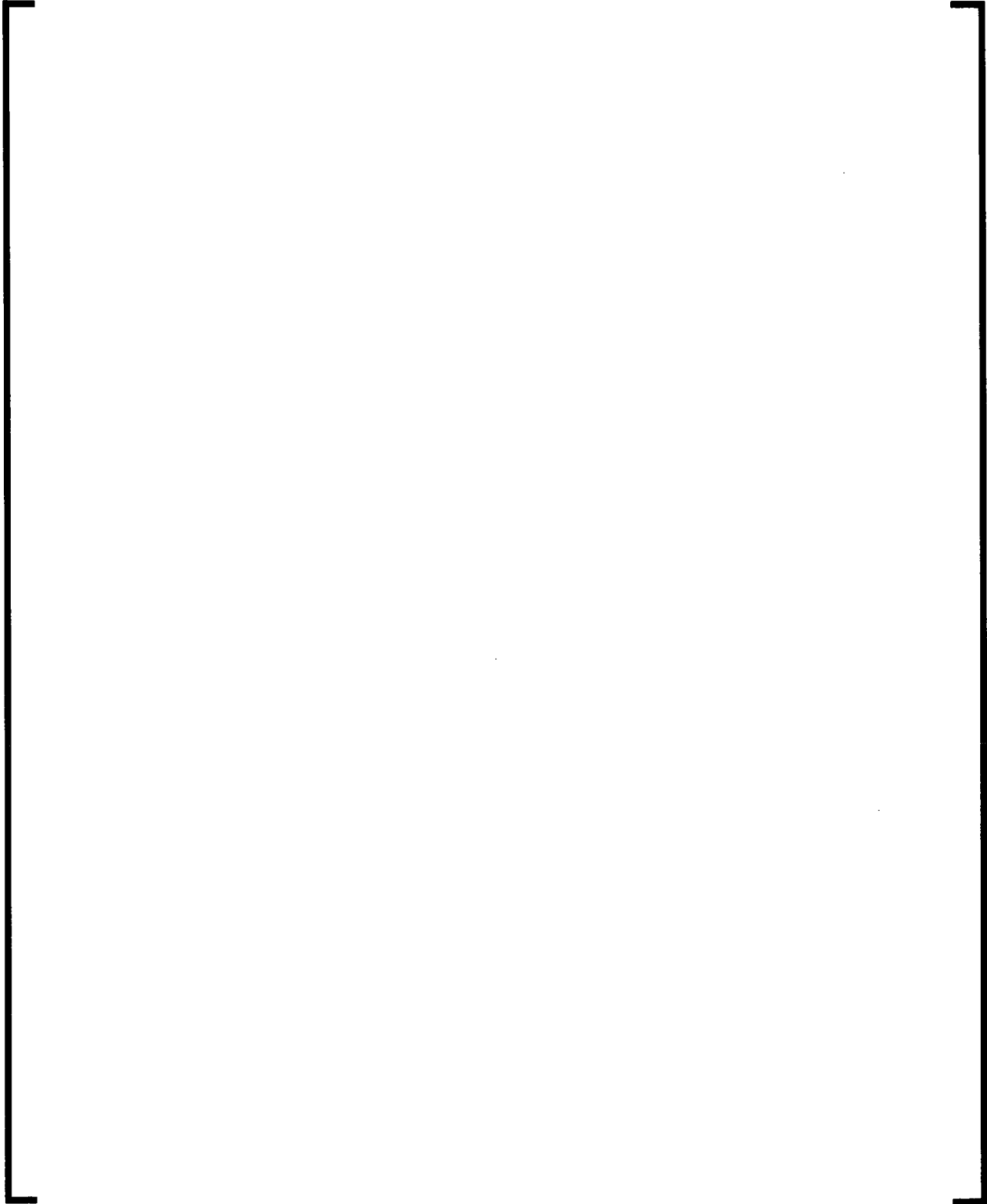


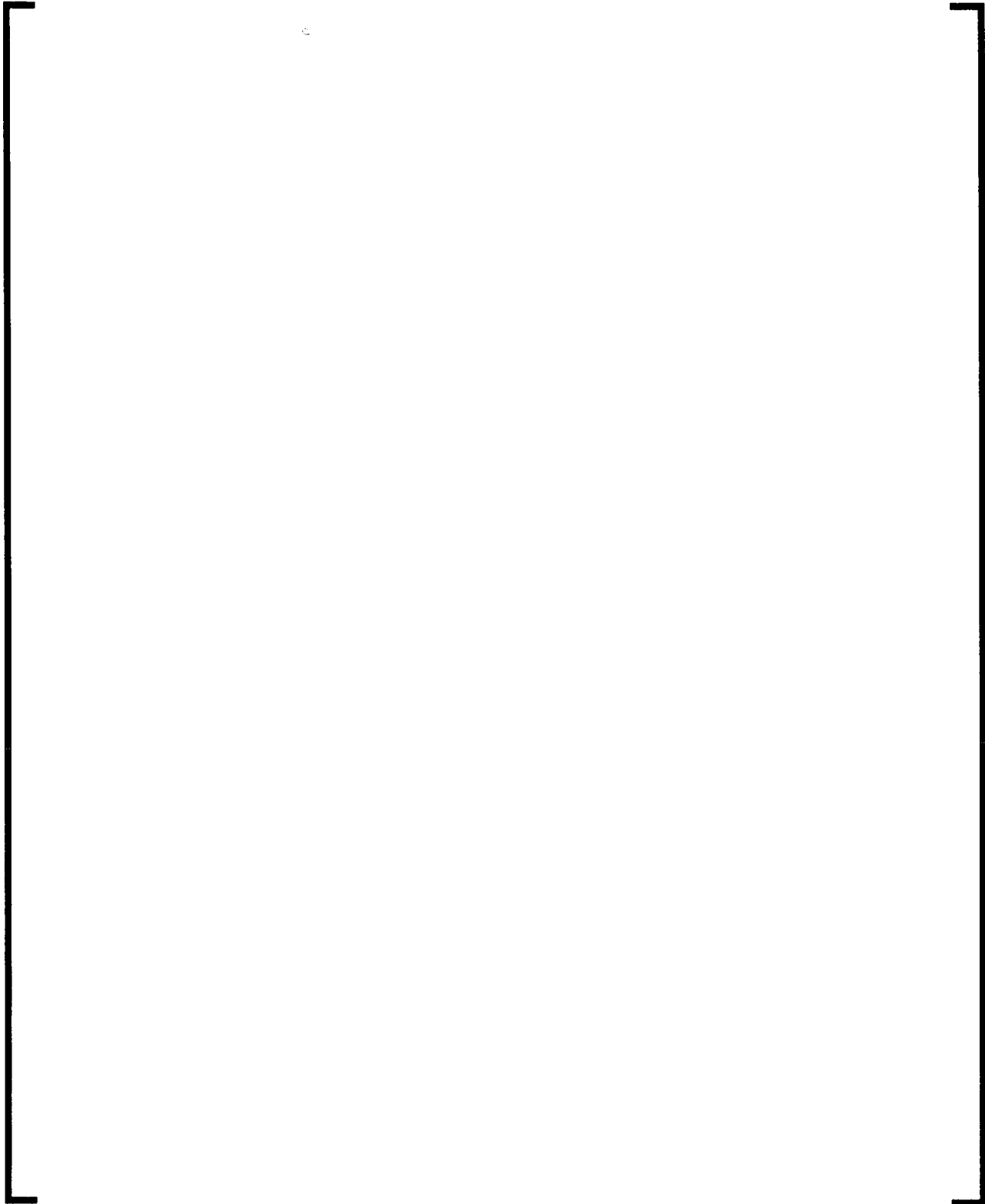


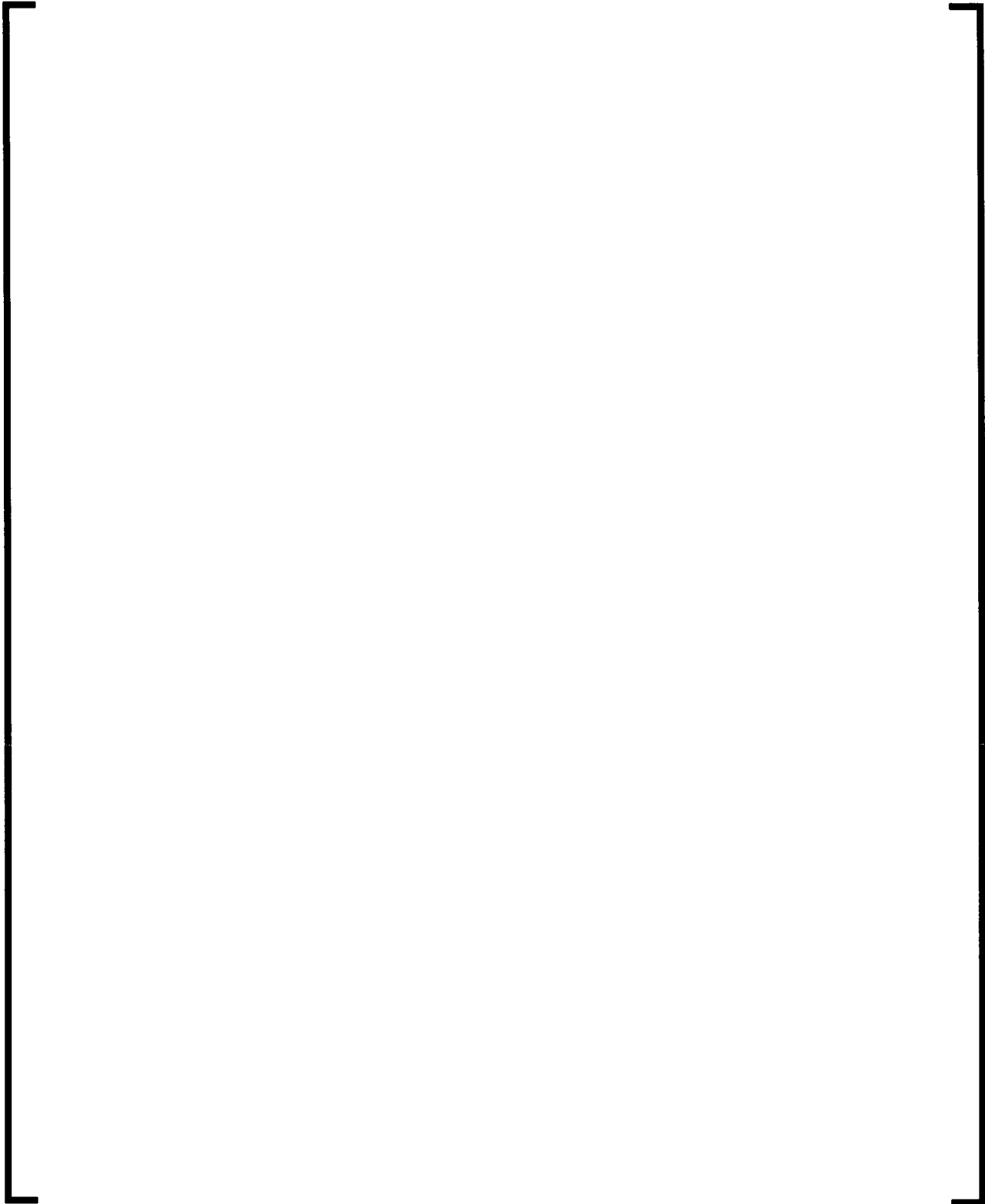


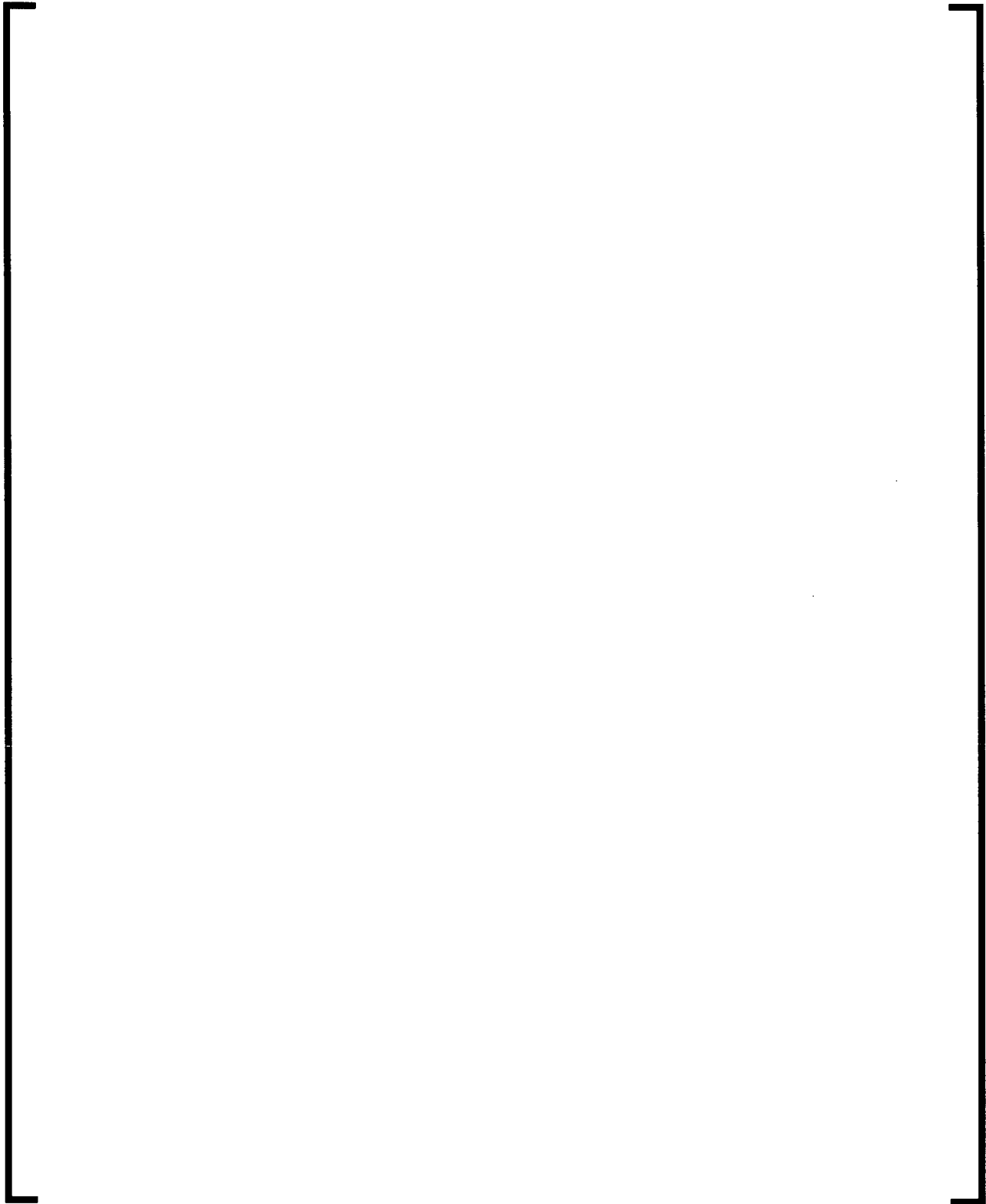


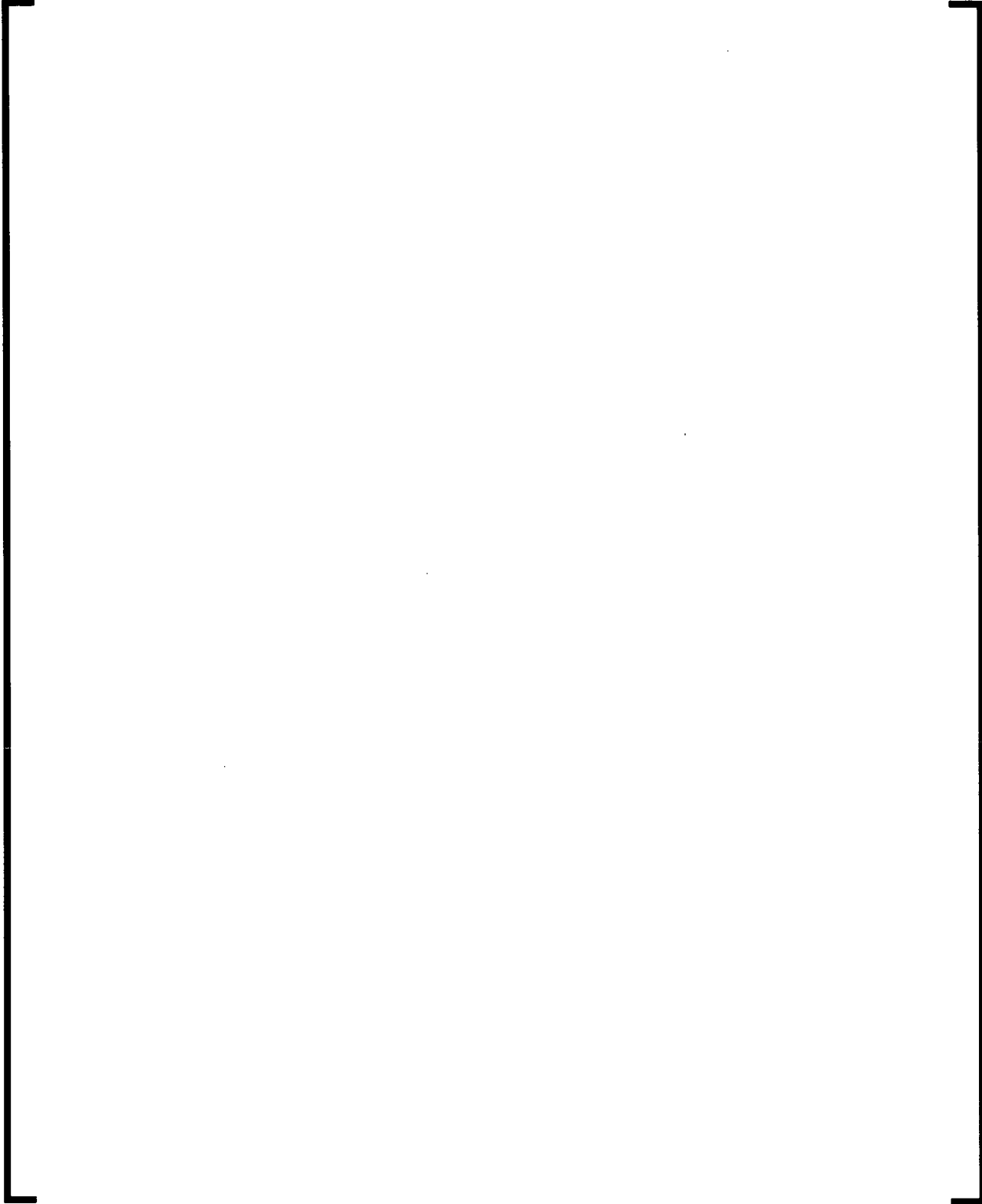


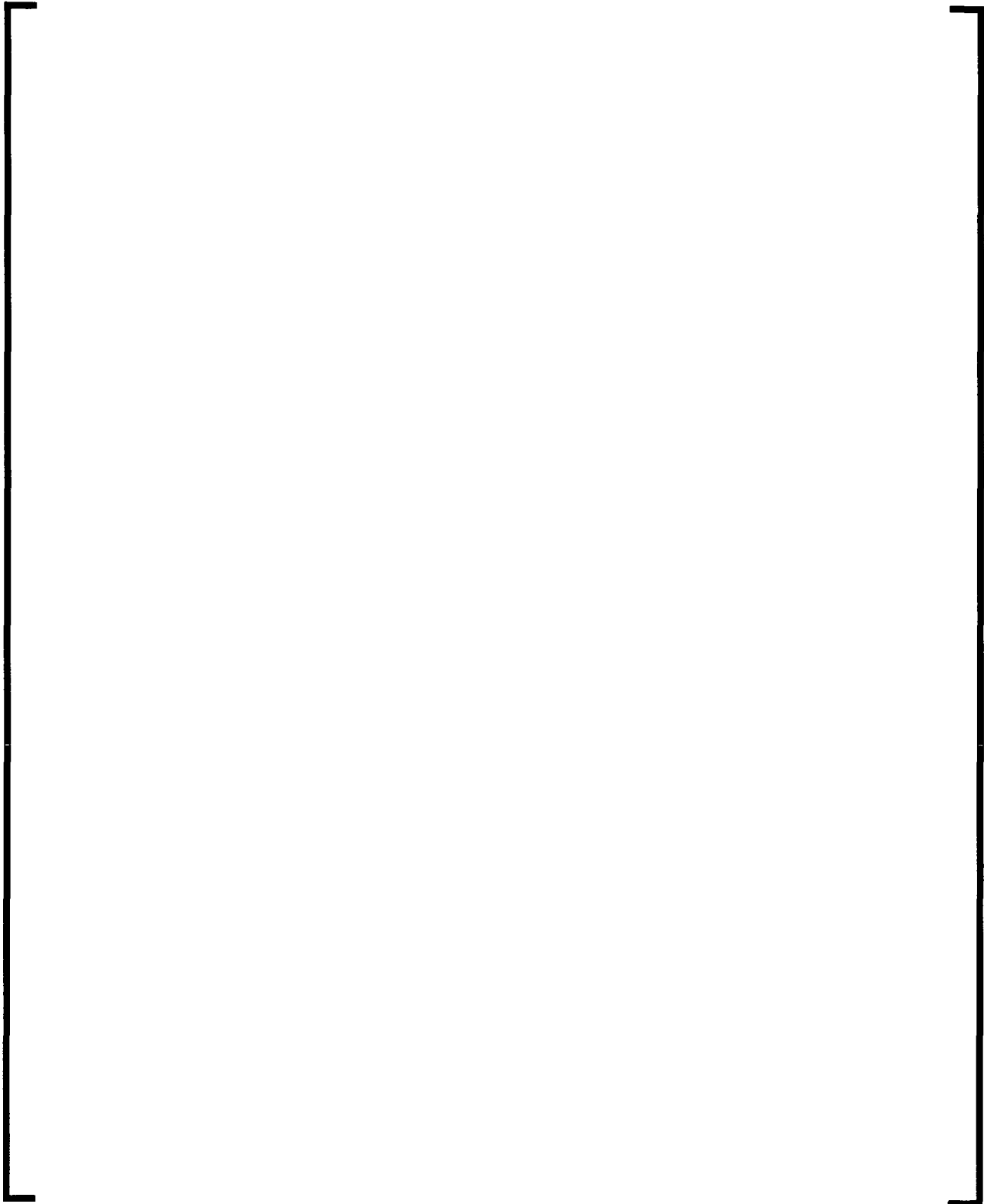


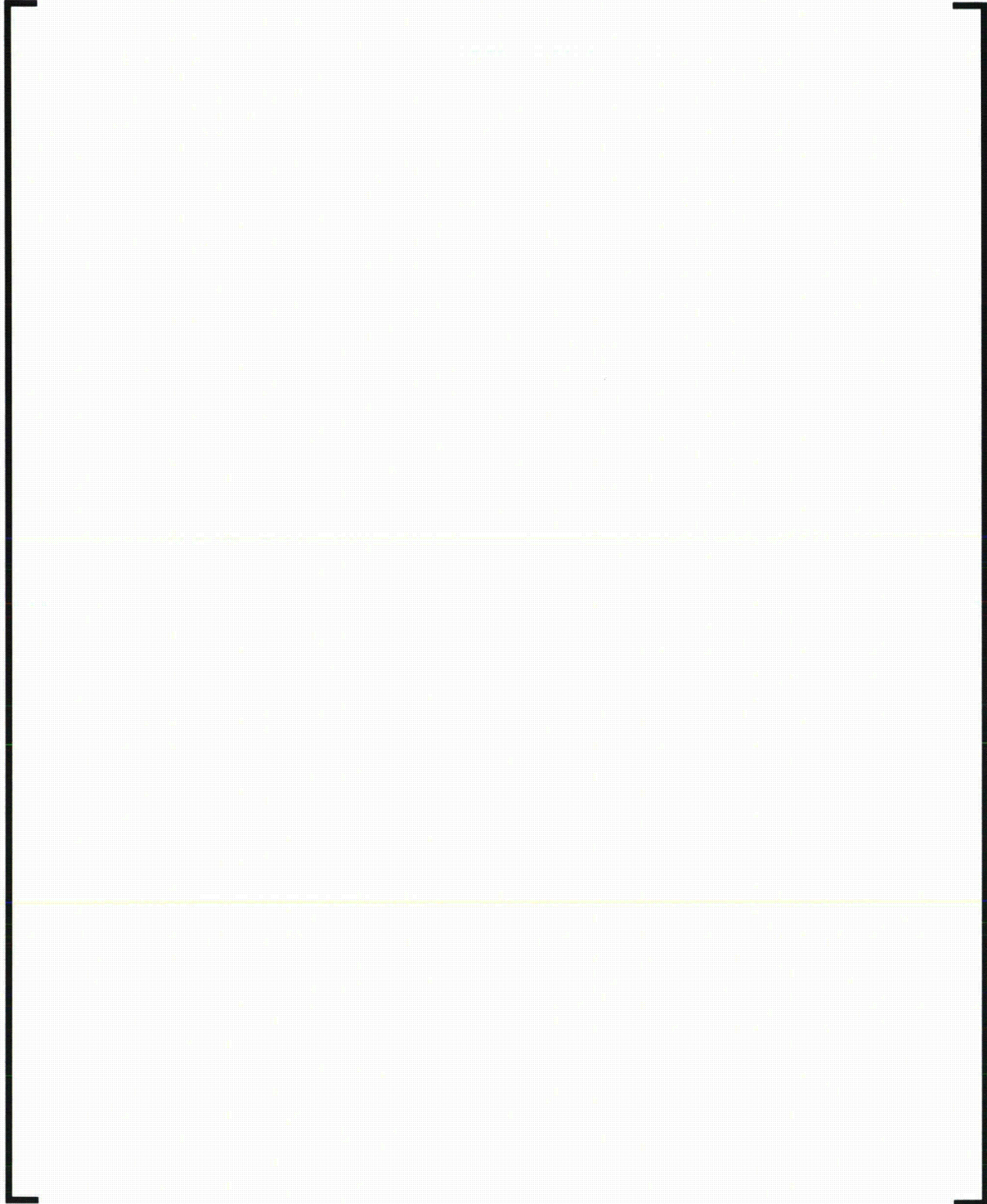


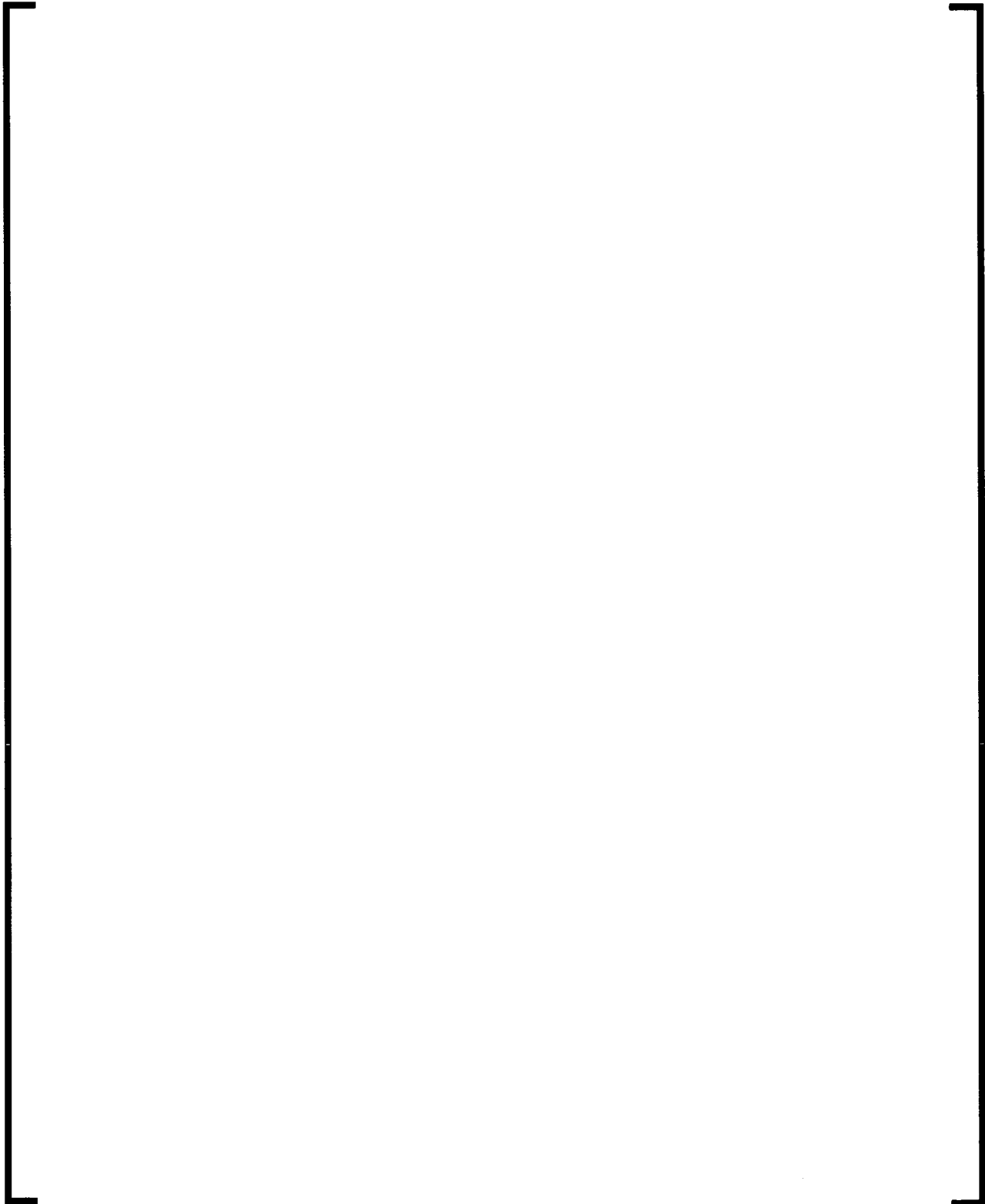


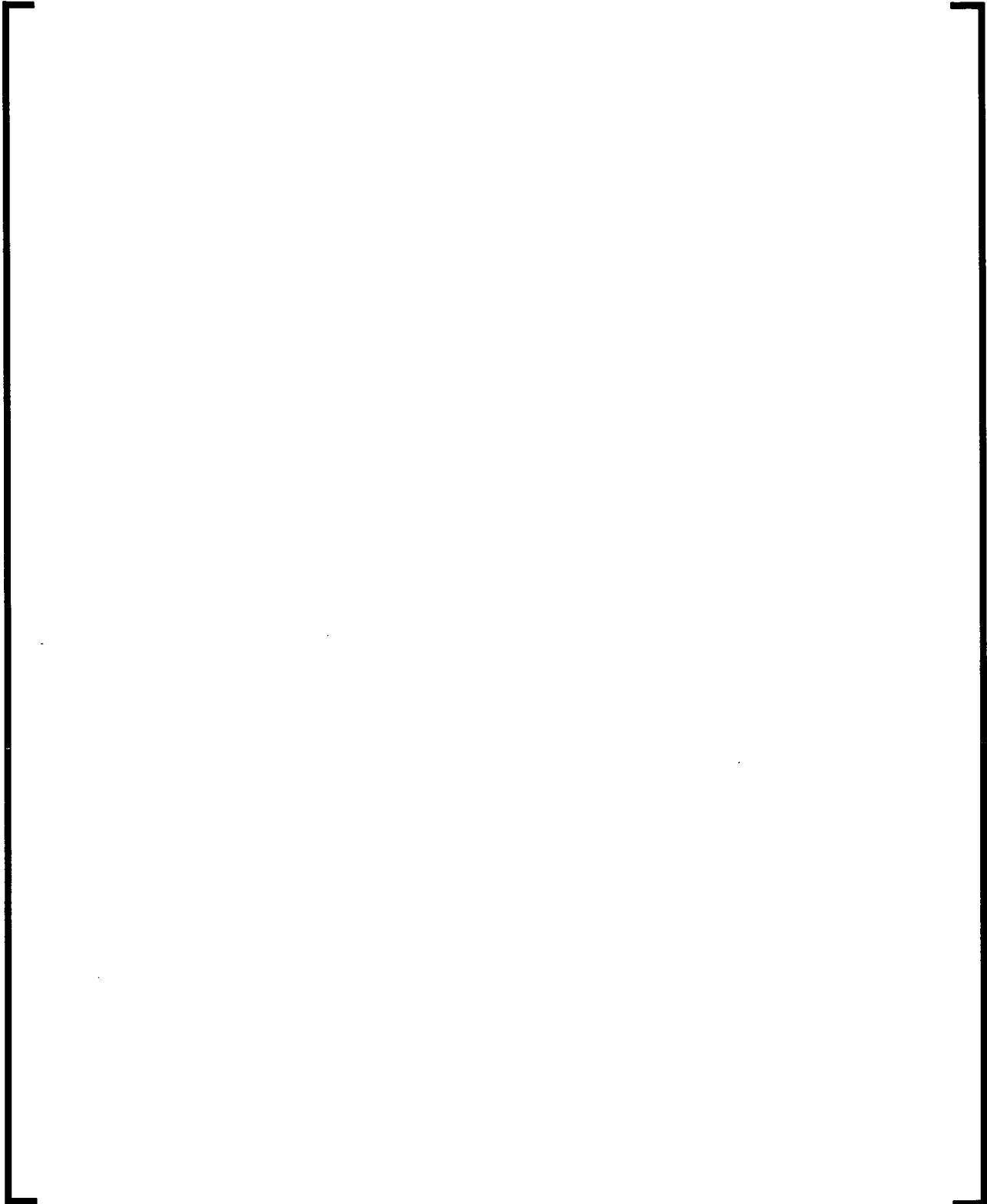


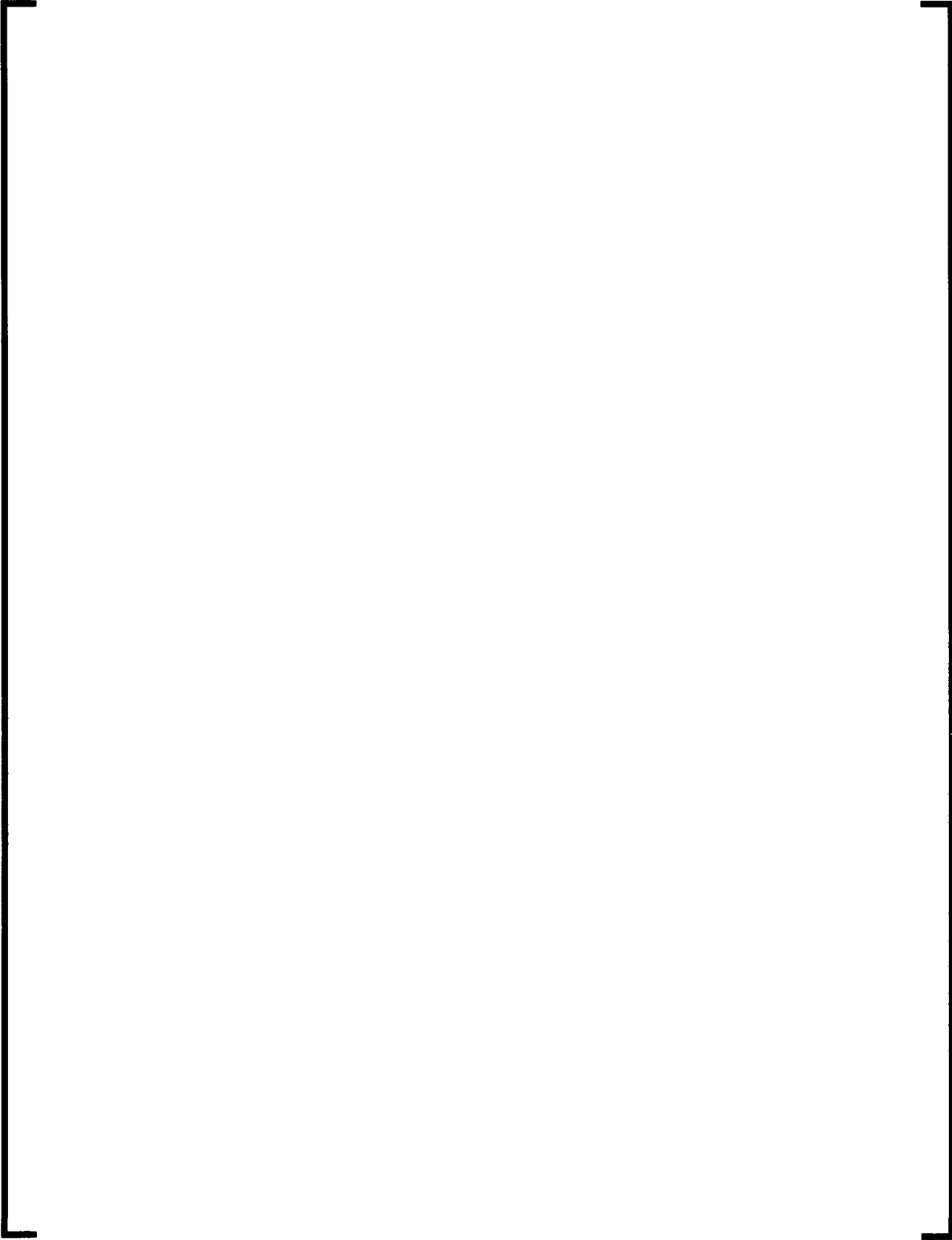


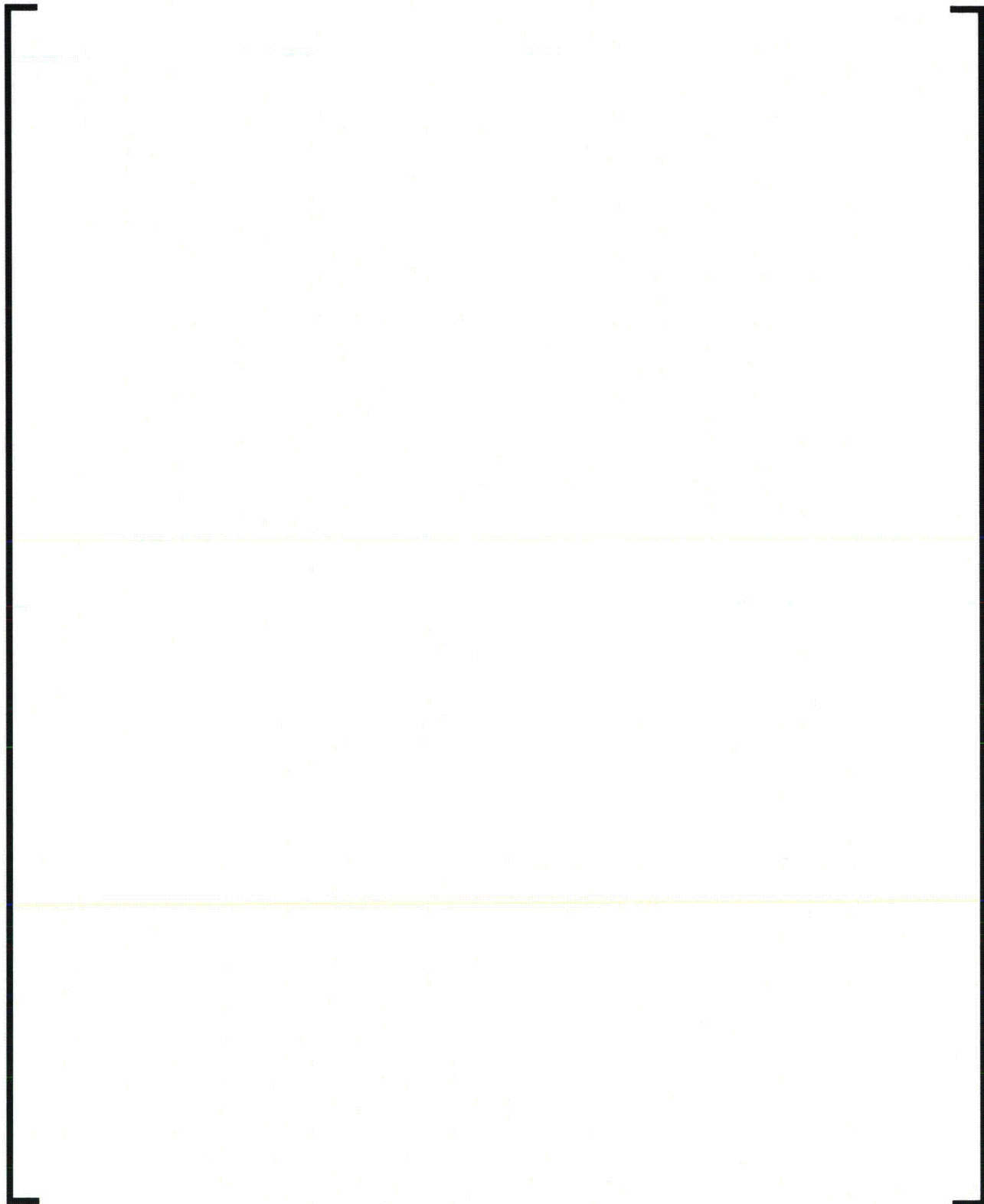












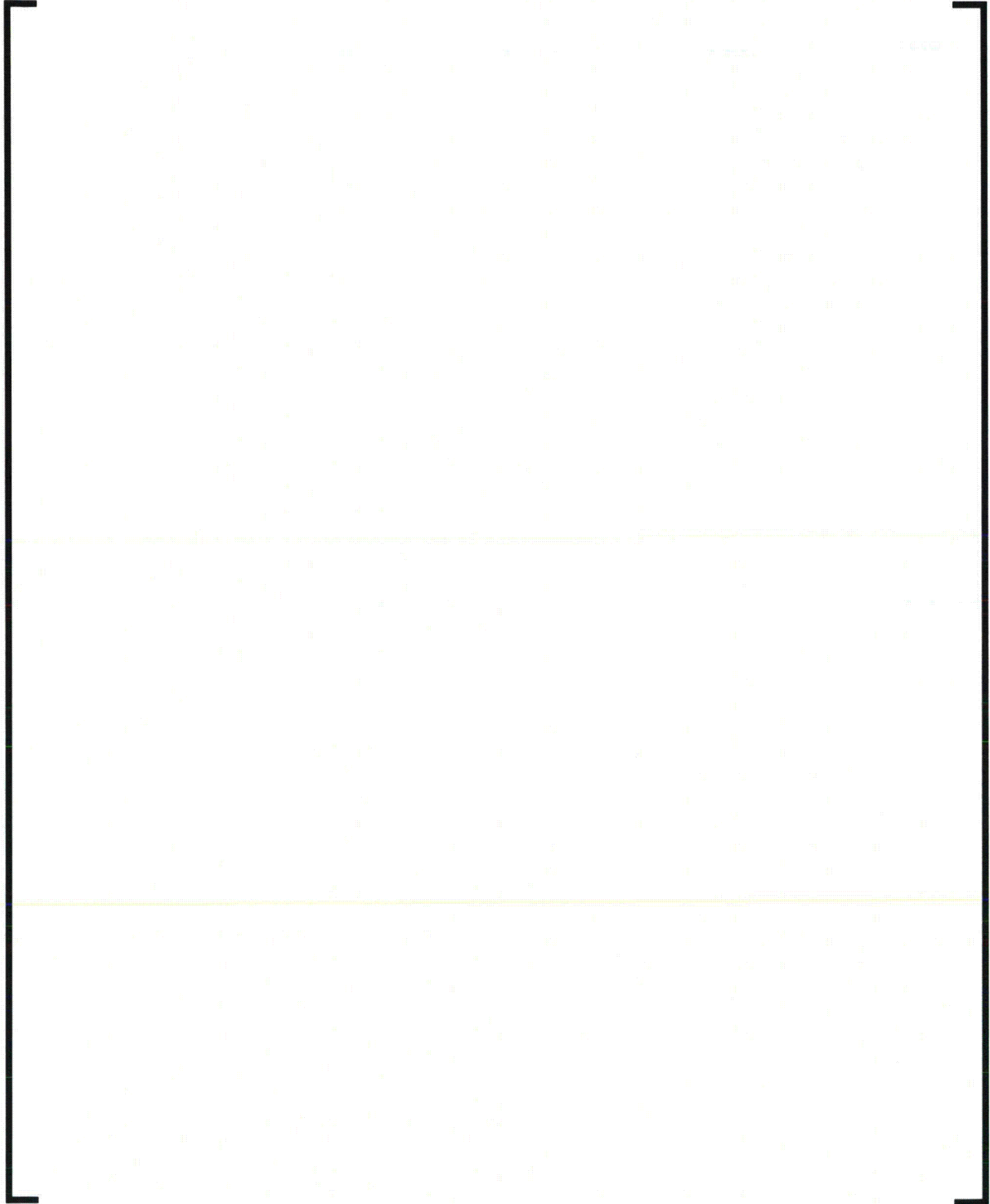




**Figure 4-20—Wet Mode Shapes for Full Scale Model (Loaded Core)**

